

1. Report No. FHWA/TX-10/0-6063-1		2. Government Accession No.		3. Recipient's Catalog No.	
4. Title and Subtitle SITE SPECIFIC WAVE PARAMETERS FOR TEXAS COASTAL BRIDGES: FINAL REPORT				5. Report Date February 2010 Published: April 2010	
				6. Performing Organization Code	
7. Author(s) Jun Jin, Chankwon Jeong, Kuang-An Chang, Youn Kyung Song, Jennifer Irish, and Billy Edge				8. Performing Organization Report No. Report 0-6063-1	
9. Performing Organization Name and Address Texas Transportation Institute The Texas A&M University System College Station, Texas 77843-3135				10. Work Unit No. (TRAIS)	
				11. Contract or Grant No. Project 0-6063	
12. Sponsoring Agency Name and Address Texas Department of Transportation Research and Technology Implementation Office P.O. Box 5080 Austin, Texas 78763-5080				13. Type of Report and Period Covered Technical Report: September 2007–August 2009	
				14. Sponsoring Agency Code	
15. Supplementary Notes Project performed in cooperation with the Texas Department of Transportation and the Federal Highway Administration. Project Title: Site Specific Wave Parameters for Texas Coastal Bridges URL: http://tti.tamu.edu/documents/0-6063-1.pdf					
16. Abstract There are about 20 coastal bridges located in hurricane evacuation routes in the State of Texas that are vulnerable to hurricane surge and wave action. Damage to these bridges could hamper emergency response and other services, and also cause tremendous economic loss. In recent devastating hurricane seasons of 2004, 2005, and 2008, several coastal highway bridges along the US coast of Gulf of Mexico suffered severe structural damages. To prevent structural failure of coastal bridges, the magnitude of wave load on coastal bridges must be determined. The objective of this research is to determine site-specific design wave parameters (i.e., wave height and wave period) that are needed in computation of wave loads and evaluation of wave effects on coastal bridges. In this project, we determined storm surge and wave parameters for four bridges using numerical models ADCIRC and SWAN. Simulation of water level including storm surge were performed with program ADCIRC, which also provides input to wave simulation. Wave parameters were determined by statistical analysis on simulation results performed with wave model SWAN at different storm surge and wind speed levels. Both wave and water level/storm surge simulations were vigorously validated with observed wave and water level data. The results of this research project will enable TxDOT to quickly implement the design methodology produced by an AASHTO/FHWA pooled fund study.					
17. Key Words Wave Forces, Wave Action, Storm Surge, Coastal Bridges, Hurricane, Wave Parameters			18. Distribution Statement No restrictions. This document is available to the public through NTIS: National Technical Information Service Springfield, Virginia 22161 http://www.ntis.gov		
19. Security Classif.(of this report) Unclassified		20. Security Classif.(of this page) Unclassified		21. No. of Pages 124	22. Price

SITE SPECIFIC WAVE PARAMETERS FOR TEXAS COASTAL BRIDGES: FINAL REPORT

by

Jun Jin, Ph.D., Assistant Professor
Chankwon Jeong, Graduate Student
Department of Maritime Systems Engineering
Texas A&M University - Galveston

and

Kuang-An Chang, Associate Professor
Youn Kyung Song, Graduate Student
Jennifer Irish, Assistant Professor
Billy Edge, Professor
Zachry Department of Civil Engineering
Texas A&M University

Report 0-6063-1

Project 0-6063

Project Title: Site Specific Wave Parameters for Texas Coastal Bridges

Performed in cooperation with the
Texas Department of Transportation
and the
Federal Highway Administration

February 2010

Published: April 2010

TEXAS TRANSPORTATION INSTITUTE
The Texas A&M University System
College Station, TX 77843-3135

TEXAS A&M UNIVERSITY AT GALVESTON
200 Seawolf Parkway
Galveston, TX 77553

DISCLAIMER

The contents of this report reflect the views of the authors, who are responsible for the facts and the accuracy of the data presented herein. The contents do not necessarily reflect the official view or policies of the Federal Highway Administration (FHWA) or the Texas Department of Transportation (TxDOT). This report does not constitute a standard, specification, or regulation. This report is not intended for construction, bidding, or permit purposes.

ACKNOWLEDGMENTS

This project was conducted in cooperation with TxDOT and FHWA. The authors thank the project director Dacio Marin, P.E. and members of TxDOT's Project Monitoring Committee, John Barton, P.E., Jon Holt, P.E. and Bonnie Longley. The research team pays tribute to all those affected by Hurricane Ike, which occurred during the conduct of the project and directly affected its robustness by providing current information.

TABLE OF CONTENTS

	Page
List of Figures	ix
List of Tables	xi
Chapter 1: Introduction	1
Chapter 2: STORM SURGE: Background and Literature Review	9
Damages to Coastal Bridges due to Storm Surges	9
Governing Equation for Storm Surge	10
Numerical Studies of Storm Surge Simulations	12
Review of Extreme-Value Statistics for Storm Surge	14
Chapter 3: Collection of Historical Wind Wave and Water Level Data	17
Historical Wind Data	17
Historical Wave Data	18
Historical Water Level Data	18
Chapter 4: STORM SURGE Study Area and Conditions	21
Chapter 5: SURGE RESPONSE FUNCTION APPROACH	29
Surge Response Function Methodology	31
Physical Scaling Laws for Surge Response Function	32
Surge Response Function from Limited Data	37
Improvement for General Use of Surge Response Functions	37
Chapter 6: Numerical Simulation Strategy	41
Numerical Models for Wave and Storm Surge Simulation	41
Wave Model SWAN	41
Hydrodynamic Model ADCIRC	42
Hurricane Surface Wind Field Modeling	44
Hurricane Selection Based on Optimal Sampling	46
Chapter 7: Hindcast of Wave Conditions during Hurricane Ike	51
Chapter 8: Extreme WAVE AND STORM Surge Estimation	59
Extreme Wave Conditions at Selected Bridge Sites	59
Surge Response Function Advancements	68
Validation and Justification of SRF Methodology	75
Chapter 9: Application of Surge Response Function for Peak Surge Estimation	77
Hurricane Carla Description	78
Comparison of Peak SRF Predictions with High-Water Mark Observations	78
Hurricane Ike Description	82
Comparison of the Extreme Surges from SRF Predictions with Peak Water Level Observations	83
Discussion of the Comparisons	85
Application of SRF Method for Flood Probability Estimation	86

Chapter 10: Summary and Discussion	93
References.....	95
Appendix: Surge Response Function Developed near 17 Texas Coastal Bridges	103

LIST OF FIGURES

	Page
Figure 1. Highway 90 Bridge Damaged during Hurricane Katrina.....	2
Figure 2. Two Bridges Damaged during Hurricane Ike.	2
Figure 3. Storm Related Forces on Coastal Bridges.	4
Figure 4. Profile of a Nonlinear Ocean Wave.....	5
Figure 5. Wind Speed in Gulf of Mexico during Hurricane Rita (2005) (Unit: m/s).....	18
Figure 6. Recorded Water Level in Galveston during Hurricane Ike (Source: NWLON).	20
Figure 7. Locations of 20 Target Bridges along Texas Coast (Red Dots).....	22
Figure 8. Bridges (Red Dots) near the Eastern Boundary of the Texas Coast.....	22
Figure 9. A Bridge (Red Dot) at Rollover Pass in Galveston.....	23
Figure 10. Bridges (Red Dots) near the Entrance of Galveston Bay.....	23
Figure 11. Bridges (Red Dots) of FM 2004 Road (Top Dot), and San Luis Pass (Bottom Dot) in Galveston.....	24
Figure 12. Bridges (Red Dots) on FM1495 Road (Left Dot) and Hwy 332 (Right Dot) near Freeport.....	24
Figure 13. Bridges (Red Dots) along Highway 35 in Matagorda Bay.....	25
Figure 14. Bridge (Red Dot) on Lyndon B. Johnson Causeway in Aransas.	25
Figure 15. Bridges (Red Dots) in Corpus Christi.	26
Figure 16. Location (Maroon Dots) of Two Damaged Bridges in Galveston during Hurricane Ike.	28
Figure 17. Hurricane Tracks and Stations for SRF Development (Irish et al., 2009).	33
Figure 18. Preliminary Dimensionless SRFs (Irish et al., 2009).	34
Figure 19. Dimensionless SRFs Using the Modified Dimensionless Alongshore Parameter (Irish et al., 2009).	36
Figure 20. SRF Prediction versus Numerically Simulated Surges (Irish et al., 2009).	36
Figure 21. Texas Coastal Map of the Study Area.....	39
Figure 22. East Coast ADCIRC Domain Grid.....	44
Figure 23. Texas Coastal Map of the Study Area. The area shaded in blue represents the varying continental shelf width (L30) along the Texas coastal.....	48
Figure 24. Storm Tracks (Solid Line) with Respect to Stations along the Texas Coast.....	48
Figure 25. Tracks for Subset I & II.....	50
Figure 26. Damage to Pelican Island Causeway.....	51
Figure 27. Damage to the Entrance Bridge to Flagship Hotel, Galveston.....	52
Figure 28. Track of Hurricane Ike and Locations of NDBC Buoys.....	53
Figure 29a. Comparison of Model and Measured SWH at Buoy 42001, 42002, and 42007.	54
Figure 29b. Comparison of Model and Measured SWH at Buoy 42019, 42020, 42035, and 42036.....	55
Figure 29c. Comparison of Model and Measured SWH at Buoy 42039 and 42040.	56
Figure 30. Contour of Model SWH before Hurricane Ike Made Landfall in Galveston Area.	57
Figure 31. Predicted Significant Wave Height during Category 3 Hurricanes (Bridge Locations Marked by Red Crosses).....	62
Figure 32. Predicted Maximum Wave Heights vs. Storm Surge Levels (Galveston Causeway and San Luis Pass Bridge).	63

Figure 33. Predicted Maximum Wave Heights vs. Storm Surge Levels (Rollover Pass and Lavaca Bay Causeway).....	64
Figure 34. Predicted Maximum Wave Heights vs. Hurricane Category (Galveston Causeway and San Luis Pass Bridge).....	65
Figure 35. Predicted Maximum Wave Heights vs. Hurricane Category (Rollover Pass and Lavaca Bay Causeway).....	66
Figure 36. Locations of 10 m and 30 m Water Depth on the Continental Shelf.....	69
Figure 37. Hurricane Tracks Selected (Green Solid Lines) to Measure the Effect of Varying Continental Shelf Width (L_{30}).....	69
Figure 38. Linear Regression of Storm Size (R_p) and the Distance between the Location of Hurricane Eye at Landfall and the Alongshore Peak Surge Location.....	70
Figure 39. The Parameter λ Variations with Respect to Varying Continental Shelf Width.....	72
Figure 40. Continental Shelf Map of the Texas Coast.....	73
Figure 41. Surge Response Functions Developed at the Three Locations in Galveston.....	74
Figure 42. $\zeta_{srf} - \zeta_{sim}$ plots.....	76
Figure 43. Hurricane Tracking Map and Elevation Stations.....	79
Figure 44. Comparison of the SRF Prediction to HWM for Hurricane Carla.....	81
Figure 45. Hurricane Ike Tracking Map and Water Elevation Stations.....	82
Figure 46. Comparison of the SRF Prediction to Peak Water Level Record during Hurricane Ike.....	85
Figure 47. Surge Response Surface Estimated with Respect to the Variation of R_p and x_o at a Fixed Location.....	88
Figure 48. Combined Surge Response Surfaces.....	92

LIST OF TABLES

	Page
Table 1. Locations of the Selected Coastal Bridges.	27
Table 2. East Coast Domain Triangular Mesh Information.....	44
Table 3. R_p and c_p Combinations for Subset I and II.	49
Table 4. Maximum Wind and Wave at Three Bridges in Galveston during Hurricane Ike.	58
Table 5. Wind Speed and Storm Surge Ranges of Saffir-Simpson Hurricane Scale.....	60
Table 6. Most Probable Extreme Wave Height H_{max} at Galveston Causeway (m).	60
Table 7. Most Probable Extreme Wave Height H_{max} at San Luis Pass Bridge (m).....	61
Table 8. Most Probable Extreme Wave Height H_{max} at Rollover Pass Bridge (m).....	61
Table 9. Most Probable Extreme Wave Height H_{max} at Lavaca Bay Causeway (m).	61
Table 10. Period of Extreme Wave T_{max} at Galveston Causeway (s).....	67
Table 11. Period of Extreme Wave T_{max} at San Luis Pass Bridge (s).	67
Table 12. Period of Extreme Wave T_{max} at Rollover Pass Bridge (s).	67
Table 13. Period of Extreme Wave T_{max} at Lavaca Bay Causeway (s).....	68
Table 14. Properties of the Parameter λ for Each Segmentation of the Texas Coastal Region ...	71
Table 15. Variation of λ in the Continental Shelf Width.	72
Table 16. Hurricane Carla Surge Estimation from HWM and SRF.	80
Table 17. Hurricane Ike Surge Estimation from Peak Surges and SRF.	84
Table 18. SRF Extreme Surge Predictions at Three Bridges in Galveston.	90
Table 19. Locations of the 17 Selected Coastal Bridges	103

CHAPTER 1: INTRODUCTION

In recent years, several hurricanes have caused structural damages to coastal highway bridges in all four states along the U.S. coast of the Gulf of Mexico. In September 2004, during Hurricane Ivan, the 2.5-mile-long I-10 twin bridges over Escambia Bay near Pensacola Florida suffered extensive structural damage. On the eastbound and westbound bridges, 58 spans were pushed off the substructure and another 66 spans were misaligned ([Talbot 2005](#)). The Florida Department of Transportation (FDOT) signed a \$26.4 million emergency contract to repair and reopen the westbound bridge within 24 days. A \$243 million project was started later to design and build a new bridge to replace the damaged bridges.

In August 2005, during Hurricane Katrina, more bridges suffered similar damage, including the I-10 twin bridges across Lake Pontchartrain in Louisiana, the US-90 bridges across Biloxi Bay ([Figure 1](#)) and Bay St. Louis in Mississippi, and I-10 bridge over Mobile Bay in Alabama ([ASCE TCLEE, 2006](#)). As a result, \$803 million was awarded for the bridge deck lifting project for the I-10 Twin Span Bridge, and \$226.8 million was awarded for the bridge replacement project for the US-90 bridge over Bay St. Louis. In total, \$2.75 billion in supplemental appropriation was awarded by the Federal Highway Administration's "Emergency Relief Program" ([Collins, 2006](#)). In September 2008, while this project was underway, Hurricane Ike made landfall in Galveston. Two bridges in Galveston, the Rollover Pass Bridge and the Pelican Island Bridge were damaged ([Figure 2](#)).



Figure 1. Highway 90 Bridge Damaged during Hurricane Katrina
The bridge was located on US-90 in Biloxi and Gulfport, Mississippi Gulf Coast (from [Gulf Coast Information System, 2006](#)).

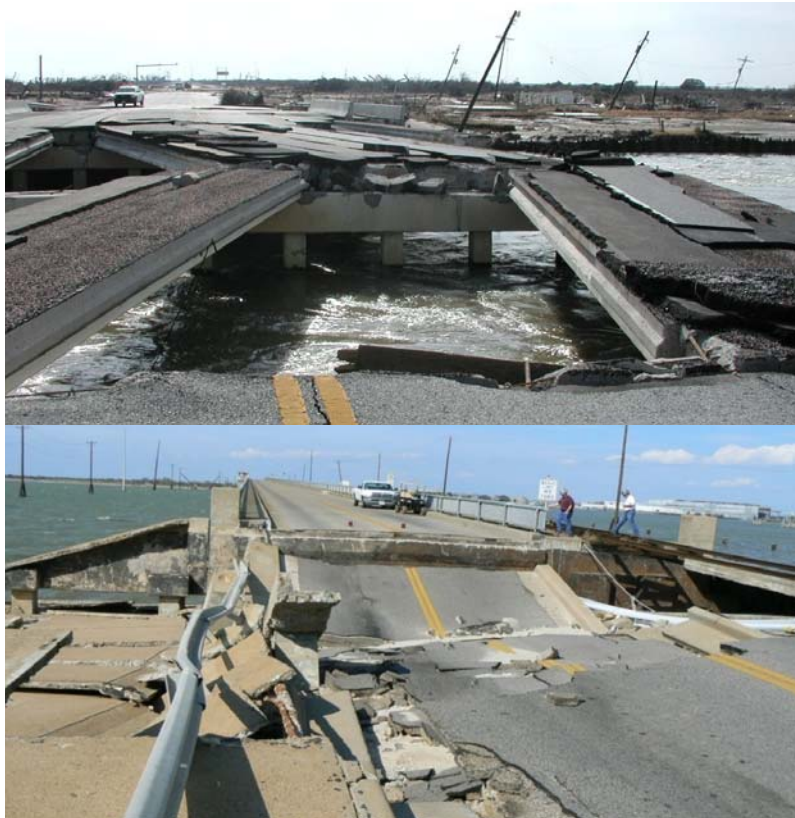


Figure 2. Two Bridges Damaged during Hurricane Ike.
Rollover Pass bridge located between the communities of Gilchrist and Caplen (top), and Pelican Island Bridge along 51st Street over the Galveston Ship Channel (bottom).

Damage resulting from hurricanes striking in 2004, 2005, and 2008 has called public attention to the importance of accurate assessment of hurricane impacts on coastal residents and structures. Especially, the stability and serviceability of coastal bridges directly exposed to intensified wave forces during hurricane events have become a main concern. There are a great number of coastal highways and bridges distributed throughout the entire Texas coast along the Gulf of Mexico. After inspection of the geography and landscape of their locations, researchers identified 20 coastal bridges closely associated with the life of nearby communities, especially during hurricane evacuation, that were suspected to be vulnerable to hurricane flooding.

To prevent structural failure of coastal bridges, the magnitude of wave load on coastal bridges must be determined. Storm-related forces on coastal bridges are illustrated in [Figure 3. Storm Related Forces on Coastal Bridges](#). Under normal conditions, the superstructure of a coastal bridge is well above still-water level and is subjected to wind force only. Wave and current forces can act only on the piles. However, during a hurricane the storm surge combines with the normal tides to create the hurricane storm tide, which may raise the mean water level to a point that part or even the entire superstructure is immersed in water, thus subjecting the superstructure to wave and current forces. Wave and current action associated with the storm surge can cause extensive damage.

Due to the fact that density of water is much larger than the density of air, the magnitude of wave and current forces is much larger than wind force. The vertical (uplift) component of wave force adds to buoyancy to counteract the gravity of bridge superstructure and, as a result, the friction between the superstructure and pile cap is reduced. Due to this reduced friction, the horizontal component of wave force adds to the current force and may push the superstructure off the pile cap if the bridge was not specifically designed for this extreme event.

To prevent wave-induced structural damage to coastal bridges, either in design of new bridges or retrofitting of existing bridges, the magnitude of wave forces on coastal bridges must be determined. The magnitude of wave force on coastal bridges depends on the following major factors: wave parameters, water depth, and geometry of bridge structure.

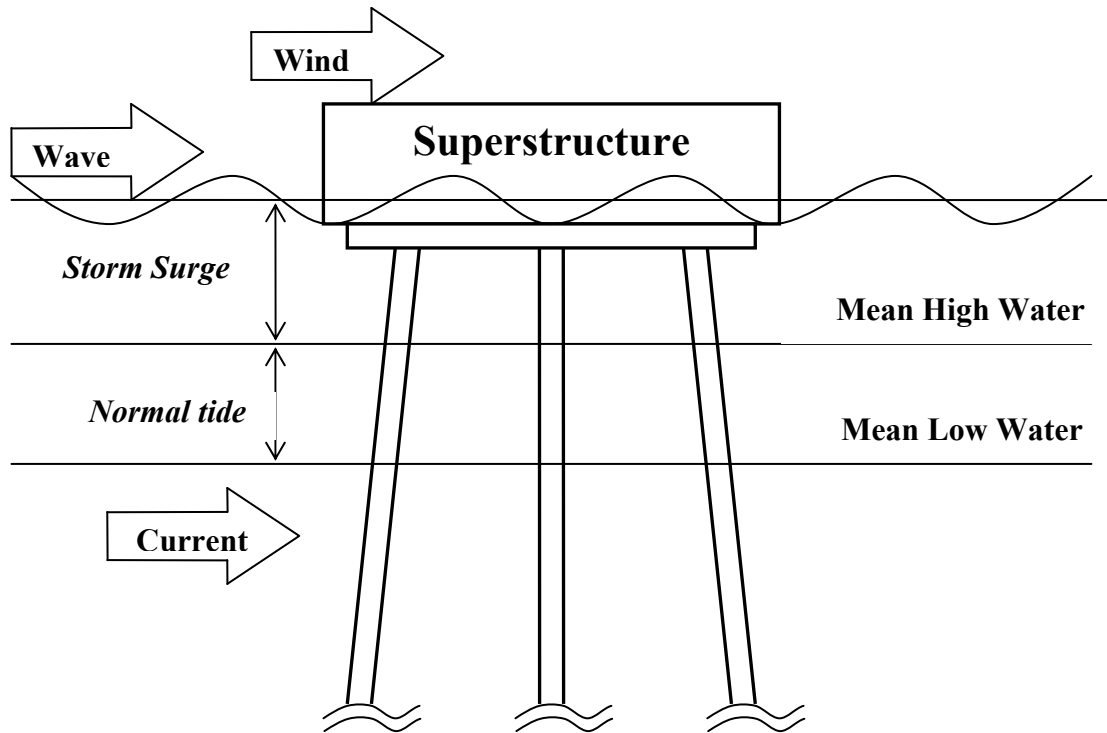


Figure 3. Storm Related Forces on Coastal Bridges.

The most critical design wave parameter is the wave height (Figure 4), which indicates the intensity of ocean waves (the energy of the sea is proportional to the square of wave height). Other wave parameters, such as wave period, wave direction, and spectral shape are also design concerns. Wave length depends on both wave period and local water depth. Water depth is mainly affected by astronomical tides, storm surge, and wave setup. Increased water depth can increase depth-limited wave heights. According to the ratio of water depth to wave length, water waves are classified as deep water, shallow water, or intermediate waves. Each wave regime requires different wave theories for the calculation of water surface profile and wave mechanics, which are needed for calculation of wave force on structures. For nonlinear waves, wave crest height, which is the distance between wave crest and still water level, is higher than half of the wave height.

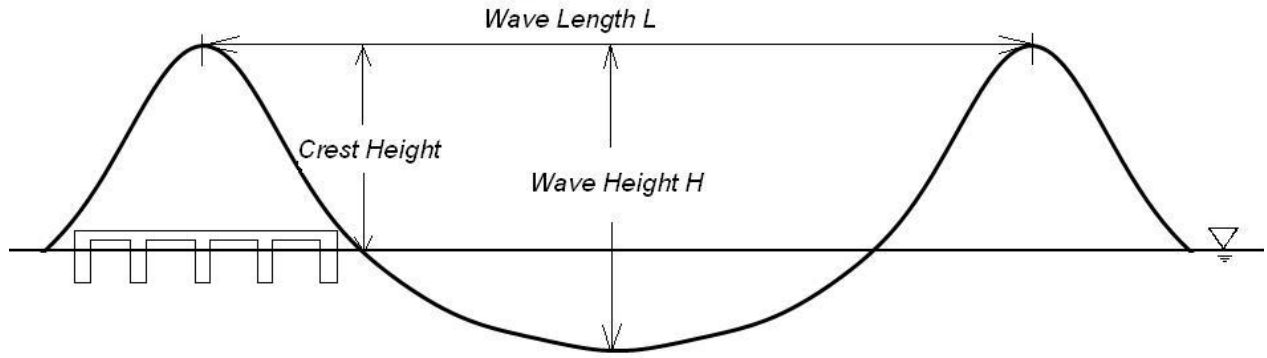


Figure 4. Profile of a Nonlinear Ocean Wave.

The length of a structure along the direction of wave propagation is important in wave analysis. If the length is much smaller than the wave length (e.g. bridge piers), the incident wave field is not significantly affected by the presence of the structure, diffraction and refraction can be ignored. Otherwise (e.g., bridge superstructure) diffraction analysis is necessary for calculation of wave load. The shape of the cross-section of superstructure affects the wave load, because the decks of bridges are often supported by parallel girders along the span length, the bottoms are not flat, and the load will affect the wave field below the bottom of superstructure.

Based on these factors, computation of wave load on bridge structures generally includes the following steps:

1. determination of site-specific design wave parameters;
2. determination of design water depth, which includes the effect of storm surge;
3. determination of wave kinetics (water particle velocity and acceleration) and dynamics (pressure) around the structure:
 - for bridge substructures, a wave theory will be selected based on design wave and water depth conditions, water practical velocity, acceleration, and pressure—it can be easily obtained from the wave theory;
 - for bridge superstructures, wave kinetics and dynamics cannot be directly obtained from wave theory—the wave field around the structure needs to be obtained through numerical or theoretical analysis; and
4. computation of wave load from wave kinetics or dynamics using established methods.

In September 2006, FHWA funded a pooled-fund study entitled “Development of Guide Specifications for Bridges Vulnerable to Coastal Storms and Handbook of Retrofit Options for Bridges Vulnerable to Coastal Storms” (study number TPF-5(130)). The objective of that project was to develop a guide specification and a handbook of retrofit strategies and options to mitigate damage to highway bridges subject to coastal storm hydrodynamic factors, and to recommend improvements for bridges in coastal environments. The project was completed in 2008. AASHTO published its *Guide Specifications for Bridges Vulnerable to Coastal Storms* (AASHTO, 2008), which gives equations for computation of wave forces on bridge structures and guidelines for determination of design wave parameters. For bridges critical to a region’s economy or safety, or for bridges where substantial repair and/or replacement costs may be incurred if damages by a coastal storm event, a Level III analysis is mandated by the AASHTO guide specifications for determination of design water level and wave parameters. The Level III analysis specified in the AASHTO guide requires extensive computer modeling of water level and waves at the bridge site. During Hurricane Ivan, the maximum significant wave height recorded by National Data Buoy Center (NDBC) buoy 42020 was 15.96m, the largest wave ever recorded in the Gulf of Mexico. According to previous statistics, it corresponds to a 40,000-year event. This aspect, combined with the huge economic cost to replace the damaged bridges, highlights the need for site-specific wave information.

The objective of this research was to determine site-specific design wave parameters (i.e., wave height and wave period) for selected bridges along Texas coast, that are needed to compute wave loads and evaluate wave effects on these bridges. In this project, storm surge and wave parameters for four bridges were determined using numerical models ADCIRC (Advance Circulation Model for Coastal Ocean Hydrodynamics) and SWAN (Simulating WAVes Nearshore). Simulation of water level including storm surge also provides input to wave simulation. As a means for more concrete quantification and reliable estimation of storm surge, a surge response function (SRF) methodology was adopted. A SRF is a parametric representation of the continuous surge response surface in a dimensionless form (Irish et al., 2009). Based on the joint probability method with optimal sampling, the surge response function approach (Resio et al., 2009) suggested that a maximum surge surface (ζ) could be described by a number of major hurricane parameters such as hurricane size, intensity, track angle, forward speed, and the relative distance to hurricane landfall location. Furthermore, the physical relationship between

the maximum surge and relevant hurricane parameters was identified and used to develop the scaled parameters characterizing spatial extent of surge (x') and hurricane surge (ζ'). These physical laws introduced in the surge response function method is beneficial since it has a potential for more reliable surge estimation since the derived dimensionless parameters allow a better interpolation for the tracks lying between the tracks where the numerical simulation data is available.

Numerical hurricane surge simulations for 15 parallel tracks entering to the Gulf of Mexico following northeasterly path were carried out. During the course of this work to determine the surge response functions at the selected bridge regions, however, a notable shifting in the location of dimensionless peak surge, i.e., the highest surge possible among all studied storm surges at a given location, has been found for those bridges located away from Matagorda Bay with respect to Matagorda Bay results studied by [Irish et al. \(2009\)](#). Also, more prominent scatter in the surge data for these storms to the right of the hurricane landfall location have been found in data distribution at the coastal stations nearby Galveston Bay. After investigation into the regional characteristics, it was found that the continental shelf width, defined here as the offshore distance from the coastline to the 30 m water depth, near the Galveston coast changes more rapidly and is much wider than those at other regions to the south. Therefore, the effect of relative storm size with respect to the continental shelf width was investigated in order to improve SRF performance.

Based on these new findings, in this study we have made a number of modifications to improve the initial surge response function so it can be applicable for all 20-target bridges over a range of geographical and hurricane meteorological parameters. We related the continental shelf width to the continental shelf parameter, λ , so the variance of bottom slope, or the area on which the storm surge is developing, is considered when predicting the peak surge location.

Wave parameters were determined by statistical analysis on simulation results performed with wave model SWAN at different storm surge and wind speed levels. Both wave and water level/storm surge simulations were vigorously validated with observed wave and water level data. For validation of storm surge simulation, the defined SRFs were applied to quantify storm surge levels at several stations in Matagorda Bay and Galveston, and the prediction is compared to High Water Marks (HWM) and water level gauge data recorded during hurricanes Carla (1961)

and Ike (2008), respectively. For validation of wave simulation, modeled significant wave height at several locations were compared to wave buoy data recorded during Hurricane Ike.

The results of this research project will enable Texas Department of Transportation (TxDOT) to quickly implement the design methodology produced by a pooled-fund study of the American Association of State Highway and Transportation Officials (AASHTO) and the Federal Highway Administration (FHWA).

The wave parameters determined in this project can be used in computation of wave forces in the design of coastal bridges and retrofitting existing bridges vulnerable to storm related damages. The scope of this research project included the following,

- collect and evaluate available wave, wind and water level (including storm surge) data along Texas coast,
- perform wave and water level simulation for extreme events, and
- perform statistical analyses to determine the value of wave parameters for locations along Texas coast for different levels of hurricane intensity.

This report documents the research work performed, methods used, and results obtained in this project.

CHAPTER 2: STORM SURGE: BACKGROUND AND LITERATURE REVIEW

This chapter identifies and discusses sources related to storm surge damage and associated issues. Discussion of additional literature review findings can be found in subsequent chapters for sources that relate to specific topics.

DAMAGES TO COASTAL BRIDGES DUE TO STORM SURGES

A storm surge is a drastic surface sea level rise caused by extreme wind and barometric pressure deficit, among other factors induced by tropical or extratropical cyclones. In addition to the direct loss of lives due to flooding, a sudden rise in the surface water level during recent hurricane seasons brought serious damages to properties and infrastructure in coastal areas. In the United States, around 53 percent of the population lives near the coast, and since 1970 there have been 2000 homes per day erected in coastal areas ([UN Atlas of the Oceans, 2000](#)). Within the Atlantic Ocean or Gulf of Mexico alone, there are more than 25.6 million people in 290,000 km of coastal land area, and more than 96,560 km of roadways are in the 100-year coastal flood plain in the United States ([Douglass et al., 2005](#)).

Many hurricane reports evidenced that this intrusion of flood water was the cause of severe damages to coastal highways and bridges along the Gulf of Mexico. Hurricane Ivan (2004) ravaged the Escambia Bay Bridge and resulted in suspension of traffic and blockage of the supply route. When Hurricane Katrina (2005) attacked the vital coastal bridges along the gulf coast including the one on the US-90 in Mississippi ([Figure 1](#)), extensive repair at public expense was required. For example, \$803 million was awarded for the bridge deck lifting project for the I-10 Twin Span Bridge in Louisiana, and \$226.8 million was awarded for the bridge replacement project for the Bay St. Louis Bridge on U.S. 90 in Mississippi. In total, \$2.75 billion in supplemental appropriation was awarded by the Federal Highway Administration's "Emergency Relief Program" ([Collins, 2006](#)). Following Hurricane Ike in 2008, the state and interstate highways along the Galveston coast, including SH 87 from the Bolivar Ferry Landing to SH 124 and IH 45-Gulf Freeway were closed due to damage and debris on the road. Their damages resulted in a \$20 million effort for repair ([Public Information Office of Texas Department of Transportation, 2008](#)).

[Padgett et al. \(2008\)](#) analyzed bridge damage mechanisms based on observations of 44 damaged bridges in Alabama, Louisiana, and Mississippi during Hurricane Katrina. According to their study, major bridge damages during hurricane events are attributed to the increased uplifting loads and impacts from debris and objects near the bridge, induced by the storm surges, and partially by high winds, scour, and malfunction of electrical and mechanical equipment due to water inundation. The overall analysis showed that the bridges with spans of the same or lower elevation than peak surge levels had experienced severe structural failure during hurricane events. For studies mainly focused on water surface response to hurricane forcing, the wave setup is estimated at about 15 percent of the total flood level ([Irish and Cañizares, 2009](#)). Therefore, in order to examine the stability of the coastal bridges in response to the storm surges, the value of 15 percent higher than the peak surge levels should be an adequate approximation for this study.

GOVERNING EQUATION FOR STORM SURGE

Storm surge levels are determined by both the hurricane meteorological conditions and the geometric characteristics of the coastal regions. The early surge prediction was highly dependent on the historical surge observations ([Resio and Westerink, 2008](#)). However, the lengths of most surge data were too short and regional extent where the data were recorded was not wide enough to adequately characterize regional geometric factors. Reliance on such limited historical data alone resulted in inaccurate characterization of surge responses to the extreme storms. Consequently, in an attempt to make more accurate surge predictions that overcome the existing data limit, researchers' efforts for surge predictions focused on developing physics-based hurricane models.

A storm surge is a sea level rise caused by wind stress and low pressure, among other factors, and can be described by three-dimensional equations of mass and momentum. However, we can limit our interest to shallow-water hydrodynamic circulation in the regions where the horizontal scale of fluid motion is much larger than the water depth. That is, assuming horizontal fluid dynamics are more dominant compared to relatively static vertical motion of the flow in the shallow-water body, and the water density is constant over the depth, the three-dimensional equation of motion and momentum can be vertically integrated to become the two-dimensional shallow-water equations ([Lynch and Gray, 1979](#)). Therefore, the conservation of mass becomes

$$\frac{\partial H}{\partial t} + \nabla_h (H\bar{u}) = 0 \quad (2.1)$$

The conservation of momentum becomes

$$\frac{\partial \bar{u}}{\partial t} + (\bar{u} \cdot \nabla_h) \bar{u} + g \nabla_h \zeta + f \hat{k} \times \bar{u} + \tau_b \bar{u} = \psi \quad (2.2)$$

where

H is total fluid depth,

u is a vertically averaged horizontal velocity,

ζ is the elevation above the mean sea level,

f is the Coriolis parameter,

τ_b is a bottom stress parameter,

∇_h is the horizontal gradient operator, and

\hat{k} is the vertical unit vector,

ψ is a forcing term.

Under hurricane forcing, ψ can be represented by the combined effect of atmospheric pressure variations ($\Delta P = P_f - P_c$) between the surface pressure at periphery (P_f) and lowest surface pressure (P_c) of the storm, surface wind stress (τ_s), and other forces (e.g., wave radiation stress and tides). The wind stress is empirically defined (Dean and Dalrymple, 1984) as a function of air density (ρ_a), a surface friction coefficient (C_f), and wind speed (U) as

$$\tau_s = \rho_a C_f U^2 \quad (2.3)$$

A setup of surface water in the deep ocean is dominated by pressure deficit due to the low atmospheric pressure at the center of a storm. Storm surge induced by the pressure deficit can be evaluated (Dean and Dalrymple, 1984) by

$$\zeta_B = \frac{\Delta P}{\gamma} \quad (2.4)$$

where

ζ_B is a setup of the surface water due to the barometric pressure deficit ΔP , and γ is the specific weight of the water.

On the other hand, storm surge generation at the coast involves more complex interactions between coastal geometry, bathymetry, and wind and pressure forcing. A linearized, steady-state storm surge on the coast can be simplified as (Resio and Westerink, 2008)

$$\zeta_c = \left(\frac{\tau}{gh} \right) W \quad (2.5)$$

where

ζ_c is storm surge at the coast,
 τ is hurricane induced wind and barometric stress,
 h is the depth of water,
 W is the continental shelf width, and
 g is the gravitational acceleration.

The close relationship between coastal surges and the geometric factors, termed as the water depth (h) and shelf width (W), implies that capturing the site-dependent characteristics makes significant impact on the accuracy of surge prediction.

Besides the two components previously mentioned, other mechanisms involved in storm surge generation are momentum transfer due to wave breaking, Coriolis acceleration, astronomical tide forcing, and the bottom friction after balanced with the surface wind stress.

NUMERICAL STUDIES OF STORM SURGE SIMULATIONS

Considering the heavy reliance of this study on numerical storm simulation results, it is critical to utilize an adequate numerical model that provides sufficient accuracy in prediction. The performance of numerical models to solve shallow-water surge problems is documented through many years of careful studies (Lynch, 1983; Westerink and Gray, 1991). Surge analysis based on numerical simulations was carefully conducted by Westerink et al. (1992 and 1994). They investigated the effect of domain size on the accuracy of prediction. They concluded that using the largest East Coast domain encompassing the Western North Atlantic Ocean, the

Caribbean Sea, and the Gulf of Mexico, and specifying open boundaries in deep ocean gave the most accurate surge predictions. That was compared to those obtained from computation on smaller grid domains including only the Gulf of Mexico, or the continental shelf near Florida coast.

As mentioned earlier, storm surge at a coast results from the interaction between meteorological wind forcing and geometric factors. On the other hand, storm surge in deep water is mainly induced by the pressure deficit and hardly affected by the surface wind stress or the offshore landscape. Therefore, storm surges at the open boundary in deep water are readily estimated by Eqn. (2.4). Furthermore, storm surges initiated from the surge rise on the deep ocean boundary and forced to propagate toward coastal regions in more natural fashion could avoid the erroneous excitement in coastal water level as well as reduce error potential due to complicated specification across the continental boundary (Westerink et al., 1991).

Westerink et al. (1991, 1992) examined improvement in the accuracy with respect to the grid refinement for coastal surge prediction. They concluded that, to obtain the relevant accuracy in surge level computation, a high degree of grid refinement is required to resolve complex geometry and rapidly varying bathymetry in shallow-water regions, while a much lower grid resolution was found to be sufficient for deep water. For efficient use of computational resources, they further developed a mesh grid with varying resolution that has coarse refinement in deep waters and gets finer toward coastal regions. It was proved that surge response obtained by using the varying-resolution grid could be identical to that obtained by using the uniformly fine grid.

To obtain flexibility in nodal densities of a mesh grid, the shallow-water equations are solved by the finite element (FE) method with various algorithms (Navon, 1988; Gray, 1982). With the development of the wave-continuity equation (WCE) (Lynch and Gray, 1979) that implements the primitive mass continuity and momentum conservation, spurious node-to-node oscillation commonly found in early FE numerical models was suppressed without artificial damping. Using the operator notation, a WCE (W) is presented (Lynch and Gray, 1979; Aldama et al., 2000; Kolar and Westerink, 2000) as

$$W \equiv \frac{\partial L}{\partial t} + \tau L - \nabla \cdot M^c = 0 \quad (2.6)$$

where

L represents the primitive form of mass continuity,

M^c represents the primitive form of momentum conservation, and

τ is the bottom friction factor.

The work by [Kinmark et al. \(1985\)](#) on refining the previous WCE resulted in the generalized wave-continuity equation (GWCE). By replacing the bottom friction factor (τ) with the weight factor (G) associated with the primitive continuity equation (L), the GWCE (W^G) is formulated as ([Luettich et al., 1991](#); [Kolar and Westerink, 2000](#))

$$W^G \equiv \frac{\partial L}{\partial t} + GL - \nabla \cdot M^c = 0 \quad (2.7)$$

Here, the G parameter has no physical meaning but is introduced as a means for describing a wide class of equations, including the wave continuity equation itself, for numerical solutions. By choosing as large value of G as possible that satisfies $G > \tau$ so [Eqn. \(2.7\)](#) has a nontrivial solution, yet the GWCE remains equivalent to the primitive WCE, the spurious oscillation problem can be avoided without artificial damping. Furthermore, by virtue of the flexibility in the value of G , the GWCE can be explicitly solved using time-independent mass matrices for elevation solutions.

The objective of the literature review in this section is to provide an overview of surge model development, to help one understand the principle and physics behind storm surge, and to build a fundamental idea of the advantages gained from the advance in modeling schemes. Therefore, lengthy description on the numerical schemes or details that require in-depth understanding about the numerical analysis method is not included here.

REVIEW OF EXTREME-VALUE STATISTICS FOR STORM SURGE

Since the 1960s, a number of efforts have been made to characterize hurricane hazards in terms of surge and frequency. Early methods depended on historical hurricane data recorded in small spatial scale over a short period. Early hurricane records did not cover more intense storms that have occurred since 1960s. Therefore, reliance on such a paucity of weak data resulted in a high degree of uncertainties in the extreme-value analysis from various factors. For example, in the design storm approach developed as a part of the standard project hurricane (SPH) work

(U.S. Department of Commerce, 1959, 1972, and 1979), a hurricane's behavior was characterized by only one parameter, typically storm intensity, and disregarded the variability of other factors. Surge levels were analyzed based on a single storm, and the design was based on environmental conditions seen in the limited historical data. Such an approach ignores possible changes in hurricane conditions in the future.

Since the period of high hurricane activity in the 1960s, many researchers put effort into developing parametric (Gumbel, 1959) or non-parametric or empirical (Borgman et al., 1992; Scheffner et al., 1996) representations of historical storm surge data, as a means for extreme surge analysis. However, such reliance on the limited historical data infers the statistics had some potential problems. First, the historical population cannot capture the changes in frequencies and intensities of storms on decadal scales. Second, this approach does not account for the spatial extent over which the hurricane surge acts.

Ho and Myers (1975) developed a statistical approach that utilizes the joint probability function to describe storm surge probability on certain condition. This method, termed as joint probability method (JPM), first specifies various hurricane parameters (x_1, x_2, \dots, x_n) , such as the storm size, intensity, speed, and so forth. With the specified parameters, the cumulative distribution function (CFD) for a hurricane with the specified condition x_1, x_2, \dots, x_n will generate surge level in excess of a certain surge value, η , is evaluated as

$$F(\eta) = \int \dots \int p(x_1, x_2, \dots, x_n) \delta[\Psi(x_1, x_2, \dots, x_n) - \eta] dx_1 dx_2 \dots dx_n \quad (2.8)$$

where

η is the threshold of the highest surge at a given location,

$p(x_1, x_2, \dots, x_n)$ is a joint probability for an event caused by the combination of variables x_1, x_2, \dots, x_n ,

$\delta[\dots]$ is the Dirac delta function,

$\Psi(x_1, x_2, \dots, x_n)$ is a numerical model for surge estimation based on the variables (x_1, x_2, \dots, x_n) , and n is the total number of hurricane parameters.

In its original form, the JPM does not acknowledge that the numerical model computation may not be 100 percent accurate and/or that the joint probabilities estimated from a small sample size may not exactly represent the parent group. Furthermore, assuming the structure of storms changes very slowly during its approach to the coast, this approach regards the hurricane

condition off the coast as the same as that at landfall, which recent data show is not true (Resio et al., 2009). Moreover, the JPM approach produces storm surge information based on the joint probabilities among a large variety of hurricane variables. Therefore, for accumulating sufficient surge data, the JMP approach requires heavy computational work.

Resio et al. (2009) suggested that improved statistical surge analysis should have a means to justify the errors. These errors may be produced by unrealistic assumptions applied in the hurricane modeling and computation, uncertainties in characterizing the joint probabilities from limited data, uncertainties in unknown events in the future, and uncertainties in possible changes in present conditions. Furthermore, careful consideration on the effect of hurricane evolution is required as hurricanes approach the coast, and to the variability in the structure of the hurricane wind field.

CHAPTER 3: COLLECTION OF HISTORICAL WIND WAVE AND WATER LEVEL DATA

In order to perform wave and storm surge simulation, we needed to collect wind field data to provide input to numerical models SWAN and ADCIRC. We also needed to collect measured wave and water level data to validate the numerical models by comparing model results and measurements at the same location.

HISTORICAL WIND DATA

We collected wind field data, which includes wind speed and direction, for the region from 98°W to 70°W, 15°N to 35° N, which encloses the entire Gulf of Mexico. The data were downloaded from the National Oceanic and Atmospheric Administration (NOAA) website (<ftp://polar.ncep.noaa.gov/pub/history/waves/>). The wind data were stored in “GRIB” (GRIdded Binary) format , which is a mathematically concise data format commonly used in meteorology to store historical and forecast weather data.

We downloaded the wind data set “WNA” which represents data from the West North Atlantic Ocean. We then extracted wind data from downloaded wind data files and rewrote it in ASCII format, which can be read with any text editor. We consolidated wind data into one single file for each year and created animation files that enabled us to identify significant storm events easily. Wind data from July 1999 to November 2007 were available. During that period, 18 storms made landfall in Texas. We examined the wind fields of these storms and selected the wind field of Hurricane Rita for wave simulation. [Figure 5](#) is a snapshot of the animation file we created, which represents the wind field of Hurricane Rita that made landfall between Sabine Pass, Texas, and Johnsons Bayou, Louisiana, on September 23, 2005. After Hurricane Ike made landfall in Galveston, we collected wind field data of Hurricane Ike and scaled it to different levels corresponding to different hurricane category in wave simulations.

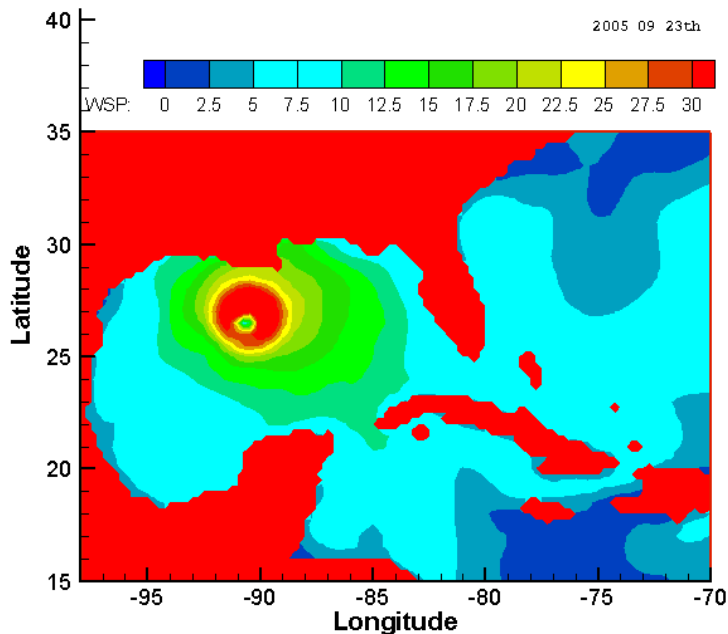


Figure 5. Wind Speed in Gulf of Mexico during Hurricane Rita (2005) (Unit: m/s).

HISTORICAL WAVE DATA

We collected wave data from the National Data Buoy Center. NDBC is a NOAA program with moored buoys and onshore/nearshore platforms (C-MAN stations) for oceanographic and meteorological observations. The real-time data are incorporated into the Texas Automated Buoy System (TABS), which is operated for the Texas General Land Office by the Geochemical and Environmental Research Group at Texas A&M University. It consists of ten TABS buoys, four NDBC buoys, and two C-MAN stations. All of the data are archived, and data subsets can be retrieved online. Available data include spectral wave density, spectral wave direction, directional wave spectrum, water level, average wave period, dominant wave period, and wave direction.

There are 11 data buoys in the Gulf of Mexico, three of them are near the Texas coast (#42019, 42030 and 42035). Measured wave data were collected and used in the validation of wave model SWAN ([Chapter 6](#)).

HISTORICAL WATER LEVEL DATA

We collected historical water level data from the National Water Level Observation Network (NWLON). NWLON is a network of tide gauge and water level stations managed by

the NOAA National Ocean Service (NOS) Centers for Operational Oceanographic Products and Services (CO-OPS). Both U.S. coastal (including the Great Lakes) and international real-time data are available. While the focus is on water level data, ancillary data are collected at many of the stations. Texas has approximately 12 data collection stations. Available data include water level and wind speed/direction.

NWLON has 175 continuously operating water level stations, 31 of them in Texas. Water level data during Hurricane Ike were collected from three stations in the Galveston area: Rollover Pass, Galveston Pier 21, and Galveston Pleasure Pier ([Figure 6](#)). The data were used to update water levels during wave simulation ([Chapter 6](#)) and also to validate the model results of ADCIRC.

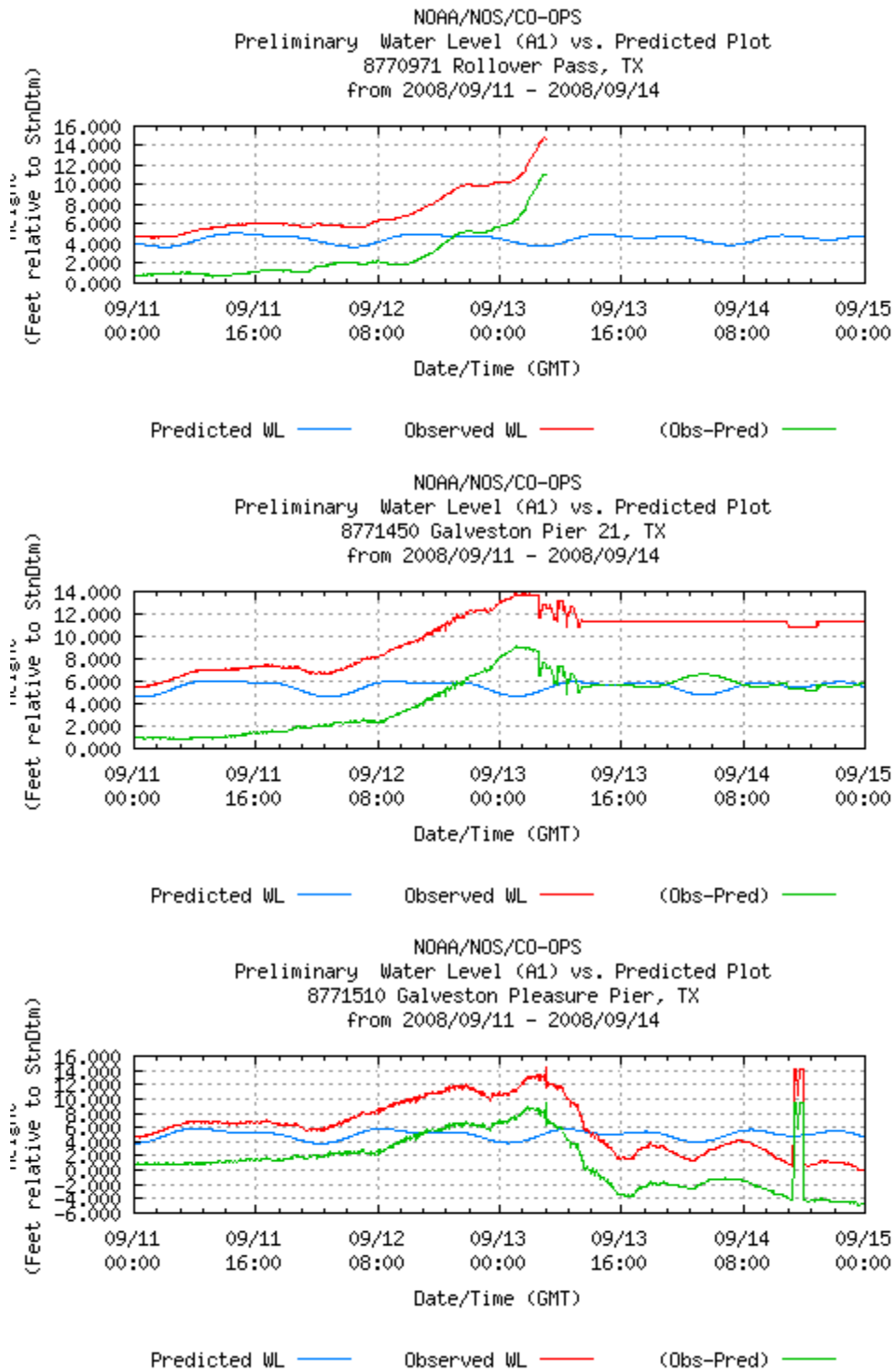


Figure 6. Recorded Water Level in Galveston during Hurricane Ike (Source: NWLON).

CHAPTER 4: STORM SURGE STUDY AREA AND CONDITIONS

Researchers examined satellite images of the Texas coast to determine an appropriate study area where high inundation was suspected. After consideration of bridge locations with respect to the regional geography, and their importance to the nearby neighborhood, 20 bridges along the Texas coast were selected for examination for their vulnerability to hurricane flooding (Figure 7). The geographical features near a subset of these bridges are shown in Figure 8 through Figure 15.

As shown through the figures, most of the bridges located on the open coast are exposed to a direct strike from incident surges and waves developed in the Gulf of Mexico and on the continental shelf, while some in the adjacent basins are subject to inundation due to flood invasion through tidal inlets or over barrier islands. Locations of the bridges are summarized in Table 1, along with the numbers of corresponding output stations specified for the hurricane simulations.

In the middle of the project period, Hurricane Ike (September 2008) emerged into the Gulf of Mexico and made landfall near Galveston. Due to this hurricane, several coastal bridges near Galveston Bay were damaged. Our target bridges include two of these severely damaged bridges (Figure 2): Rollover Pass bridge (Figure 9, and on the top of Figure 2) located in Bolivar Peninsula, and Pelican Island bridge (Figure 10, and on the bottom of Figure 2) located in Galveston. These damaged bridges cut off the public transportation system, delayed restoration after the disaster (Jones, 2009), and cost about \$7 million to repair (Rapple, 2008).

The estimation of storm surge levels near these selected bridges can be made through numerical simulations and SRF. Surge development is determined by hurricane meteorology and geographic properties of the region, such as bay geometry, variation in bathymetry, and shoreline shape. Since our target bridges occur over a wide range of the Texas coast, an enormous number of storm surge simulations would be required to assess flooding probability with a traditional JPM approach. However, by adopting the SRF approach introduced by Resio et al. (2009), the number of simulations required for characterizing the site-dependent surge response behavior may be dramatically reduced.



Figure 7. Locations of 20 Target Bridges along Texas Coast (Red Dots).
(Google Satellite Images, 2009a)



Figure 8. Bridges (Red Dots) near the Eastern Boundary of the Texas Coast.
Jetty Road (right) and Martin Luther King Jr. Drive (Hwy 82, left) are located near the eastern boundary of Texas (Google Satellite Image, 2009b).



Figure 9. A Bridge (Red Dot) at Rollover Pass in Galveston.
(Google Satellite Image, 2009c)

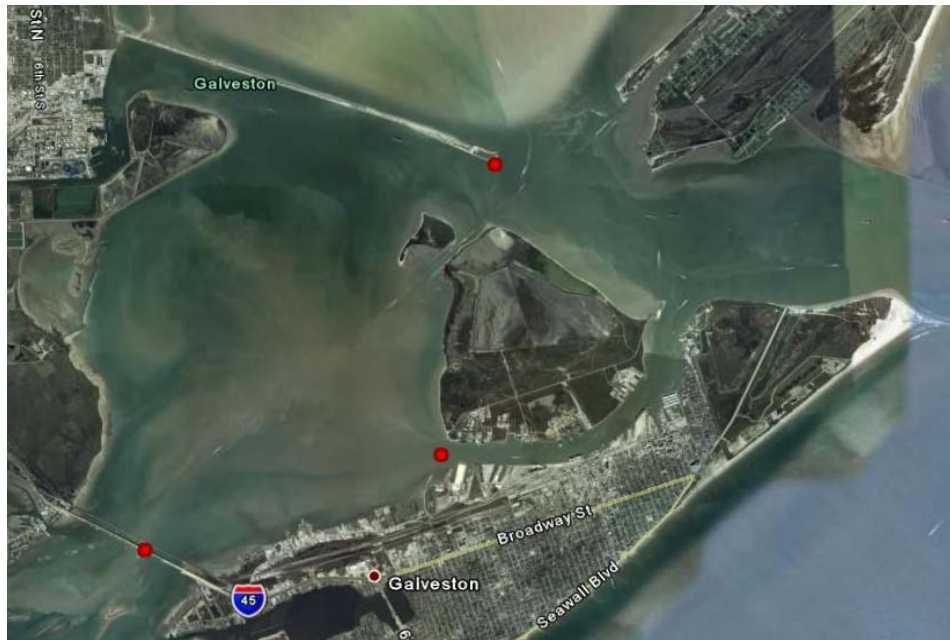


Figure 10. Bridges (Red Dots) near the Entrance of Galveston Bay.
Bridges are located on the Texas City Dike Road (top dot), Pelican Island bridge (middle dot), Galveston Causeway (bottom dot) near the entrance of the Galveston Bay (Google Satellite Image, 2009d).



Figure 11. Bridges (Red Dots) of FM 2004 Road (Top Dot), and San Luis Pass (Bottom Dot) in Galveston.
(Google Satellite Image, 2009e)

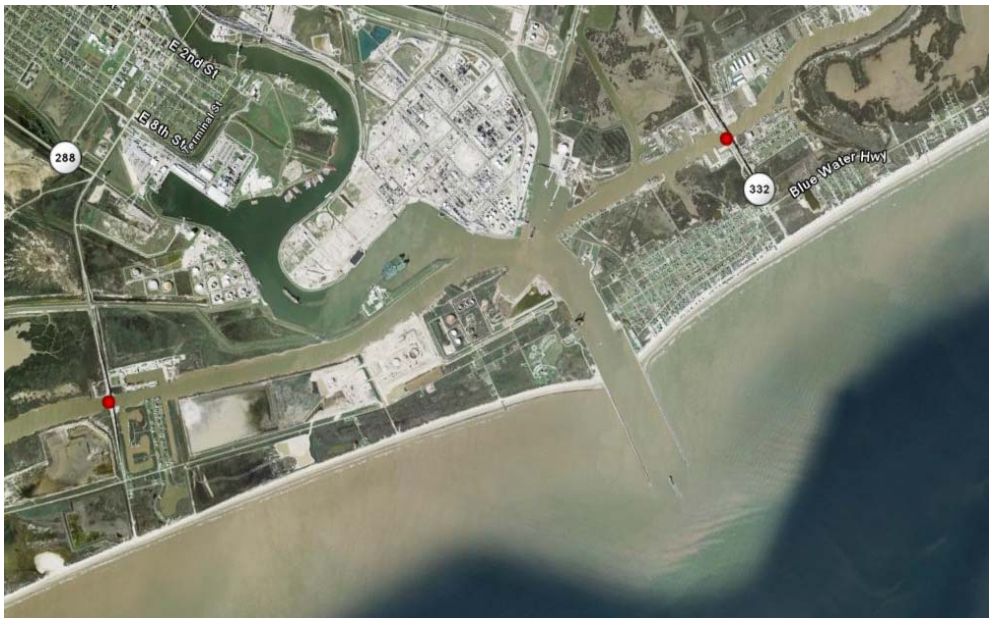


Figure 12. Bridges (Red Dots) on FM1495 Road (Left Dot) and Hwy 332 (Right Dot) near Freeport.
(Google Satellite Image, 2009f)

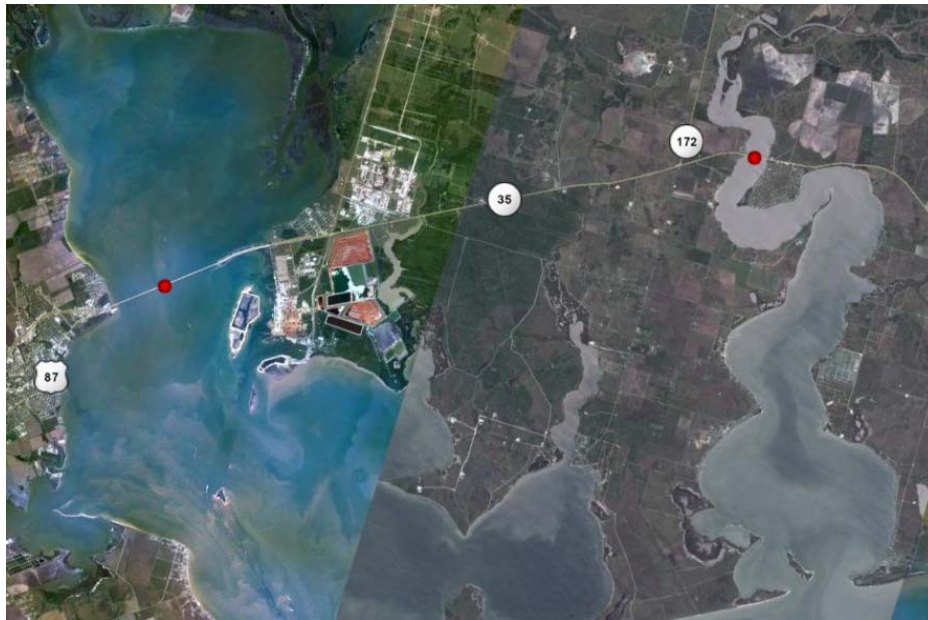


Figure 13. Bridges (Red Dots) along Highway 35 in Matagorda Bay.
(Google Satellite Image, 2009g)

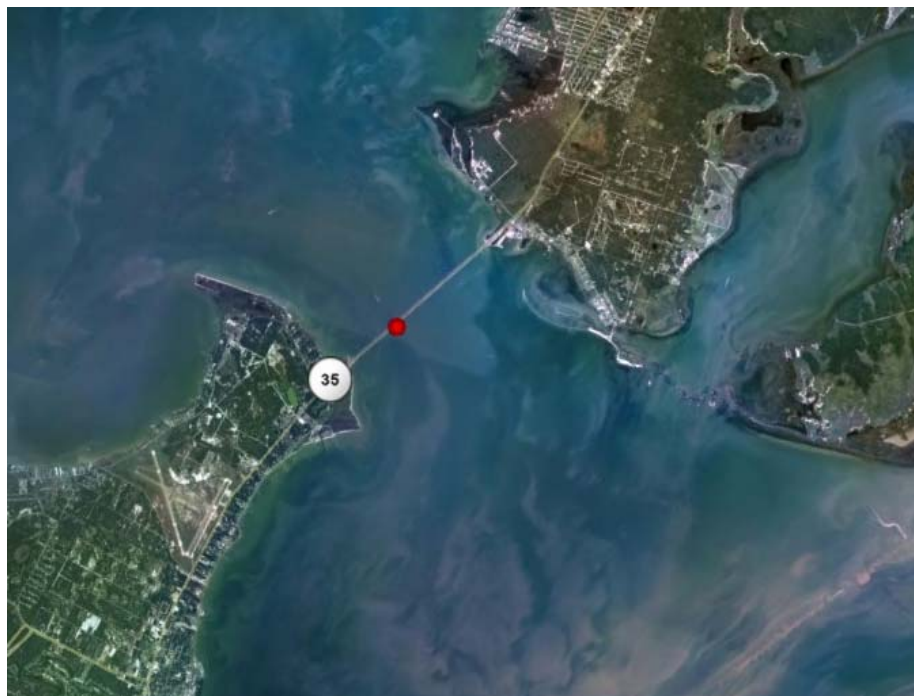


Figure 14. Bridge (Red Dot) on Lyndon B. Johnson Causeway in Aransas.
(Google Satellite Image, 2009h)



Figure 15. Bridges (Red Dots) in Corpus Christi.
One bridge on State hwy Park Road 53, two bridges on State Hwy Park Road 22, one on the Padre Island Drive, one bridge over the industrial canal, and two bridges on Cemetery Road, Nueces Bay Causeway (Google Satellite Image, 2009i).

Table 1. Locations of the Selected Coastal Bridges.

Bridge No.	Stn. No.	Description	Lon.	Lat.	Location
1	45	State Hwy Park Road 22_No.1	-97.214	27.619	Corpus Christi
2	47	State Hwy Park Road 22_No.2	-97.240	27.635	
3	48	Kennedy Causeway	-97.261	27.658	
4	51	Padre Island Bridge	-97.312	27.680	
5	53	Nueces Bay Causeway 1	-97.395	27.813	
6	55	Nueces Bay Causeway 2	-97.370	27.844	
7	59	Cemetery Road	-97.104	27.884	
8	65	Johnson Causeway	-97.020	28.120	
9	84	Port Lavaca	-96.598	28.650	Matagorda
10	88	Weedhaven	-96.432	28.732	
11	116	FM1495 Road	-95.341	28.922	Galveston
12	117	Hwy 332	-95.293	28.956	
13	127	San Luis Pass	-95.122	29.082	
14	130	FM 2004 Road	-95.207	29.213	
15	141	Galveston Causeway	-94.885	29.295	
16	142	Pelican Island Bridge	-94.824	29.311	
17	147	Texas City Dike Road	-94.810	29.363	
18	157	Rollover Pass	-94.500	29.508	
19	181	Martin Luther King Jr. Drive (Hwy 82)	-93.895	29.766	
20	182	Jetty Road	-93.853	29.696	

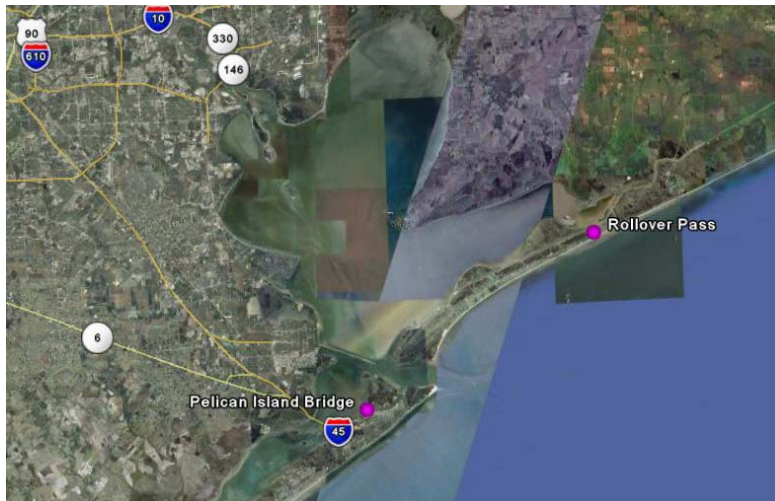


Figure 16. Location (Maroon Dots) of Two Damaged Bridges in Galveston during Hurricane Ike.
(Google Satellite Image, 2009j)

CHAPTER 5: SURGE RESPONSE FUNCTION APPROACH

In order to measure the uplift force and impact of debris on the selected coastal bridges during hurricanes, prediction of flood level derived hurricane meteorology is required. There is only scarce historical hurricane data available at these bridges, and it is difficult to estimate the storm surge probability from the historical record alone. Therefore, storm surge data at each bridge location had to be accumulated through numerical simulations. In an effort to avoid a heavy computational burden imposed by the great amount of hurricane simulations typically required to quantify surges over a wide range of storm conditions along the entire Texas coast, optimal sampling from a synthetic hurricane wind field database was carried out.

Following the modified JPM approach suggested by [Resio et al. \(2009\)](#), researchers selected hurricane parameters that have the most dominant effects on the storm surge response. Subsets for storm surge simulations were determined based on careful combination of the selected parameters. The storm surge model for evaluating extreme surge levels near the 20 selected target bridges was developed. Finally, the simulated surge data were analyzed to develop parameterized surge response functions in order to evaluate surges on wide range of hurricane meteorological conditions near the target bridges.

To develop the improved methodology for surge hazard analysis, [Resio et al. \(2009\)](#) introduced a modified joint probability method implementing the SRFs. In this method, the number of variables used for joint probability in Eqn. (3.8) is limited to only those hurricane parameters that have the most dominant effects on surge response, based on physical reasoning. This process is called optimal sampling, and the original JPM is now revised to become the Joint Probability Method with Optimal Sampling (JPM-OS). The JPM-OS specifies the error term, ε , to incorporate the storm surges with uncertainties from various sources. That is, the effect of variation in surges due to other factors than those classified as dominant factors is regarded as negligible and grouped into the error term.

The strength of the surge response approach is that it characterizes the storm surge response of surface water by physical correlations between surges and the meteorological hurricane parameters. As discussed earlier, a large portion of storm surge is generated by hurricane wind stress and pressure deficit forcing. Consequently, it would physically make sense

that the dominant parameters in JPM should correspond to those parameters utilized to describe the wind field. The hurricane wind field can be parameterized with respect to the location of eye, storm size, intensity, forward speed and angle, and pressure profile peakedness. Therefore, the modified joint probability distribution with reduced dimensions, where the error term is separated from the probability distribution, is integrated into the CDF

$$F(\eta) = \int \dots \int p(c_p, R_p, v_f, \theta_l, x_o, B) p(\varepsilon | \eta) H[\eta - \Psi(\vec{X}) + \varepsilon] dx_1 dx_2 \dots dx_n d\varepsilon \quad (5.1)$$

$$\Psi(\vec{X}) = \Psi(c_p, R_p, v_f, \theta_l, x_{eye}, B) \quad (5.2)$$

where

R_p is the storm pressure radius,

c_p is the storm central pressure,

B is the pressure field structure peakedness (Holland B, 1980),

x_{eye} is the location of storm eye,

v_f is the storm forward speed,

θ_l is the storm approach angle, and

$\Psi(\vec{X})$ is a numerical model or system.

Here the error term ε also provides a means to include other effects on the water levels, such as tides and waves.

The storm surge probability expressed as Eqn. (5.2) is even more reduced by using mean value of the profile shape factor, Holland B (\bar{B} , 1980). By considering the Holland B as constant (Resio et al., 2009), the dimensions of storm surge joint probability can be reduced to

$$p(\vec{X}) = p(c_p, R_p, v_f, \theta_l, x_{eye}) \quad (5.3)$$

Finally, the continuous hurricane probability is obtained as

$$F(\eta) = \int \dots \int p(c_p, R_p, v_f, \theta_l, x_{eye}) p(\varepsilon | \eta) H[\eta - \Psi(\vec{X}) + \varepsilon] dx_1 dx_2 \dots dx_n d\varepsilon \quad (5.4)$$

Eqn. (5.4) shows that hurricane distribution of surge level η can be represented by a continuous function of primary hurricane parameters. If we make our focus on the maximum

surge level η_{\max} at an arbitrary location (x, y) against random sets of hurricane condition, the Eqn. (5.4) may be re-written as

$$\eta_{\max} = \phi(c_p, R_p, v_f, \theta_l, x_{eye}) \quad (5.5)$$

where ϕ represents the surge response function characterizing the correlations between surges and the dominant hurricane parameters.

SURGE RESPONSE FUNCTION METHODOLOGY

Resio et al. (2009) performed intensive numerical studies to examine the sensitivity of storm surge level to the dominant hurricane parameters. They concluded that the surge behavior was mainly affected by hurricane intensity ($\Delta P = P_f - c_p$), where P_f is a far-field pressure, and storm size (R_p). On the other hand, surge variations with respect to storm approach angle (θ_l) or speed (v_f) are seen to be somewhat less important (Irish et al., 2009). That is, for two close locations, a fixed value of approach angle (θ_l) and speed (v_f) can be used as an initial evaluation of surge response. Therefore, at a spatial point $(x, y)_n$ where the storm approach angle with respect to shoreline orientation (θ_l) and speed (v_f) may be regarded as a fixed value of k and m , respectively, the maximum storm surge ζ can be described in terms of hurricane meteorology; $\Delta P, R_p, (x, y)$, and a location of eye at landfall (x_o, y_o) as (Irish et al., 2009)

$$\zeta(x, y) = \phi_{km} \left([x, y], \Delta p, R_p, [x_o, y_o] \right) \quad (5.6)$$

The SRF approach, required for efficient use of the JPM-OS, enables reliable estimation for the extreme surge flood levels based on a reasonably selected sample. In addition, it provides a means to account for errors due to uncertainties in assumptions and simplifications made during the surge development process. Eqn. (5.6) shows that, at a given location, the maximum storm surge surface (ζ) can be described by a continuous function of hurricane parameters and site-dependent geographic properties. Irish et al. (2009) developed dimensionless parameters based on physical scaling laws that relate the hurricane meteorology and location to the maximum surge levels. Products of the scaling process were interpolated to construct a SRF, demonstrating the continuous surge response behavior on various hurricane conditions with

respect to the alongshore extent. Furthermore, [Irish et al. \(2009\)](#) provided a standard for optimal sampling for surge response analysis in order to minimize the computational requirement for hurricane model simulation while maximizing the use of existing discrete sets of surge data.

The following sections present the physical scaling laws used to derive the dimensionless storm surge parameters. We will then discuss how this method is improved and applied for extreme surge prediction in the vicinity of the Texas coast.

Physical Scaling Laws for Surge Response Function

[Irish et al. \(2009\)](#) performed 75 numerical storm surge simulations along a stretch of the Texas coast near the Matagorda Bay. The investigation focused on storms propagating toward the coast of Matagorda Bay with an approach angle of less than 17° with respect to shore-normal along four parallel tracks spaced 30 km apart from each other (the circles mark sample output locations, [Figure 17](#)).

The 75 synthetic hurricanes varied in intensity (C_p) from 900 mb to 960 mb, and in size (R_p) from 11 km to 65 km. For each track, at least five different properties were specified for storm intensity in order to create the synthetic hurricane wind field, in combination with at least five storm size specifications. The changes in coastline and nearshore bathymetry within the study area are slow and smooth, and the four stations specified for surge output recording are close to each other. Forward speed and Holland B of each hurricane were specified as 5.7 m/s and between 1.27 and 1.00, respectively, which are typical values for hurricanes in Gulf of Mexico.

From the simulated surge results, [Irish et al. \(2009\)](#) identified a linear correlation between the storm size and the alongshore distance between the eye at landfall and the location of peak surge. The relationship was described by using a parameter λ as

$$x_{peak} - x_o \cong \lambda R_p \quad (5.7)$$

where

x_{peak} is the alongshore distance to the location of the peak surge,
 x_o is the alongshore distance to the location of eye at landfall, and
 R_p is the hurricane pressure radius.

Note that spatial extent was measured along the shoreline at the open coast, for purpose of evaluating storm surge responses with respect to the variation in relative distance from the eye of storm to the arbitrary point.

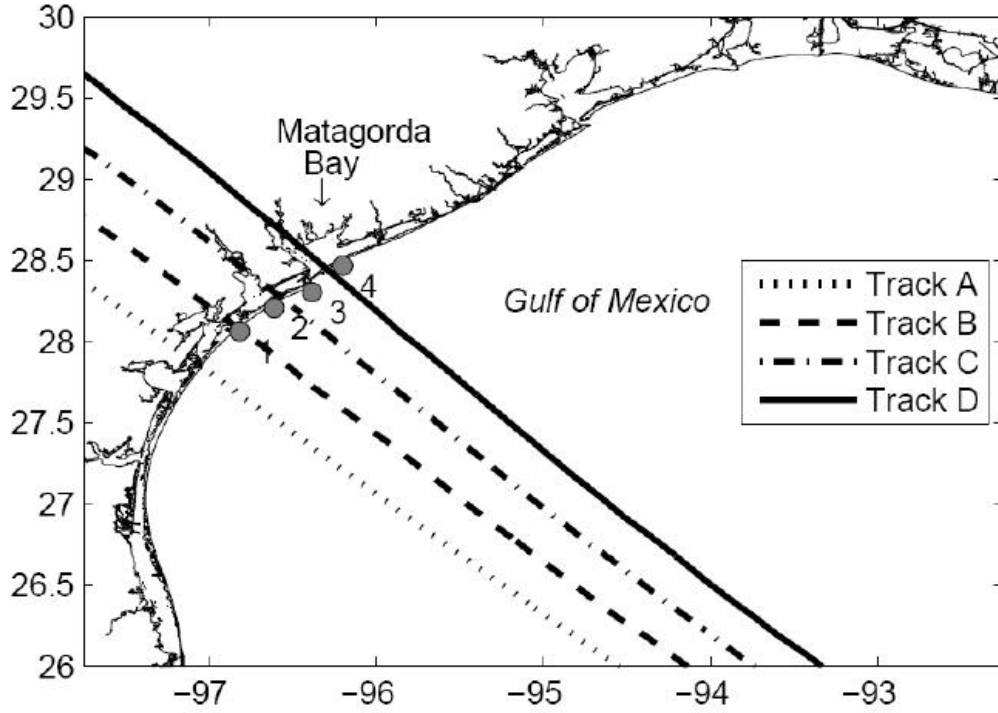


Figure 17. Hurricane Tracks and Stations for SRF Development (Irish et al., 2009).
The circles mark sample output locations.

For extreme-value statistics, our interest was in higher surge events. A dimensionless alongshore dimension (x') representing the distance from landfall of a hurricane to the point of interest (i.e., the location of a surge monitoring station) was defined as

$$x' = \frac{x - x_o}{R_p} - \lambda \quad (5.8)$$

We also defined a dimensionless surge parameter (ζ') by normalizing the simulated surge levels by hurricane intensity as

$$\zeta' = \frac{\gamma \zeta}{\Delta p} + m_x \Delta p \quad (5.9)$$

The first term in Eqn. (5.9) accounts for storm surge as a response to the momentum transfer due to the surface wind stress. The second term accounts for additional wind-drag effect. The coefficient m_x is a site-dependent coefficient and determined by linear regression.

Figure 18 shows plots of the two dimensionless parameters defined by Eqns. (5.8) and (5.9). Overall data distribution follows a single distribution function. However, there were a few prominent scatters near the peak of the distribution. In analyzing those storms, which did not follow the trend, it was determined that these storms were relatively small storms making landfall close to the point of interest. This class of relatively small storms was classified as storms with $R_p < R_{thres}$ and $-\lambda < x' < \lambda$, and the threshold size was estimated by inspection to be $R_{thres} = 25$ km, in the vicinity of Matagorda Bay.

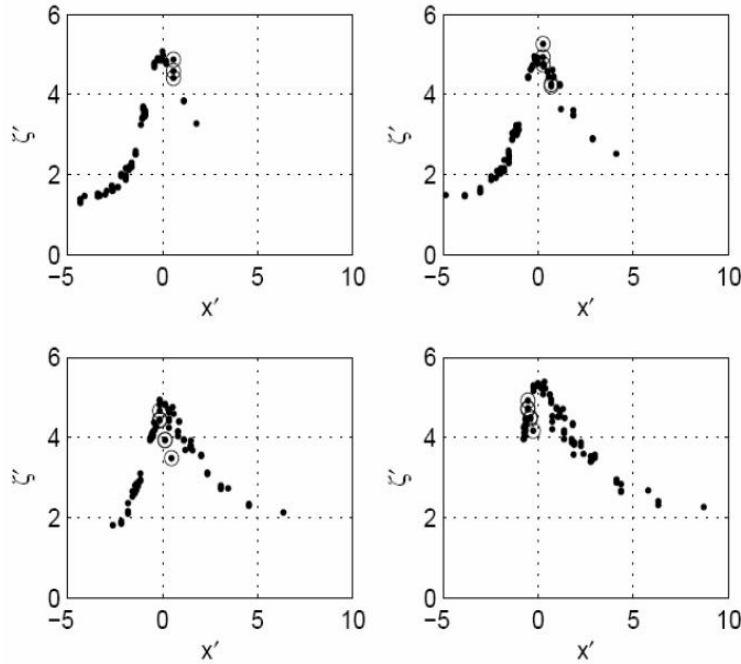


Figure 18. Preliminary Dimensionless SRFs (Irish et al., 2009).

SRFs were developed by using all simulated storms on all four tracks for Locations 1 (top left), 2 (top right), 3 (bottom left), and 4 (bottom right).

Circled storms are those with $R_p < 25$ km and $-\lambda < x' < \lambda$.

To collapse this class of storms into the single distribution function obtained before, the dimensionless alongshore parameter (x') was revised and redefined:

$$x'_2 = x' - F(1 - R')H(1 - R') \quad (5.10)$$

where R' is the dimensionless hurricane size defined as $R' = R_p/R_{thres}$, and $H(1-R')$ is the Heaviside function defined as

$$H(1 - R') = \begin{cases} 0 & (R' \geq 0) \\ 1 & (\text{otherwise}) \end{cases} \quad (5.11)$$

$F(1-R')$ is a ramp function defined as:

$$F(1 - R') = \begin{cases} a_1(1 - R') + b_1 & (\lambda \leq x' \leq 0) \\ a_2(1 - R') + b_2 & (0 \leq x' \leq \lambda) \\ 0 & (\lambda \leq |x'|) \end{cases} \quad (5.12)$$

The coefficients a_1 , a_2 , b_1 , and b_2 of the ramp function were evaluated by linear regression between the quantity $(1-R')$ and the difference between the value of x' and x_2' corresponding to ζ' from existing surge distributions. [Figure 19](#) shows the plots of revised dimensionless parameters. The figure shows that the data distribution follows a single trend after the secondary effects from small storms are considered.

The relationship between x_2' and ζ' were formulated through curve-fitting using a three-term Gaussian distribution function as

$$\Phi(x') = a_1 e^{-\left(\frac{x'-b_1}{c_1}\right)^2} + a_2 e^{-\left(\frac{x'-b_2}{c_2}\right)^2} + a_3 e^{-\left(\frac{x'-b_3}{c_3}\right)^2} \quad (5.13)$$

By applying the least square regression method, curve-fitting coefficients a_1 , b_1 , c_1 , a_2 , b_2 , c_2 , a_3 , b_3 , and c_3 were determined ([Figure 19](#)). [Irish et al. \(2009\)](#) reported R -squared values of curve-fits at the four stations are between 0.97 and 0.99. The comparison of the predicted surges from the SRF (ζ_ϕ) to the numerically simulated surges (ζ_{sim}) showed the root-mean-square (RMS) errors varied from 13 cm to 24 cm ([Figure 20](#)), and is on the order of the numerical simulation accuracy.

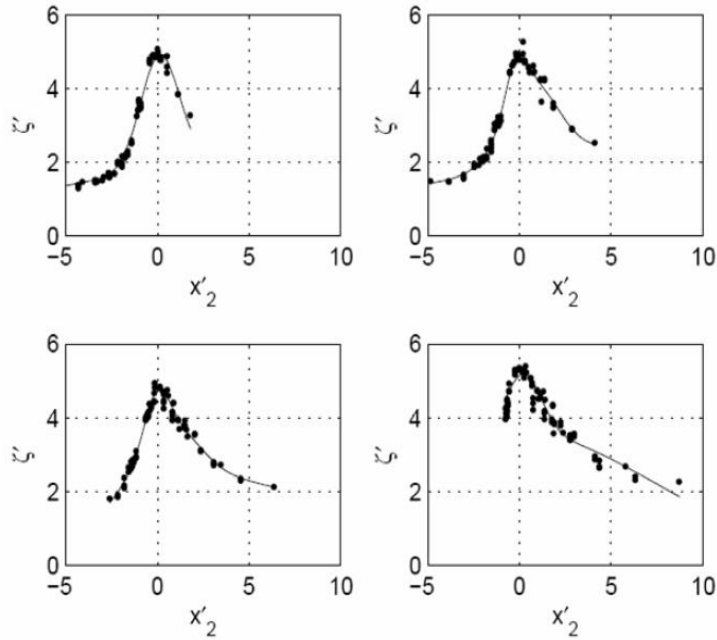


Figure 19. Dimensionless SRFs Using the Modified Dimensionless Alongshore Parameter (Irish et al., 2009).

SRFs were developed by using all simulated storms on all four tracks for Locations 1 (top left), 2 (top right), 3 (bottom left), and 4 (bottom right). Solid line shows 3-term Gaussian fit to data.

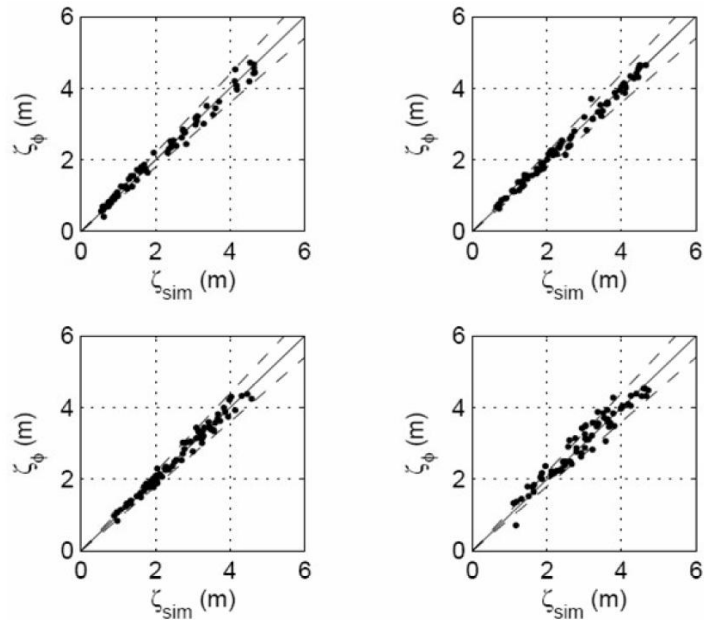


Figure 20. SRF Prediction versus Numerically Simulated Surges (Irish et al., 2009).

Predicted surge using curve-fitted SRF, based on all four tracks, versus numerically simulated surge at Locations 1 (top left), 2 (top right), 3 (bottom left), and 4 (bottom right). Solid line indicates an exact match while dashed lines indicate $\pm 10\%$ about an exact match.

Surge Response Function from Limited Data

[Irish et al. \(2009\)](#) further examined the use and accuracy of dimensionless SRFs from limited data sets. First, in order to examine the maximum track spacing for accurate SRF development, 75 hurricanes were sorted into three groups: hurricane tracks separated as:

Group 1 – 30 km (0.25°),

Group 2 – 60 km (0.50°), and

Group 3 – 90 km (0.75°).

The SRF developed from hurricanes in the third group was found to be as accurate as that generated from the first group, as long as data exist on both sides of $x'_2 = 0$, and in the vicinity of the peak in the SRF. Therefore, up to 90 km intervals between the storm tracks were found to be sufficient for defining the hurricane sample to be used for developing accurate SRFs. In addition, the authors showed that storm surges from only two discrete storm intensities, $C_p = 900$ mb and 960 mb, were sufficient to generate the SRF with the same order of accuracy compared to what was generated from all 75 numerical simulations. Analysis of those limited data sets proved that the use of the SRF approach can effectively reduce the numerical simulation requirement by at least 75 percent without sacrificing surge estimation accuracy.

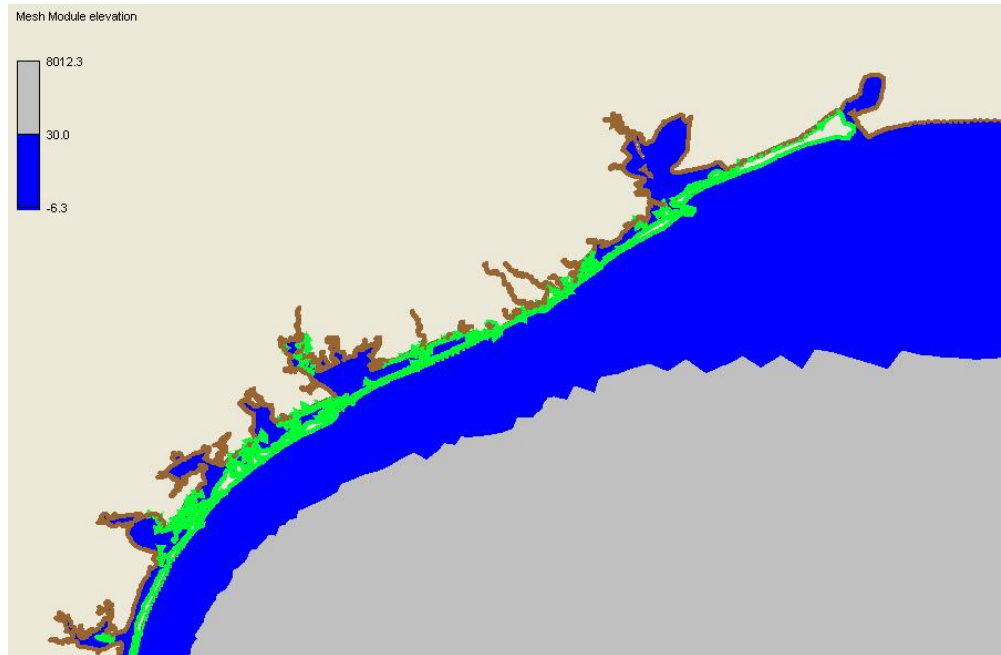
IMPROVEMENT FOR GENERAL USE OF SURGE RESPONSE FUNCTIONS

In their original work, [Irish et al. \(2009\)](#) focused on the open coast near Matagorda Bay. In this region, the relative impact of alongshore change in topographic (i.e., bottom slope) and geographic (i.e., shoreline orientation) conditions from location to location was insignificant. The assumption of slowly varying shoreline conditions was thus applied. Additionally, the storms for all storm surge simulations were forced with one forward speed and approach angle. Therefore the SRF work of [Irish et al. \(2009\)](#) excludes the effects of different forward speeds, approaching angles, and variation in regional bathymetry.

On the other hand, the coastal bridges selected in this study are widely distributed throughout the Texas coast. The spatial coverage for this study is thus expanded to include three main Texas bays: Galveston, Corpus Christi, and Matagorda. Consequently, some assumptions and simplifications applied to the previous work were reevaluated. In particular, application of SRFs to comprise a wider range of the Texas coast should take the effects of varying bottom slope, or continental shelf width into account. The storm surge level at the coast is affected by

bottom slope of the site as expressed in Eqn. (3.5). It was found that more than 75 percent of surge is generated as the hurricane moves over the continental shelf in depths shallower than 30 m (Irish and Resio, 2009). Figure 21 shows the Texas coast map displaying the coastline shape and the continental shelf expansion from the coast to the 30 m water depth contour. The contour is termed L30 hereafter. The figure clearly shows that L30 gets rapidly wider, while the change in shoreline orientation remains insignificant. As a result, the change in L30 in relation to surge generation is investigated in this study. We investigate the need to redefine the site-dependent coefficients and introduce a new parameter that accounts for the effect of changes in such geographical conditions.

In the derivation of dimensionless surge (ζ'), Irish et al. (2009) did not explicitly include the effect of storm size in the physical scaling law in Eqn. (5.9). However, a number of recent studies for hurricane impact analysis have proved that both the size and the intensity of storms play important role in surge generation (Irish et al., 2008; Powell and Reinhold, 2007; Resio and Westerink, 2008). Through analysis of both the historical records and numerical computation, it was further evidenced that a storm of moderate intensity with a large size could generate more devastating storm surges (Katrina in 2005, Ike in 2008) than a storm of stronger intensity but a smaller size (Irish et al., 2008). Recognizing the contribution of storm size to storm surge generation, the work to establish physical law relating size to storm surge level is in process. Meanwhile, in this study additional effects due to differences in the size of simulated storms were resolved through the additional wind drag effects (m_x) in the original dimensionless surge (ζ' , Irish et al., 2009).



The area shaded in blue represents the varying continental shelf width (L_{30}) along the Texas coastal line.

Figure 21. Texas Coastal Map of the Study Area.

CHAPTER 6: NUMERICAL SIMULATION STRATEGY

In order to develop sufficient wave and storm surge data to develop site-specific wave parameters, and define and refine SRFs at the selected coastal bridges, numerical simulations were conducted to compute wave and storm surge levels in the regions of interest. This section presents a detailed description on the numerical simulations. The following information describes the numerical wave model SWAN and storm surge model ADCIRC, and model setup, hurricane selection, and specification of elevation stations on the open coast.

NUMERICAL MODELS FOR WAVE AND STORM SURGE SIMULATION

Wave Model SWAN

Wave model SWAN is used in this project for wave simulation. SWAN is a third-generation wave model developed at the Technical University of Delft in the Netherlands (Booij et al., 1999; Ris et al., 1998; and Ris et al., 1999).

In SWAN the waves are described with the two-dimensional wave action density spectrum. The independent variables are the relative frequency σ (as observed in a frame of reference moving with current velocity) and the wave direction θ (the direction normal to the wave crest of each spectral component). The action density is equal to the energy density divided by the relative frequency: $N(\sigma, \theta) = E(\sigma, \theta)/\sigma$. In SWAN this spectrum may vary in time and space. The model is based on the following spectral action balance equation:

$$\frac{\partial}{\partial t} N + \frac{\partial}{\partial x} c_x N + \frac{\partial}{\partial y} c_y N + \frac{\partial}{\partial \sigma} c_\sigma N + \frac{\partial}{\partial \theta} c_\theta N = \frac{S}{\sigma} \quad (6.1)$$

where N is the action density (= spectral energy/ σ), θ is the wave direction, and c_x and c_y are components of the wave propagation velocity. The first term on the left-hand side of equation (6.1) represents the rate of change of action in time and the second and the third terms represent the propagation of action in the $(x; y)$ space. The fourth and fifth terms represent, respectively, the frequency shift and refraction induced by depth and currents. The source/sink term (S) on the right hand side of (6.1) represents the effects of generation, dissipation (due to breaking, bottom-friction, and whitecapping), and nonlinear wave-wave interactions. Reflection and diffraction

induced by structures are incorporated in an ad-hoc manner (Booij et al., 1997), because the governing equations are based on energy balance rather than mass-momentum balance. The governing equation is solved using finite differences for a spectral or parametric input specified along the boundaries (Booij et al., 1999; Ris, 1997).

SWAN can use either rectilinear or curvilinear computational grids with a uniform grid size in either case. The grid size in SWAN is independent of the water depth, although it should be small enough to resolve the changes in bathymetric, wind, and wave fields. The boundaries of SWAN computational grid are either land or water. The land boundary absorbs all incoming waves (reflection is not accounted for). Input wave conditions can be defined along the water boundaries if observations or results from another model run are available (e.g. Rogers et al., 2002). The model has been widely used and validated by several investigators including the navy (Rogers et al., 2002; Booij et al., 1999; Zubier et al., 2003).

Hydrodynamic Model ADCIRC

For accurate and detailed surge analysis, a storm surge model has to incorporate the key features discussed in this section, including

- a large-scale grid domain specifying the open boundary in deep water;
- a sufficient grid refinement on the coastal regions, including the adjacent basins; and
- the flexibility in node density.

In this study, storm surge elevation was simulated using the advanced hydrodynamic model, ADCIRC-2DDI (Luettich et al., 1991; Westerink et al., 1994). ADCIRC is a surface water circulation model coded using a finite element scheme in space and using a finite different method in time to solve the GWCE, discussed previously.

ADCIRC can be forced by specifying free surface elevations (due to tidal potential or barometric pressures deficit), normal flow, surface stress (due to hurricane wind or wave radiation), and landscape features such as barriers, bridge piers, etc. These boundary conditions can be specified on the nodes along the circumference and/or within the grid domain.

The ADCIRC model provides several options that improve its computational performance. These include the selection of operational mode, external mode (ADCIRC-2DDI), or internal mode (ADCIRC-3DL), as well as parallel (MPI-run) or serial processing. In internal mode, ADCIRC computes the vector form of surface water velocities by solving the three-

dimensional wave equations with the primitive conservation of momentum. In external mode, ADCIRC computes the scalar of surface water elevations by solving the depth-integrated, two-dimensional wave equations with the primitive conservation of mass. ADCIRC execution in external mode saves both central processing unit (CPU) time and data storage, requiring on the order of one-third that required for the three-dimensional computation. [Westerink et al. \(2008\)](#) showed that ADCIRC with this configuration performs well for surge simulations. Typical computation error for surge simulation is estimated at 20 to 30 cm (1 foot).

ADCIRC is capable of running on multiple processors in parallel by decomposing the mesh grid and related input files into multiple numbers of smaller pieces, assigning each piece of work to an independent CPU, and then reassembling the output from each CPU back together. In this way, it saves time taken to complete the total simulation as well as eases the computational burden laid on a single CPU.

ADCIRC is currently utilized to solve free surface circulation and sediment transport problems by various professional research groups in national institutions including the U.S. Army Corps of Engineers, Federal Emergency Management Agency (FEMA), National Laboratory for Civil Engineering (LNEC), National Oceanic and Atmospheric Administration (NOAA), and U.S. Naval Research Laboratory (NRL).

As a model domain, the east coast computation domain of [Westerink et al. \(2008\)](#) was used. This grid includes the Western North Atlantic Ocean, the Caribbean Sea, and the Gulf of Mexico ([Figure 22](#)). The east coast domain specifies open boundaries along the 60°W meridian, and the grid refinement widely varies from about 0.400° in the deep ocean to 0.005° nearshore and in inland bays ([Westerink et al., 1992 and 1994](#)). Especially, it highly resolves the regional bathymetry near the Texas coast and adjacent bays and waterways. Detailed grid information is listed in [Table 2](#).

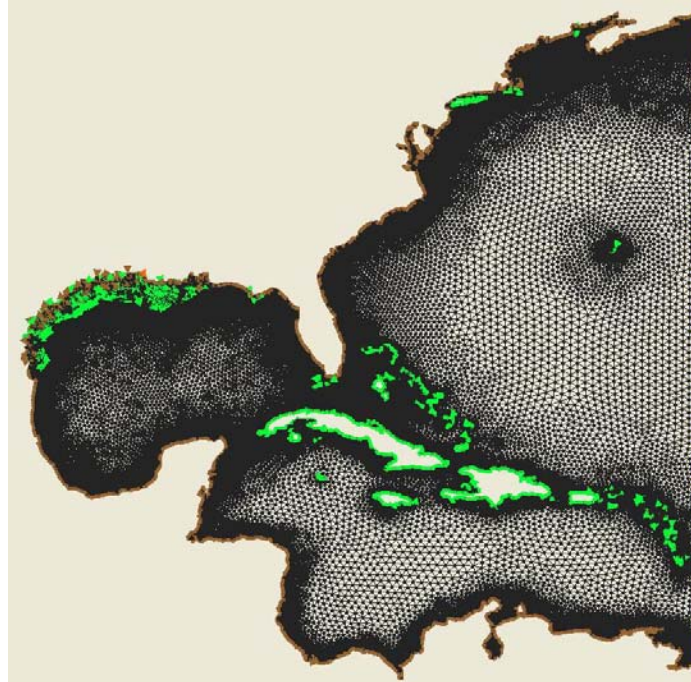


Figure 22. East Coast ADCIRC Domain Grid.

Table 2. East Coast Domain Triangular Mesh Information.

Area [km ²]	Maximum Bathymetry [m]	Minimum Bathymetry [m]	Number of Nodes	Number of Elements	Grid size (Approximation, degree)		Grid size (Approximation, meter)	
					Maximum	Minimum	Maximum	Minimum
8.3522×10 ⁶	7,858.09	(-)71.67	1,344,247.00	2,628,785.00	0.400	0.005	46,000	100

HURRICANE SURFACE WIND FIELD MODELING

Besides the capability of storm surge modeling, the accuracy of the surge prediction heavily depends on the accuracy of the specified hurricane forcing. For hurricane simulations, ADCIRC takes hurricane wind and boundary field files containing the information on surface wind and pressure at each time step as input for forcing. Several input wind field sources are available, including reanalyzed historical wind fields (i.e., HWINDS) (Powell and Reinhold, 2007). In this study, however, we emphasized parameterization of the surge response so a parametric wind field model is used.

For developing hurricane wind fields, the Planetary Boundary Layer (PBL) model of Thompson and Cardone (1996) is thus utilized. This PBL model is derived from the vertically

averaged, horizontal equation of motion with respect to a moving cartesian coordinate system with its origin at the center of the eye (Chow, 1971; Cardone et al., 1992). The vertically integrated momentum flux is related to the surface stress, and the wind and pressure fields are represented with respect to hurricane parameters including central pressure (c_p), storm size (R_p), storm forward speed (v_f), and peakedness (B) (Holland, 1980). During model development, it was assumed that the vortex flux within the PBL is horizontally homogeneous, steady state, and that the structure of a hurricane wind field changes slowly (over periods longer than one hour). Therefore, properties of those hurricane parameters are specified at one-hour intervals and, based on this information, the PBL model computes the wind velocities and pressure at the nested grid points at specified time steps.

For this study, in order to adequately resolve the temporal surge response as the hurricane moves over the continental shelf and the landmass, wind speed and pressure were set to be read every 15 minutes in a format compatible to ADCIRC file specification. The PBL model uses a moving coordinate system so the origin of the nested grid always coincides at the center of the hurricane. The nested domain is constructed by overlapping seven regular grids, each with progressively coarser grid spacing (1.25 km, 2.5 km, 5 km, 10 km, 20 km, 40 km, and 80 km) from the origin of the coordinate system. Therefore, grid refinement can be efficiently adjusted so the complete grid has high resolution near the center of the eye and low resolution outside the radius where spatial variation in hurricane wind diminishes. The PBL model converts wind (x and y directions) and pressure information into a format compatible to ADCIRC specification so the PBL output is directly used as wind and pressure field input forcing for ADCIRC storm surge simulation. Given the hurricane forcing, ADCIRC calculates surface wind stress following Garratt's (1977) relationship as

$$\frac{\tau_x}{\rho_o} = C_{D,x} \frac{\rho_a}{\rho_o} |W_{10}| W_{10,x} \quad (6.2)$$

$$\frac{\tau_y}{\rho_o} = C_{D,x} \frac{\rho_a}{\rho_o} |W_{10}| W_{10,y} \quad (6.3)$$

where

τ_x, τ_y is wind stress in the x and y direction, respectively,

$\frac{\rho_a}{\rho_o}$ is ratio of air density to average density of seawater,

$W_{10,x}, W_{10,y}$ is the x and y component of wind velocity vector at a 10 m height in units of m/s,

$|W_{10}|$ is wind speed at a 10 m height in units of m/s, and

C_D is Garratt's (1977) frictional drag coefficient defined as

$$C_{D,x} = (0.75 + 0.067W_{10,x}) \times 10^{-3}$$

$$C_{D,y} = (0.75 + 0.067W_{10,y}) \times 10^{-3}$$

The PBL specifies the hurricane pressure field P_c following the exponential law (Holland B, 1980) as

$$P_c = P_{eye} + \Delta P e^{-(R_p/r)^B} \quad (6.4)$$

where

P_{eye} is pressure at the eye of the storm, I

ΔP is pressure deficit,

r is the distance from the eye of the storm, and

R_p is a pressure scale radius in PBL model.

Including Holland B for the parametric expression of observed hurricane intensity also improves the accuracy in the maximum wind speed (U_{max}) estimation for the hurricane

$$U_{max} = \left(\frac{B}{\rho_a e} \right)^{1/2} (p_n - p_c)^{1/2} \quad (6.5)$$

where e is the base of the natural logarithms. Consequently, the storm surge levels, which would be related to the square of the wind speeds (Irish et al., 2008), were also estimated by linear proportion to the Holland B .

HURRICANE SELECTION BASED ON OPTIMAL SAMPLING

For this study, sensitivities of surge response to the variation in both forward speed and approach angle were assumed insignificant. Therefore, only storms propagating with 5.7 m/s forward speed and less than 17° of angle with respect to shoreline orientation, a typical forward

speed and angle of historical hurricanes in Gulf of Mexico (Irish et al., 2009), were considered. Holland B was held constant at 1.27 until the hurricane is over 50 km from landfall; at this point, the hurricane's Holland B was to decrease slowly to 0.9.

As demonstrated previously, the SRF redefines a continuous surge response surface, with respect to relative alongshore distance from the location of the hurricane eye to the position of interest. In order to measure the alongshore distance, and to investigate the surge responses to varying continental shelf slope, additional 215 elevation stations were specified along the ocean coastline. Accepting the concept of an idealized shoreline that the surge response at 10 m depth nearshore can represent the overall surge response behavior along the adjacent continental shelf (Irish et al., 2009), the stations were specified along the 10 m depth contour throughout the Texas open coast (Figure 20. SRF Prediction versus Numerically Simulated Surges (Irish et al., 2009)).

In addition to the 4 tracks investigated through the preceding work of Irish et al. (2009), a total of 18 storm tracks, 30 km apart from each other, were specified to cover the entire study area Figure 20. SRF Prediction versus Numerically Simulated Surges (Irish et al., 2009)). Specifically, the synthetic storms along eight parallel tracks were selected for surge investigation in the Galveston area; and for the Corpus Christi region six more parallel tracks were selected.

In the study, storm size (R_p) and intensities (c_p) were specified based on the investigation of the discrete data set of Irish and Resio (2009). While the storm tracks were somewhat densely placed in order to capture the effect of spatial variability in continental shelf width, if any, subsets for storm size and intensity combinations were alternately applied for each track to optimize numerical simulation requirements. That is, if the subset for the first, third, and fifth tracks (near Galveston) consists of at least nine different combinations of size and intensity properties for each track (subset I), the second and the fourth tracks were specified with combinations of only two discrete intensities (960 mb and 900 mb) and a single moderate size (subset II) (Figure 23. Texas Coastal Map of the Study Area). Table 3. R_p and c_p Combinations for Subset I and II. lists the combinations of storm size and intensity selected for subset I and subset II. Accordingly, synthetic hurricane wind fields were created with intensity between 960 mb and 900 mb, and size between 11 and 65 km.

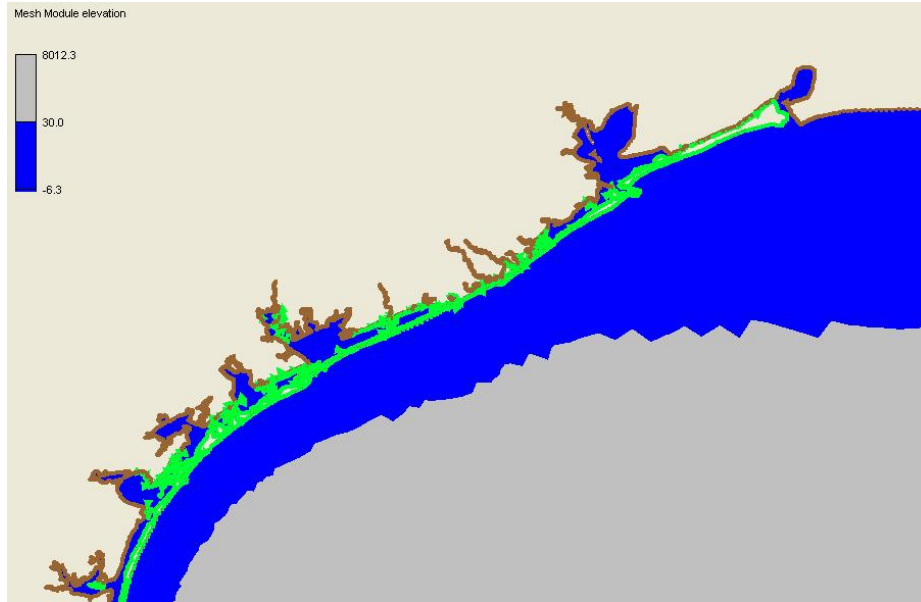


Figure 23. Texas Coastal Map of the Study Area. The area shaded in blue represents the varying continental shelf width (L30) along the Texas coastal line.

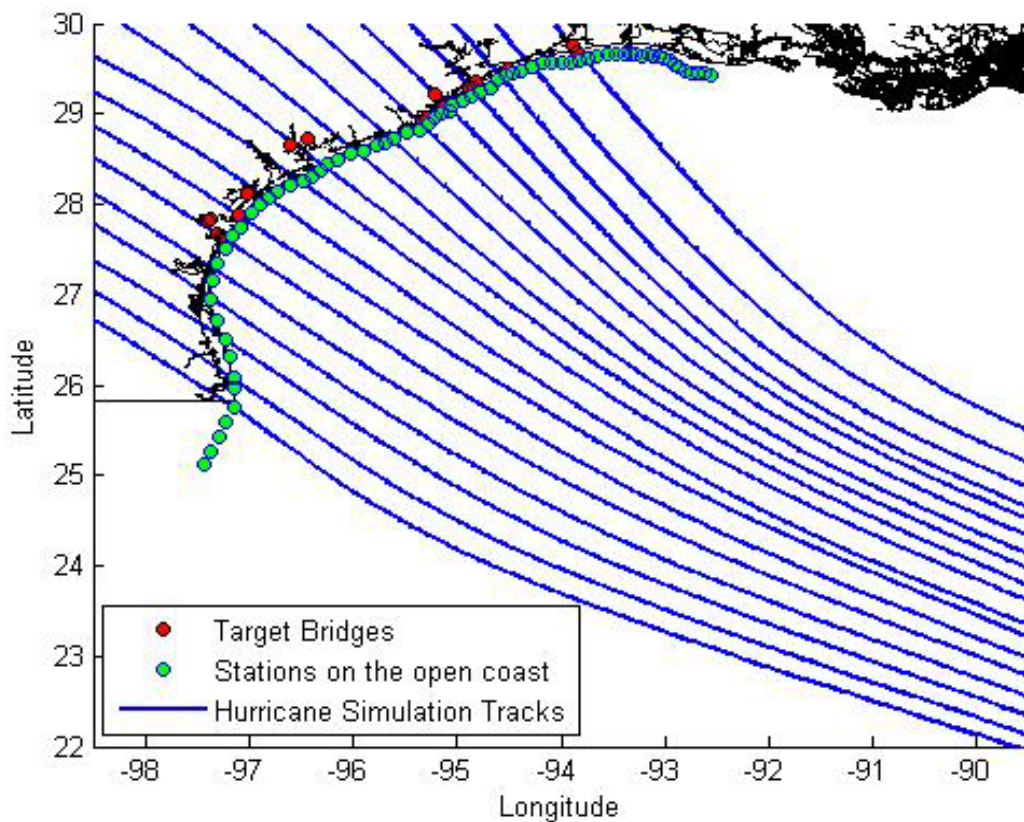


Figure 24. Storm Tracks (Solid Line) with Respect to Stations along the Texas Coast.
The green dots aligned along the shoreline represent the elevation stations while red dots indicate the target bridges.

As mentioned previously, the computations of barometric pressures and wind velocities were specified every 900 seconds and saved in two separate files in a format compatible to ADCIRC model specification. With these wind field files as meteorological forcing input, along with the other inputs for grid and boundary conditions, more than 105 ADCIRC hurricane simulations were conducted. With the refined grid, approximately 1300 CPU hours were requested to complete a single run for a storm of 6 days duration with 0.5-second time increment. To alleviate the computation burden the simulations were run on multiple processors (32, 64, 72, or 88) depending on platform and parallel configuration of the computational platform. The ADCIRC computation produced the time history of storm surges with the typical accuracy of 20 to 30 cm (Westerink et al., 2008).

Table 3. R_p and c_p Combinations for Subset I and II.

Subset I					Subset II				
x_{eye}	y_{eye}	v_f	c_p	R_p	x_{eye}	y_{eye}	v_f	c_p	R_p
[Lon.]	[Lat.]	[km/s]	[mb]	[km]	[Lon.]	[Lat.]	[km/s]	[mb]	[km]
-95.65	28.75	5.7	960	20.4	-95.35	28.90	5.7	960	32.8
-95.65	28.75	5.7	960	38.9	-95.35	28.90	5.7	900	32.8
-95.65	28.75	5.7	960	66.0					
-95.65	28.75	5.7	930	14.8					
-95.65	28.75	5.7	930	32.8					
-95.65	28.75	5.7	930	47.8					
-95.65	28.75	5.7	900	11.1					
-95.65	28.75	5.7	900	27.6					
-95.65	28.75	5.7	900	40.4					

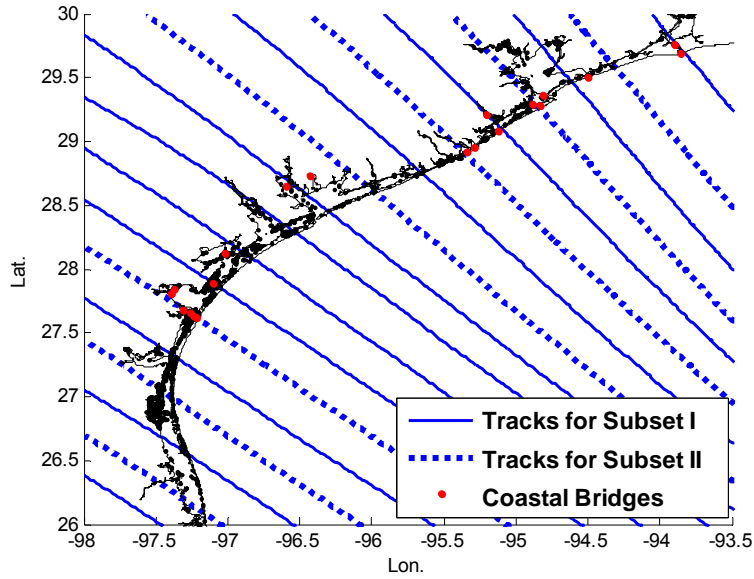


Figure 25. Tracks for Subset I & II.

The solid lines are the tracks for hurricane simulations for subset I consisting of minimum 9 combinations of R_p and c_p . The dashed lines are the tracks for hurricane simulations for subset II consisting of minimum 2 combinations of R_p and c_p as shown in Table 4. R_p and c_p Combinations for Subset I and II.

CHAPTER 7: HINDCAST OF WAVE CONDITIONS DURING HURRICANE IKE

On September 13, 2008, at 2:10 a.m. CDT, Hurricane Ike made landfall at Galveston, Texas. Although it was only a Category 2 hurricane (wind speed 96-110 mph), it generated storm surge equivalent to a Category 4 hurricane. As a result, it is ranked as the third most destructive hurricane (behind Hurricane Andrew 1992 and Hurricane Katrina 2005) that has made landfall in the United States. The Rollover Pass Bridge was damaged during Hurricane Ike .

The Pelican Island Causeway ([Figure 26](#)) was also damaged during the hurricane, which forced Texas A&M University at Galveston to relocate to College Station for the remainder of the semester. The entrance bridge to Flagship hotel was also damaged ([Figure 27](#)).

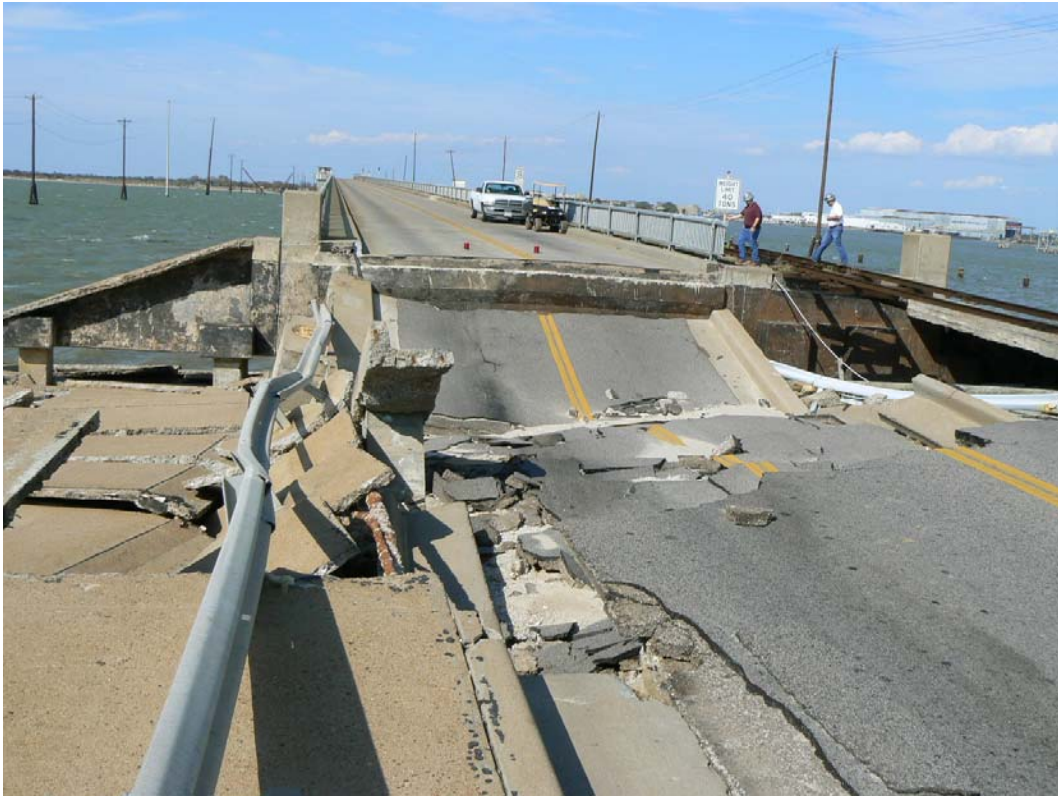


Figure 26. Damage to Pelican Island Causeway.



Figure 27. Damage to the Entrance Bridge to Flagship Hotel, Galveston.

We collected wind field data from NOAA and modeled the entire Gulf of Mexico. Wind hindcast was performed for September 11 to September 15, 2008. We used water level data collected from the three stations in Galveston to update the water level. We used measured wave data from NDBC buoys to validate our wave hindcast. The track of Hurricane Ike and locations of NDBC buoys are shown in [Figure 28](#). Comparison of model significant wave height (SWH) results and buoy measurement at NDBC buoys are given in [Figure 29](#) ([29a](#), [29b](#), and [29c](#)). Buoy 42003 stopped transmitting data during the passage of Hurricane Gustav in August 2008, therefore it was not included in the comparison.

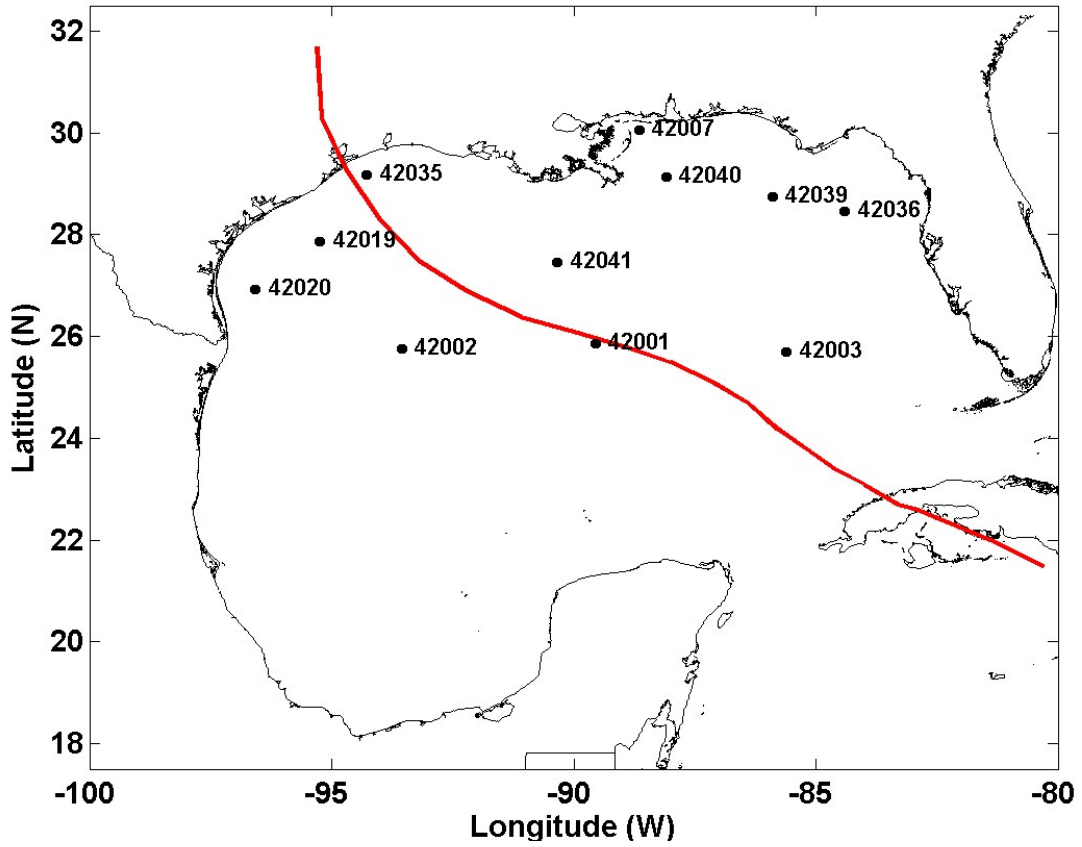


Figure 28. Track of Hurricane Ike and Locations of NDBC Buoys.

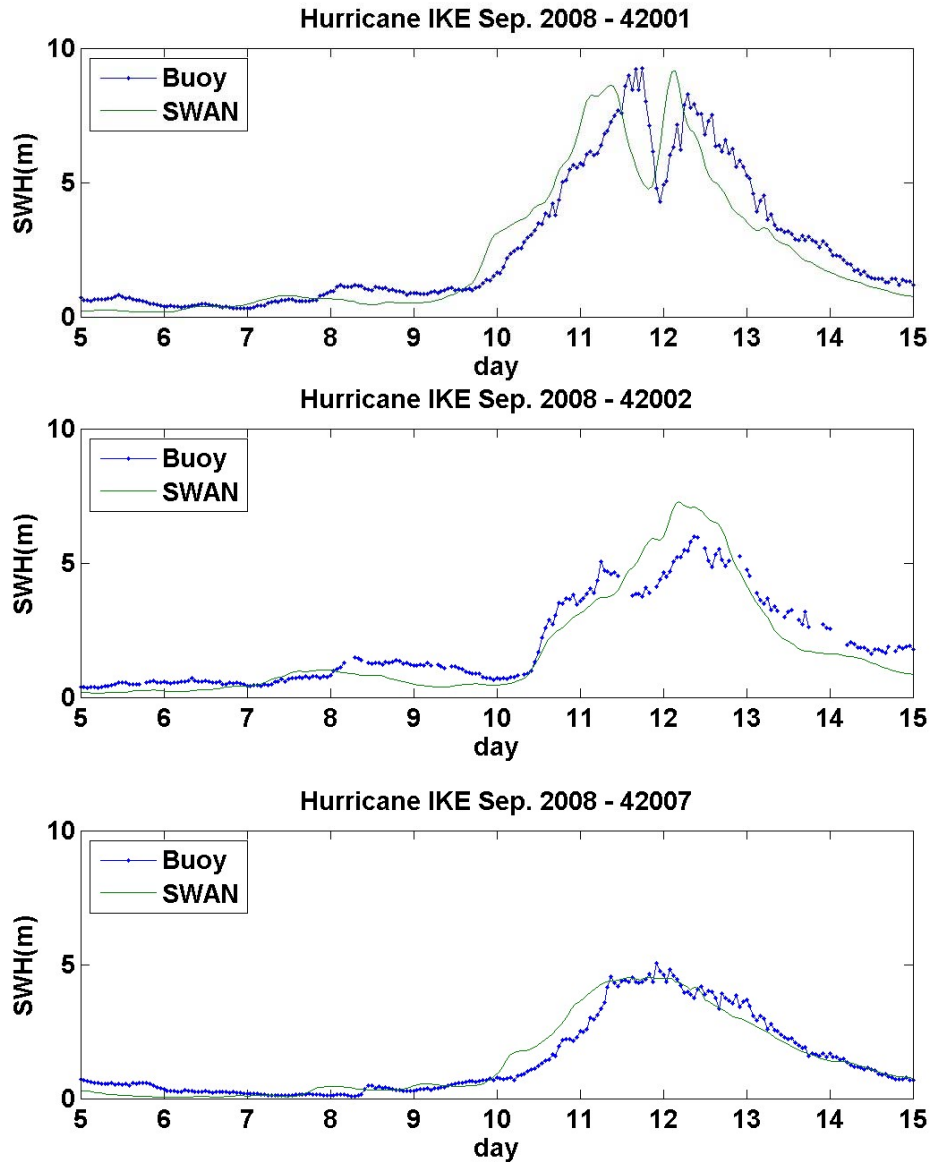


Figure 29a. Comparison of Model and Measured SWH at Buoy 42001, 42002, and 42007.

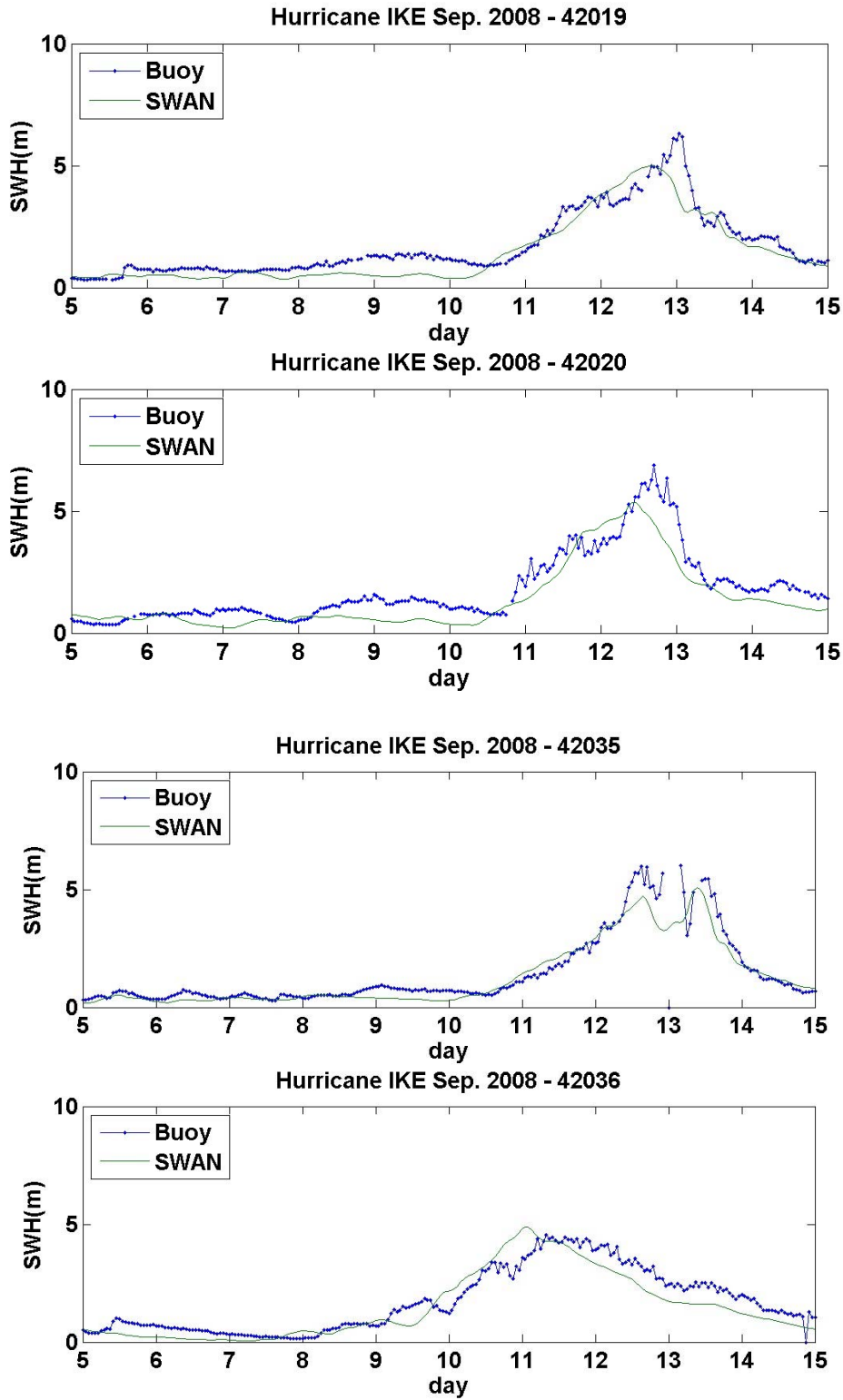


Figure 29b. Comparison of Model and Measured SWH at Buoy 42019, 42020, 42035, and 42036.

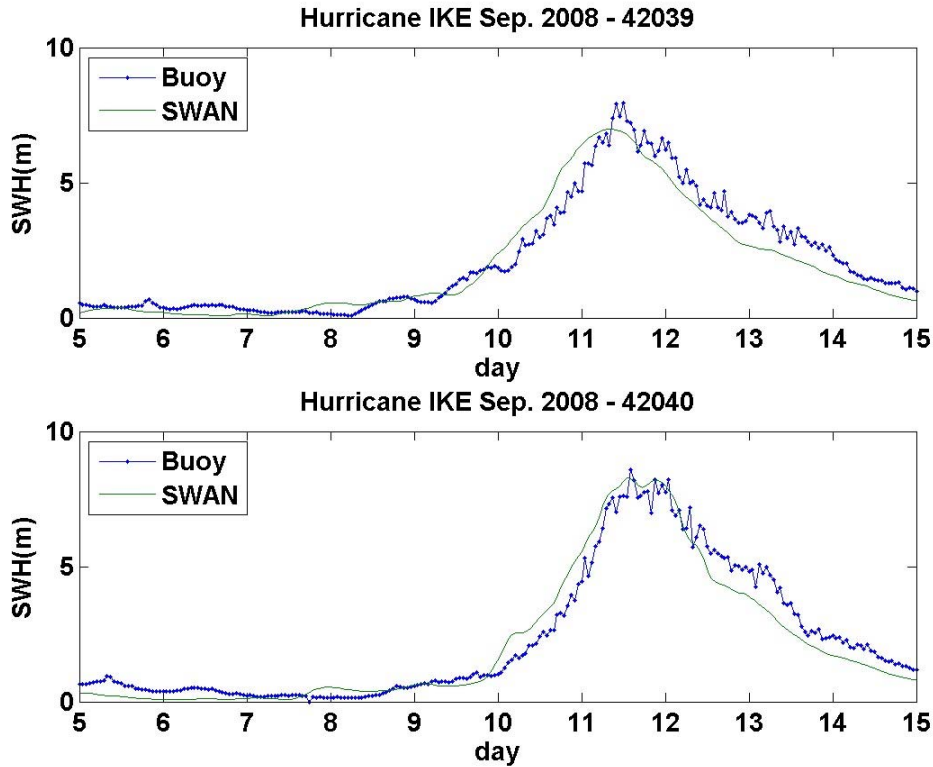


Figure 29c. Comparison of Model and Measured SWH at Buoy 42039 and 42040.

Comparisons shown in [Figure 29](#) indicate that the wave model SWAN reproduced the wave conditions during Hurricane Ike with high accuracy. It is noticeable that for Buoy 42001, which lies directly on the track of Ike, the wave height has two peaks ([Figure 29a](#)). This is caused by the relatively small wind speed in the Hurricane eye.

In order to provide more detailed information on wave height in Galveston area during Hurricane Ike, we constructed a refined-grid domain for Galveston area. Grid size for the domain is $0.003^\circ \times 0.003^\circ$. As shown in [Figure 30](#), this grid size is able to capture the complicated boundary of Galveston Bay.

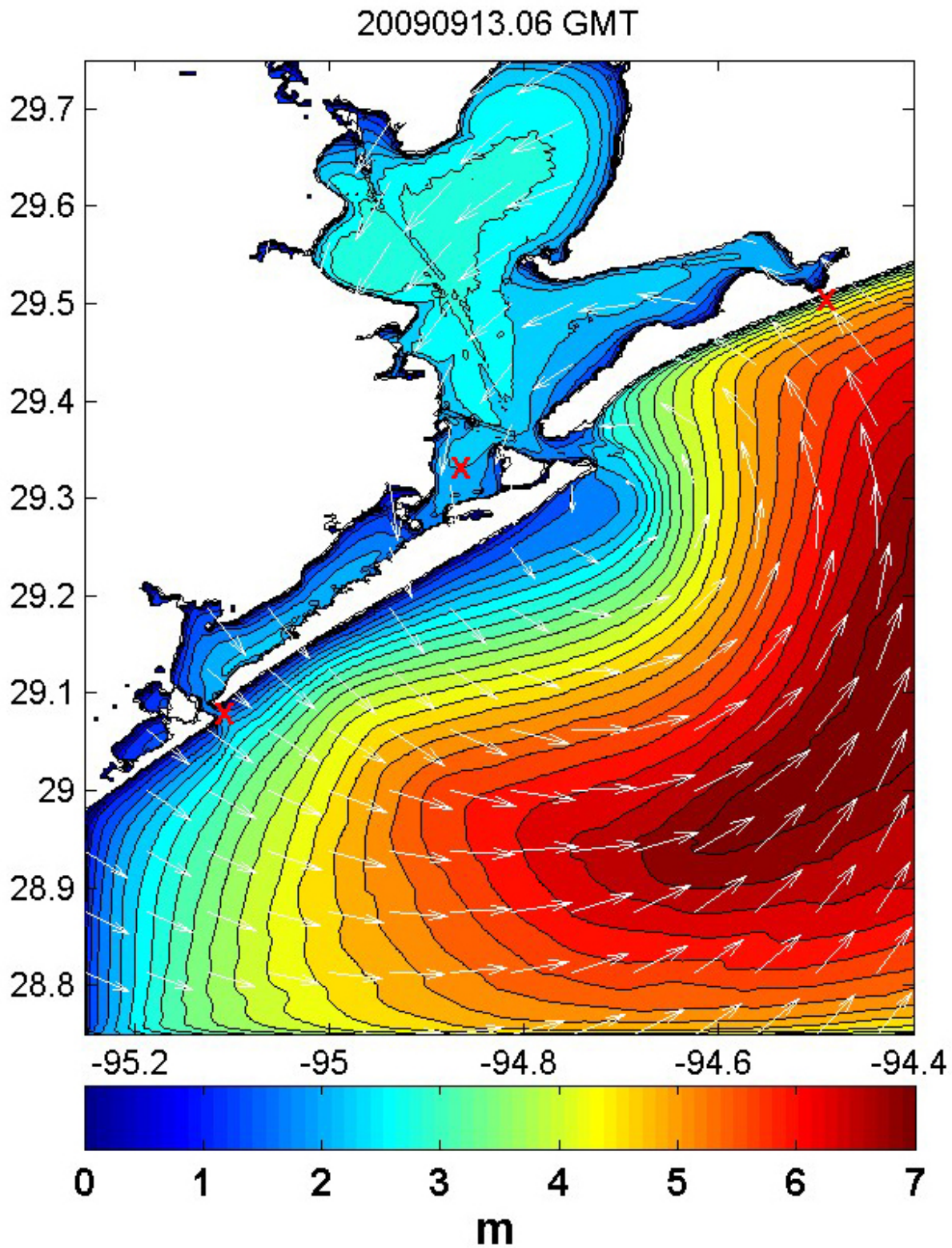


Figure 30. Contour of Model SWH before Hurricane Ike Made Landfall in Galveston Area.

We extracted significant wave height at three bridges in the area (Table 5). The maximum wave height at Galveston Causeway was 2.39 m, at San Luis Pass Bridge was 2.41 m, and at Rollover Pass was 2.49 m. The Rollover Pass Bridge is located to the east of the hurricane track, while the other two bridges are to the west of the hurricane track. Stronger wind of a hurricane is on the east side.

Table 5. Maximum Wind and Wave at Three Bridges in Galveston during Hurricane Ike.
The maximum values are highlighted in bold.

Time (CDT)	Galveston Causeway		San Luis Pass Bridge		Rollover Pass	
	wind(m/s)	wave (m)	wind(m/s)	wave (m)	wind(m/s)	wave (m)
2009/9/12/ 4am	13.27	1.07	13.18	1.00	13.57	0.44
2009/9/12/ 7am	14.72	1.20	14.62	1.17	15.07	0.53
2009/9/12/ 10am	16.11	1.35	16.00	1.33	16.51	0.65
2009/9/12/ 1pm	17.94	1.49	17.84	1.58	18.39	0.80
2009/9/12/ 4pm	20.49	1.45	20.31	1.46	21.11	0.71
2009/9/12/ 7pm	24.47	1.76	24.08	1.84	25.30	1.05
2009/9/12/ 10pm	32.93	2.39	30.71	2.41	34.70	2.05
2009/9/13/ 1am	32.54	2.28	39.53	1.89	46.23	2.49
2009/9/13/ 4am	40.33	1.92	31.52	1.29	39.77	2.05
2009/9/13/ 7am	27.01	1.32	24.31	1.34	27.12	1.86
2009/9/13/ 10am	17.31	0.90	16.12	0.25	17.83	1.09

CHAPTER 8: EXTREME WAVE AND STORM SURGE ESTIMATION

EXTREME WAVE CONDITIONS AT SELECTED BRIDGE SITES

We were initially instructed to consider three bridges for modeling in this project, San Luis Pass Bridge, Galveston Bay Causeway, and Lavaca Bay Causeway. After Hurricane Ike, the Rollover Pass Bridge was added to our study. In order to determine design wave parameters for the four bridges, we performed wave simulation using hurricane wind speed corresponding to different hurricane wind scale.

The current Saffir-Simpson Hurricane Scale (SSHS), which was developed in 1971, is mainly based on expected hurricane wind speed. Although it includes storm surge ranges (see [Table 6](#)) and other storm-related information, the storm surge information included in SSHS is not accurate, as illustrated by Hurricane Ike. Hurricane Ike made landfall with Category 2 winds, however the storm surge at Galveston was equivalent to Category 4-5 storm surge. Many residents in the Galveston area did not evacuate because the storm was predicted as only a SSHS Category 2 or 3. Other examples include: Hurricane Charley in 2004 made landfall with Category 4 winds but with weaker storm surge equivalent to the Category 2 range; and Hurricane Katrina in 2005 made landfall with Category 3 winds but with stronger storm surge equivalent to the Category 5 storm range. Because storm surge is a product of many factors not considered in SSHS such as storm size and forward speed, and bathymetry and characteristics of the coastline in the landfall location, storm surge values for each category are not exactly related to wind speed and are frequently incorrect in storm predictions. Due to above mentioned reason; we decided to run wave simulation at different storm surge levels for each level of hurricane wind.

For each bridge, we performed 40 wave simulations at 5 different wind speed levels and 8 storm surge levels. To generate maximum waves at these bridges, wind directions were set normal to coastline ([Figure 31](#)). The most probable extreme wave height, H_{max} , was calculated assuming the wave height follow Rayleigh distribution,

$$H_{max} = 0.706H_s\sqrt{\ln(N_z)} \quad (8.1)$$

where N_z is the number of waves during the duration of one hour, H_s is the significant wave height obtained from wave simulations. The results are listed in [Table 7](#) through [Table 10](#), and plotted

versus storm surge level (Figure 32 and Figure 33) and hurricane category (Figure 34 and Figure 35). Period of the maximum waves are listed in Table 11 through Table 14.

As shown in Figure 32–37, for all four bridge sites extreme wave heights are in general linearly related to storm surge and are less dependent on wind speed. For example, at Rollover Pass Bridge, the extreme wave heights are almost the same at different wind speed levels.

Table 6. Wind Speed and Storm Surge Ranges of Saffir-Simpson Hurricane Scale.

	Sustained Wind Speed range		Storm Surge Range	
	mph	km/h	ft	m
Category 1	74-95	119-153	4-5	1.2-1.5
Category 2	96-110	154-177	6-8	1.8-2.4
Category 3	111-130	178-209	9-12	2.7-3.7
Category 4	131-155	210-249	13-18	4.0-5.5
Category 5	>155	>250	>18	>5.5

Table 7. Most Probable Extreme Wave Height Hmax at Galveston Causeway (m).

Hurricane Scale	Storm Surge (m)							
	0	1	2	3	4	5	6	7.2
Category 1	1.63	2.27	2.88	3.49	4.02	4.29	4.48	4.69
Category 2	1.69	2.38	2.98	3.64	4.27	4.86	5.24	5.49
Category 3	1.77	2.54	3.19	3.80	4.46	5.11	5.74	6.41
Category 4	1.86	2.58	3.43	4.11	4.74	5.38	6.05	6.74
Category 5	1.98	2.83	3.57	4.26	4.94	5.86	6.51	7.27

Table 8. Most Probable Extreme Wave Height Hmax at San Luis Pass Bridge (m).

Hurricane Scale	Storm Surge (m)							
	0	1	2	3	4	5	6	7.2
Category 1	1.78	2.38	2.81	3.41	4.03	4.66	5.26	6.13
Category 2	1.85	2.46	3.02	3.60	4.18	4.85	5.40	6.15
Category 3	1.95	2.66	3.14	3.69	4.35	5.03	5.63	6.36
Category 4	2.15	2.73	3.40	4.03	4.59	5.19	5.81	6.51
Category 5	2.57	3.19	3.69	4.30	4.98	5.67	6.26	6.99

Table 9. Most Probable Extreme Wave Height Hmax at Rollover Pass Bridge (m).

Hurricane Scale	Storm Surge (m)							
	0	1	2	3	4	5	6	7.2
Category 1	0.78	1.83	2.35	3.08	3.75	4.33	4.87	5.71
Category 2	0.88	1.84	2.36	2.93	3.68	4.35	5.04	5.80
Category 3	1.04	1.82	2.29	2.91	3.56	4.35	4.99	5.78
Category 4	1.09	1.85	2.38	2.97	3.63	4.23	4.82	5.56
Category 5	0.93	2.07	2.62	3.21	3.88	4.52	5.17	5.88

Table 10. Most Probable Extreme Wave Height Hmax at Lavaca Bay Causeway (m).

Hurricane Scale	Storm Surge (m)							
	0	1	2	3	4	5	6	7.2
Category 1	1.58	2.14	2.73	3.34	3.87	4.36	4.82	5.40
Category 2	1.61	2.30	2.85	3.47	4.06	4.64	5.18	5.70
Category 3	1.70	2.46	3.11	3.72	4.31	4.92	5.48	6.16
Category 4	1.77	2.51	3.21	4.01	4.65	5.27	5.86	6.55
Category 5	1.98	2.80	3.53	4.19	4.83	5.50	6.41	7.13

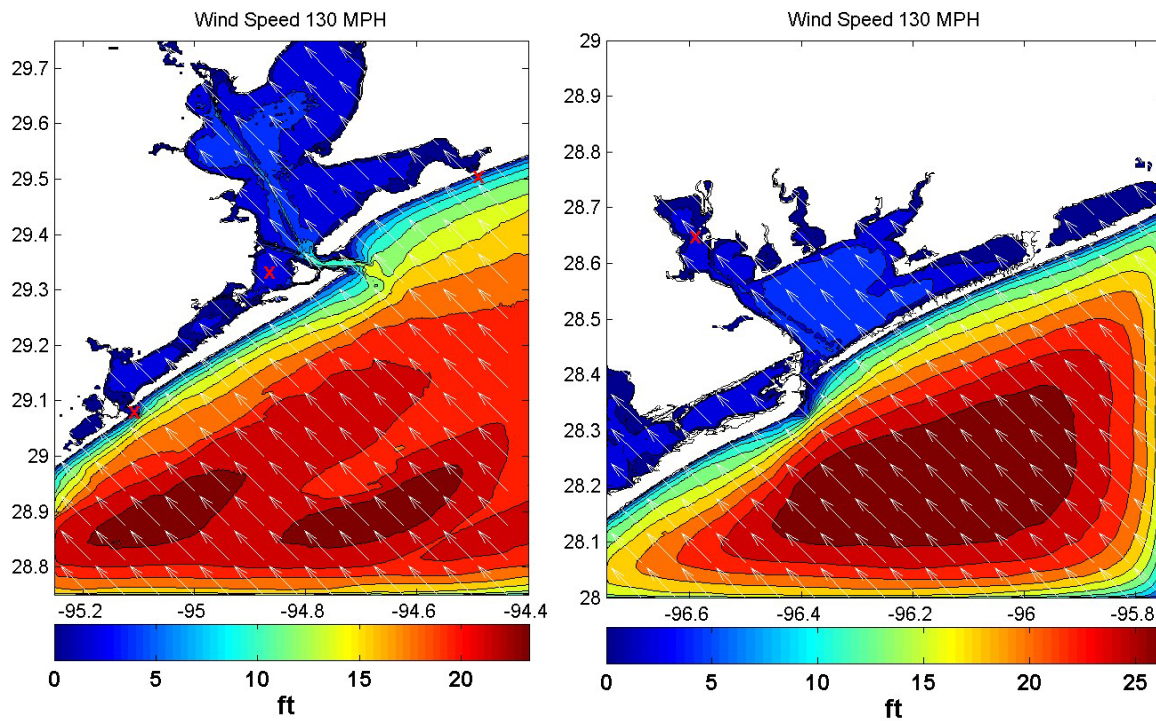


Figure 31. Predicted Significant Wave Height during Category 3 Hurricanes (Bridge Locations Marked by Red Crosses).

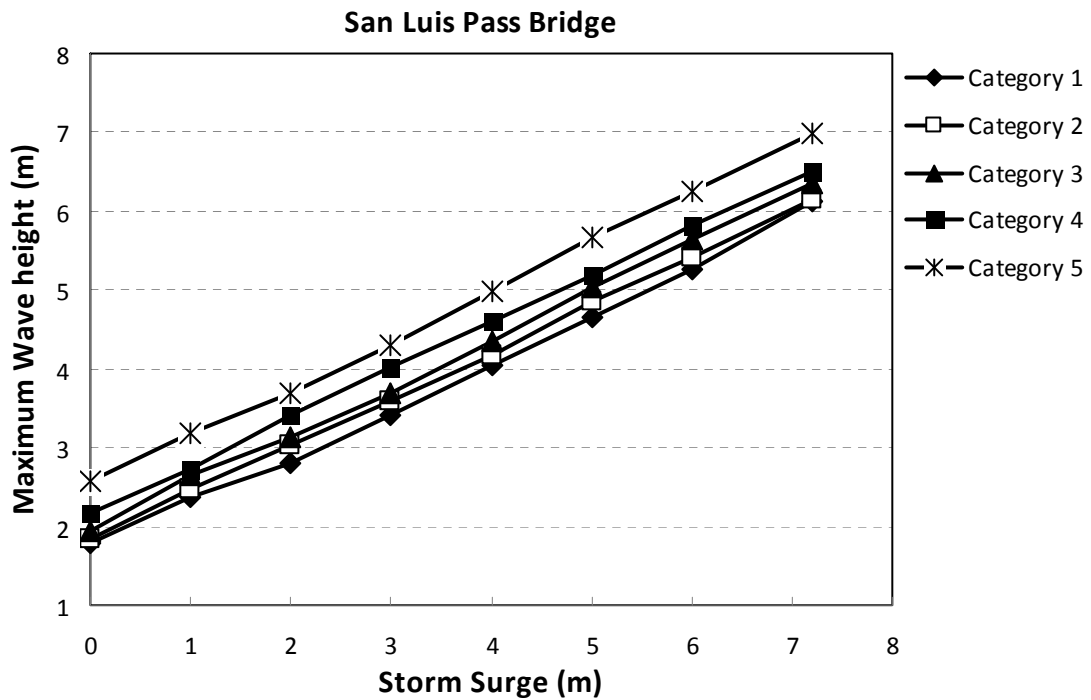
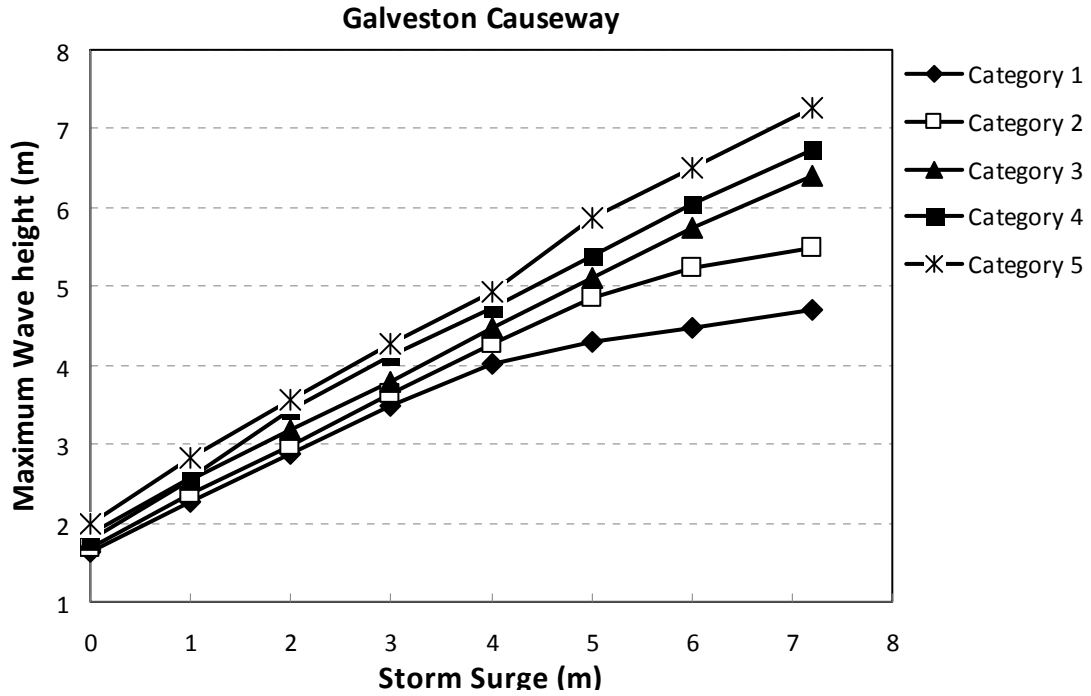


Figure 32. Predicted Maximum Wave Heights vs. Storm Surge Levels (Galveston Causeway and San Luis Pass Bridge).

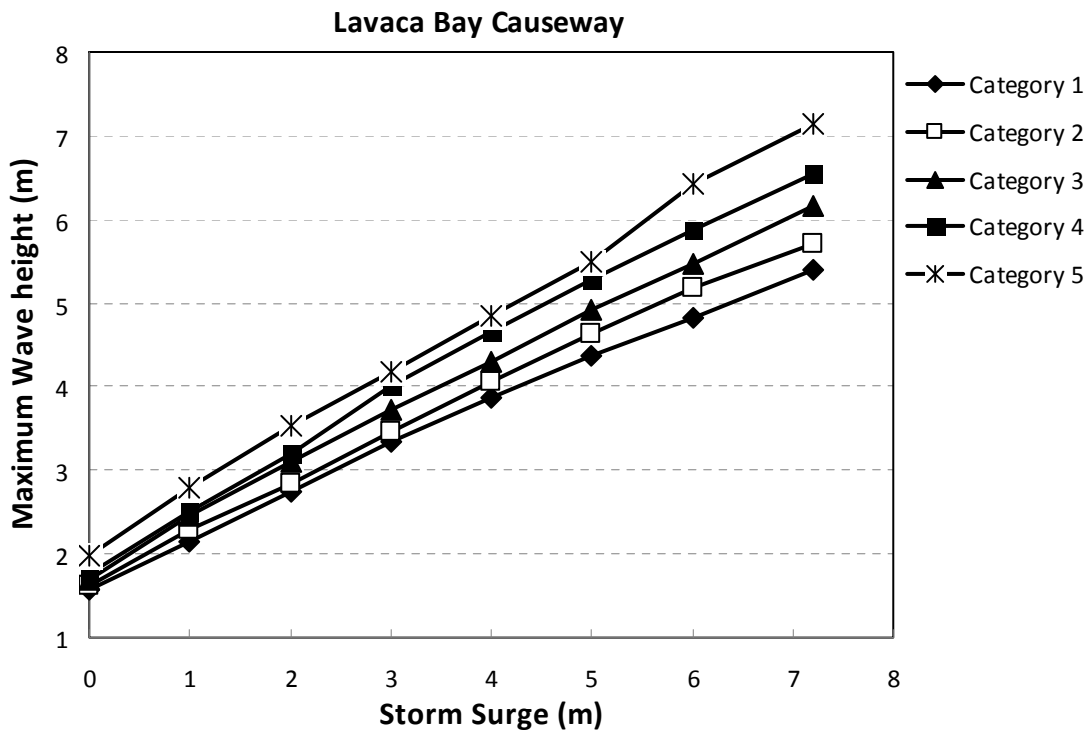
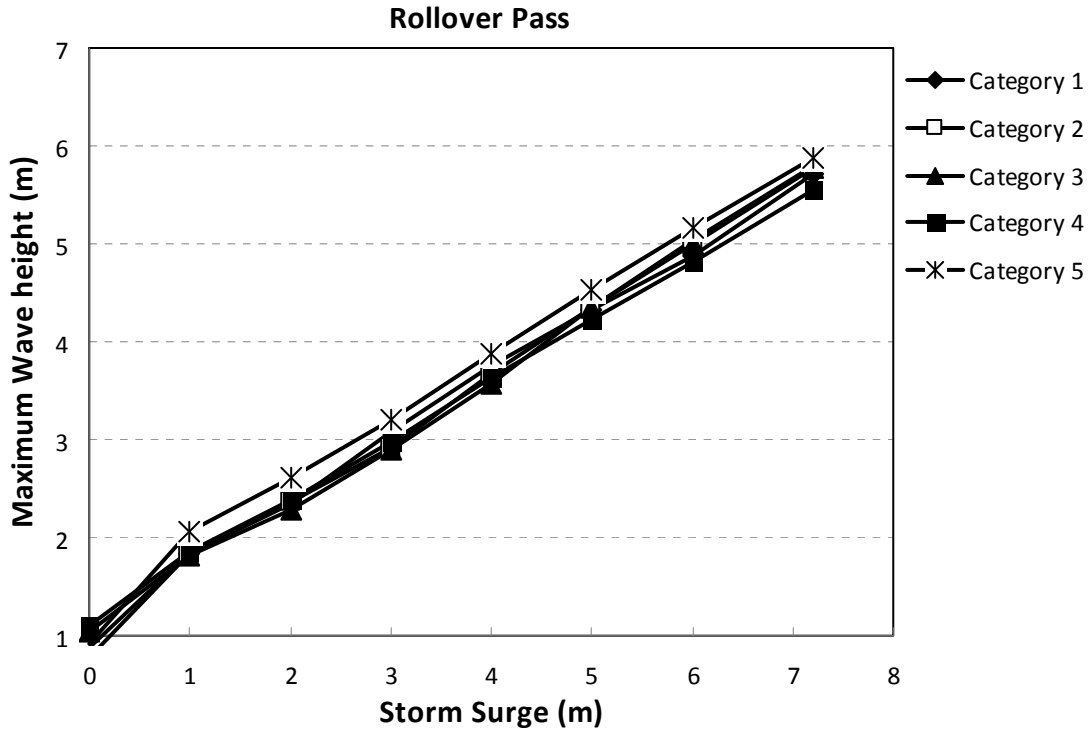


Figure 33. Predicted Maximum Wave Heights vs. Storm Surge Levels (Rollover Pass and Lavaca Bay Causeway).

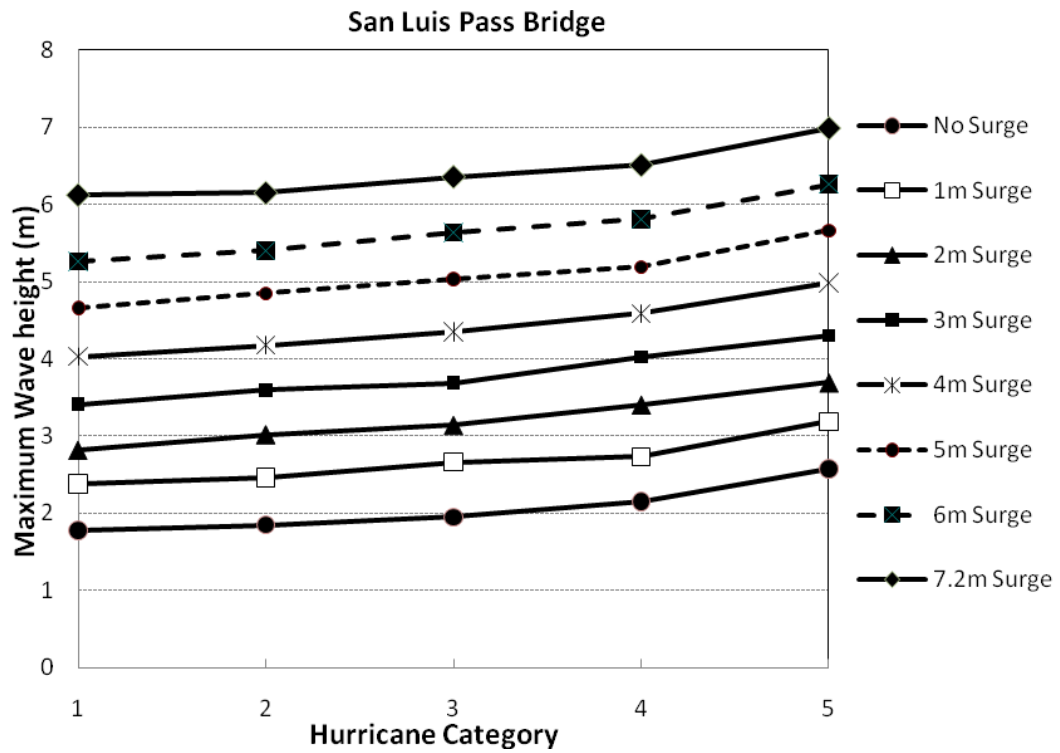
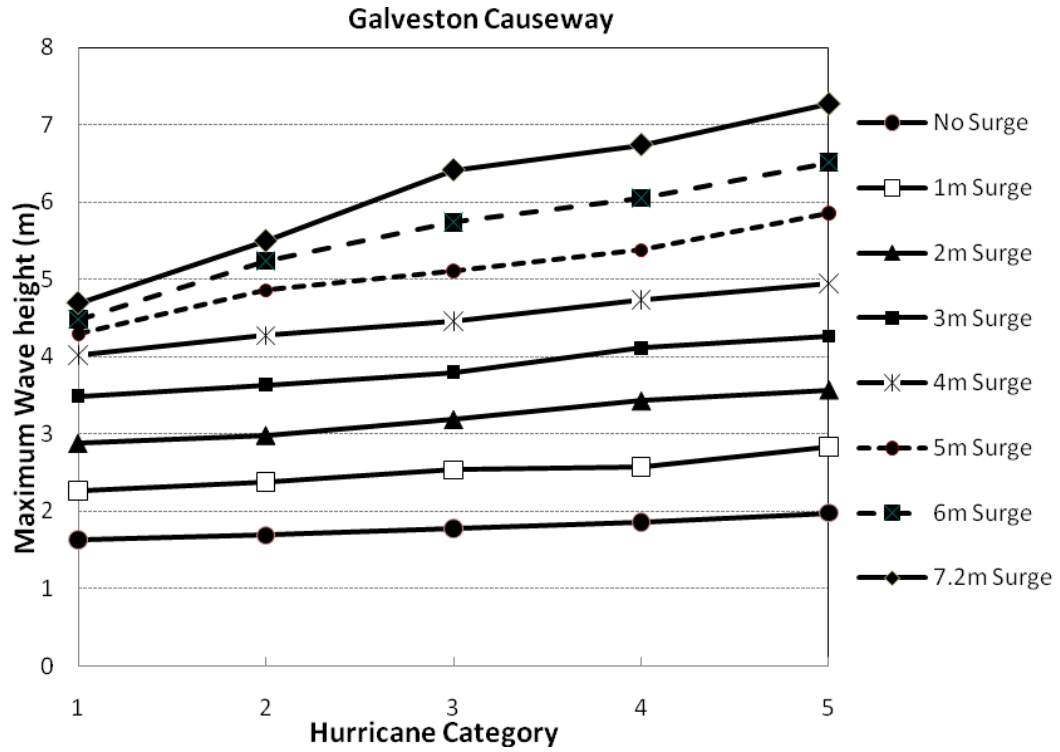


Figure 34. Predicted Maximum Wave Heights vs. Hurricane Category (Galveston Causeway and San Luis Pass Bridge).

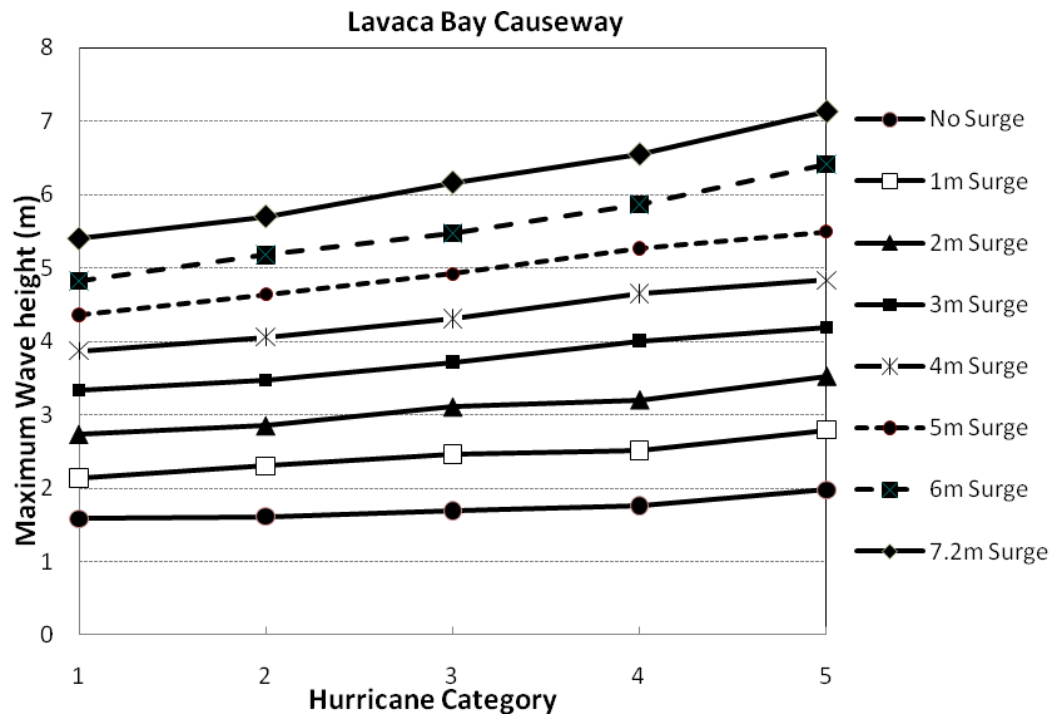
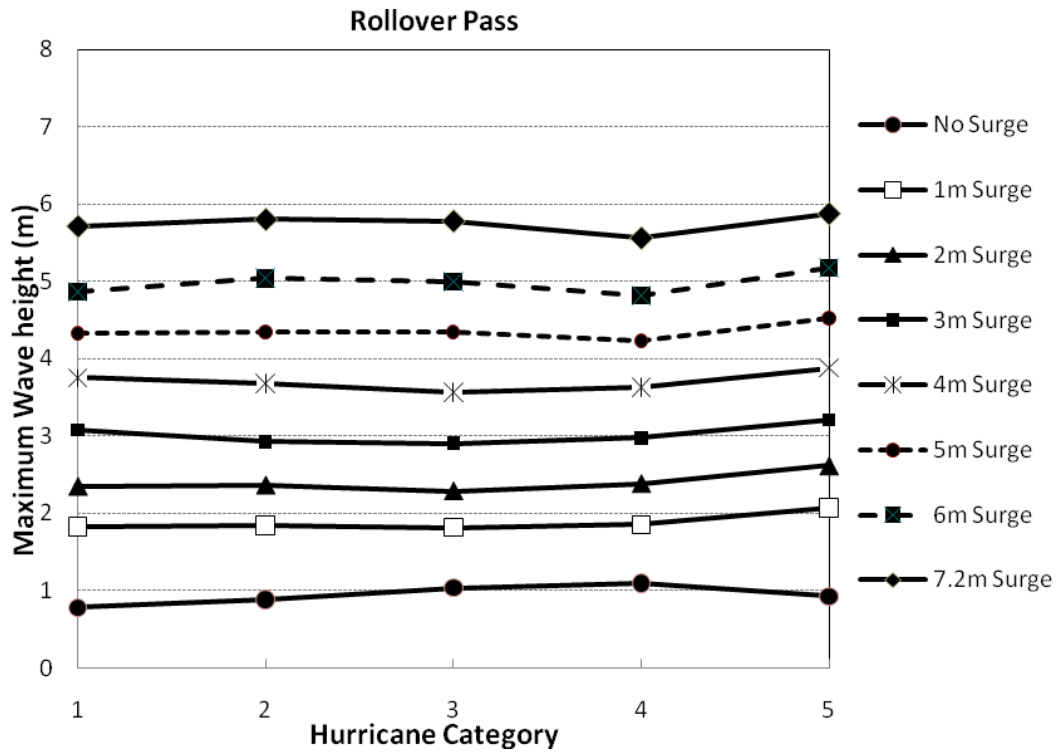


Figure 35. Predicted Maximum Wave Heights vs. Hurricane Category (Rollover Pass and Lavaca Bay Causeway).

Table 11. Period of Extreme Wave Tmax at Galveston Causeway (s).

Hurricane Scale	Storm Surge (m)							
	0	1	2	3	4	5	6	7.2
Category 1	2.75	3.33	3.67	4.45	4.45	4.45	4.45	4.45
Category 2	2.75	3.33	4.04	4.04	4.89	4.89	4.89	4.89
Category 3	2.50	3.03	3.67	4.45	4.45	5.39	5.39	5.39
Category 4	3.03	5.39	3.33	3.67	4.45	4.89	4.89	5.93
Category 5	4.04	4.89	5.93	6.53	7.18	4.45	4.89	5.39

Table 12. Period of Extreme Wave Tmax at San Luis Pass Bridge (s).

Hurricane Scale	Storm Surge (m)							
	0	1	2	3	4	5	6	7.2
Category 1	2.75	3.67	8.70	9.58	9.58	9.58	9.58	9.58
Category 2	2.75	4.45	5.93	6.53	8.70	7.91	9.58	9.58
Category 3	2.75	2.75	5.93	7.18	6.53	7.18	7.91	8.70
Category 4	2.75	4.89	5.39	5.93	7.18	7.91	7.91	8.70
Category 5	2.75	3.03	5.39	5.93	5.93	5.93	6.53	7.18

Table 13. Period of Extreme Wave Tmax at Rollover Pass Bridge (s).

Hurricane Scale	Storm Surge (m)							
	0	1	2	3	4	5	6	7.2
Category 1	4.04	6.53	6.53	7.18	6.53	7.91	10.54	10.54
Category 2	3.67	5.93	5.93	7.18	7.91	7.91	7.91	8.70
Category 3	4.04	4.89	5.39	5.93	5.93	6.53	7.18	7.91
Category 4	4.04	4.89	4.89	5.39	5.39	5.93	6.53	6.53
Category 5	3.03	4.04	4.45	4.89	4.89	4.89	4.89	5.39

Table 14. Period of Extreme Wave Tmax at Lavaca Bay Causeway (s).

Hurricane Scale	Storm Surge (m)							
	0	1	2	3	4	5	6	7.2
Category 1	2.75	3.33	4.04	4.45	4.89	5.39	5.93	5.93
Category 2	2.75	3.03	3.67	4.45	4.89	5.39	5.39	6.53
Category 3	3.03	3.33	3.67	4.04	4.89	5.39	5.93	5.93
Category 4	4.89	5.93	7.18	3.67	4.45	4.89	5.39	5.93
Category 5	4.45	5.39	6.53	7.91	8.70	8.70	4.89	5.39

SURGE RESPONSE FUNCTION ADVANCEMENTS

The storm simulation data were analyzed to determine the dimensionless SRF parameters based on the physical scaling laws of [Irish et al. \(2009\)](#), and then refined to account for continental shelf width.

First, the effect of varying coastline configuration on the spatial extent of storm peak surges was studied. As discussed previously, the location of the peak surge should be analyzed in relation with the continental shelf width or L_{30} . To measure L_{30} , several pairs of ocean stations were specified to locate at the 10 m and 30 m water depth each orthogonal to shoreline orientation. Alongshore distance between two 10 m depth stations were set with simulated hurricane landfall spacing, which is 30 km ([Figure 36](#)). To measure the alongshore peak surge distance ($x-x_{peak}$), however, a minimum of nine combinations of storm surge results along the 10 tracks were utilized ([Figure 37](#)). The size parameter λ was determined from surge data simulated throughout the Texas coast as a means to account the effect of varying L_{30} for the SRF.

By linear regression, the relationship between L_{30} and the alongshore extent to highest surge was investigated, along with the storm size. The increase in steepness of the linear interpolation (or λ) with wider L_{30} and increasing storm size (R_p) is observed in the analysis ([Figure 38](#)). Therefore, it was concluded that the simplification of slowly varying coastal geography was not valid for SRF development within the wide range of conditions seen on the Texas coast.

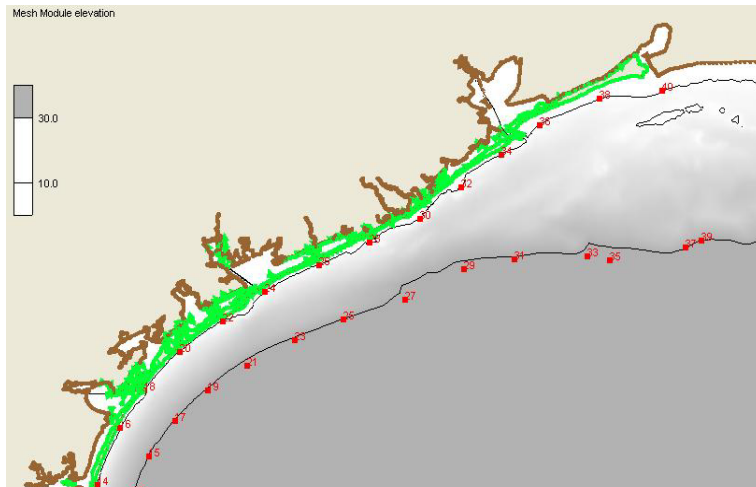


Figure 36. Locations of 10 m and 30 m Water Depth on the Continental Shelf.

A pair of two depth indicators was specified on virtual orthogonal line with respect to shoreline orientation to measure L_{30} .

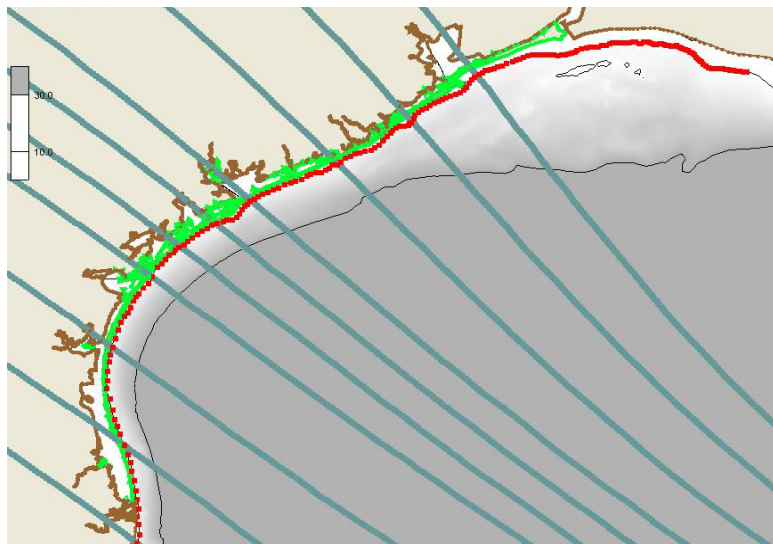


Figure 37. Hurricane Tracks Selected (Green Solid Lines) to Measure the Effect of Varying Continental Shelf Width (L_{30}).

From the bottom left across the top right: track 1, 3, 5, 7, 8, 9, 10, 12, 14, 16, and 17. The solid line in black marks the 30 m water depth contour while the red dots represent the elevation stations specified at 10 m water depth in the coast.

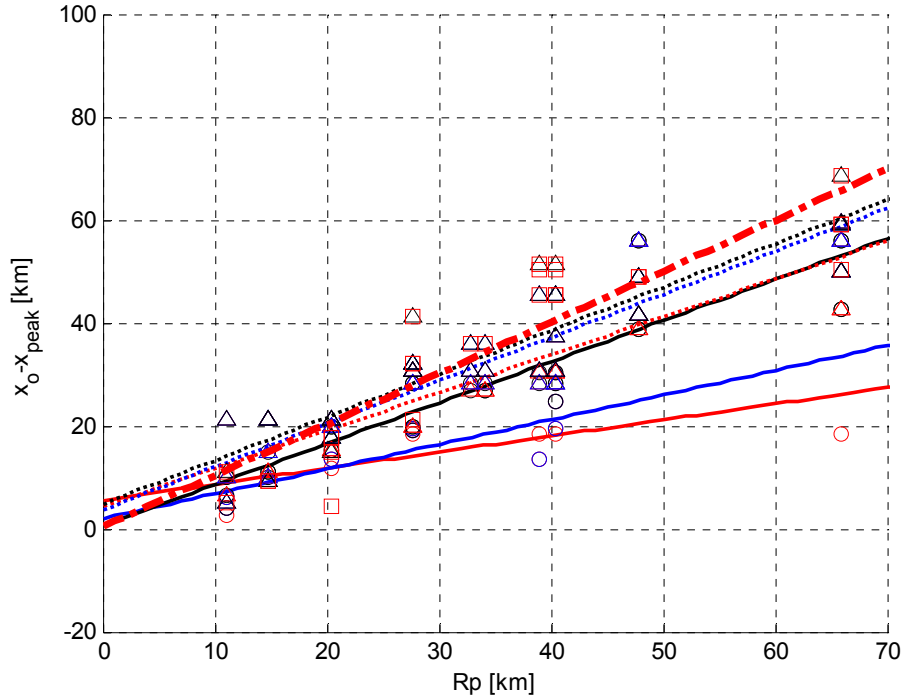


Figure 38. Linear Regression of Storm Size (R_p) and the Distance between the Location of Hurricane Eye at Landfall and the Alongshore Peak Surge Location.

The slope of each interpolation is used to determine the slope parameter, λ .

To incorporate the different geographical conditions, the total study area was divided into three parts depending on the variability in the parameter λ (Table 15): the coastal regions near Corpus Christi, Matagorda Bay, and Galveston. By partitioning the continuous coastal regions into three spatial ranges, the previously used simplification of slowly varying coastal configuration is then applied within each segment of the coast (i.e., Galveston, Matagorda Bay, and Corpus Christi).

Table 15. Properties of the Parameter λ for Each Segmentation of the Texas Coastal Region.

Selection of λ and storm tracks applied for each study area		
Coastal Region	λ	Track I.D.
Corpus Christi	0.74	5,7,8,9
Matagorda Bay	0.84	7,8,9,10,12
Galveston	0.99	10,12,14

Table 16 lists the variation in λ estimated from storms propagating over the corresponding L_{30} . These are also plotted in Figure 39. This figure shows that the distribution of the λ with respect to L_{30} can be categorized into three groups depending on their slopes – the magnitude of increase in λ with uniform variation in L_{30} . If we visualize the range of the continental shelves classified in the same group on the continental shelf map (Figure 39), it is seen that the overall geography of the continental shelf shape along the Texas coast can be divided into three segments (Figure 40, separated by the solid lines) based on the λ variation.

In addition to the correlation between L_{30} and λ , it is seen that the λ variation also corresponds to the change in the shoreline orientation. Therefore, it is expected that, by examining the correlation among L_{30} , R_p , λ , and the shoreline orientation θ_f , the SRF may also provide a means to characterize the regional geographical features in the parametric function. The effects of such a varying costal topography can be resolved by assuming that the interaction between the hurricane meteorology and the geographical factors in the region can be captured by the surge responses to the hurricanes approaching the vicinity of the area of interest. Therefore, when determining the site-dependent coefficients, such as λ and m_x , reflecting the regional characteristics, only storm simulation results from selectively chosen tracks were utilized. For example, for the evaluation of λ and m_x for bridges located in the Corpus Christi area, only the storm surge data obtained from storms simulated along track No. 5 to No. 9 was used.

Table 16. Variation of λ in the Continental Shelf Width.

3 - pair		
Track ID	L_{30} [km]	λ
1,2,3	19.6	0.26
2,3,4	20.6	0.36
3,4,5	21.3	0.49
4,5,6	23.5	0.70
5,6,7	25.4	0.69
6,7,8	28.0	0.79
7,8,9	30.1	0.74
8,9,10	33.1	0.84
9,10,11	35.7	0.81
10,11,12	39.5	1.01
11,12,13	41.7	1.12
12,13,14	47.9	1.01

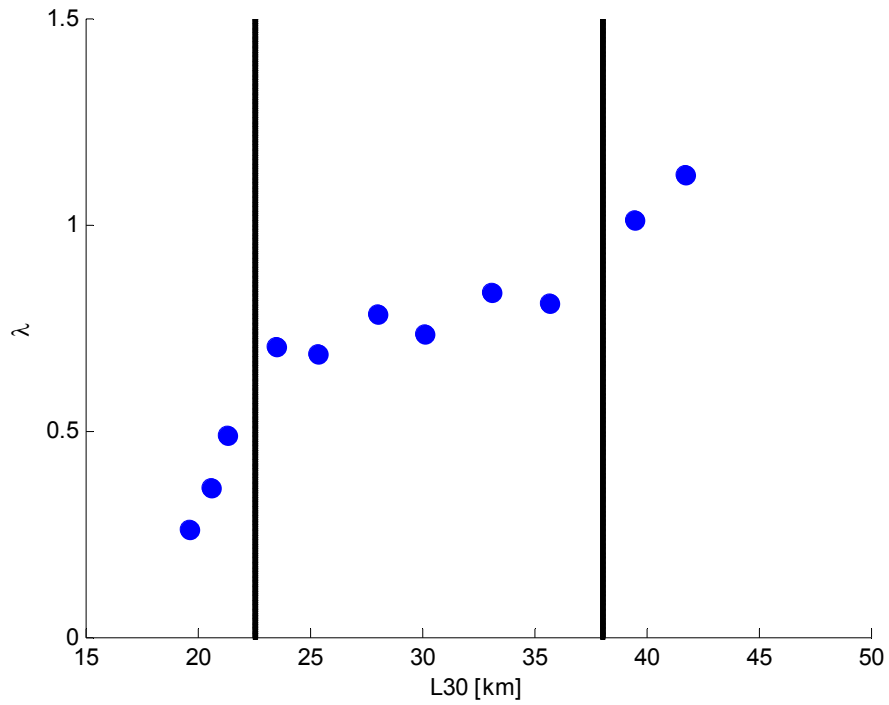


Figure 39. The Parameter λ Variations with Respect to Varying Continental Shelf Width.

The solid lines separate the research area into three segments.



Figure 40. Continental Shelf Map of the Texas Coast.

The dark shade represents the continental shelf extension to the 30 m water depth (L_{30}). The red box represents the alongshore range of L_{30} within which the parameter λ shows a similar tendency in the distribution with respect to L_{30} .

The parameter λ along with the surge simulation data were used to determine the dimensionless SRF parameters (x_2' and ζ') following the methods presented the previous sections. The obtained sets of x_2' and ζ' were curve-fitted. Based on the data, the three-term Gaussian function in adjusting peak width was found to be the most suitable for defining the SRF, as shown in the work of [Irish et al. \(2009\)](#). Moreover, the region to the right side of the hurricane eye is most influenced by the hurricane forcing due to the hurricane meteorology in the northern hemisphere. Therefore, SRF behavior has some asymmetry with respect to $x_2' = 0$. In an effort to find a way to improve the fitting, two pairs of three-term Gaussian functions were separated defined based on the right and left sides of the data. This way scattering near the peak of SRF was minimized. A smoother curve with its peak at the center (the location of $x_2' = 0$) was developed. This curve-fitting approach also reflects the asymmetry of the surge behavior. Accordingly, SRFs near the 20 selected bridge locations were developed in a form of the asymmetric three-term Gaussian function.

As discussed before, the SRF is a site-dependent function. Therefore for the 20 target bridges 20 independent SRFs were developed. The SRFs for the bridges are presented in the [Appendix](#), and three of these SRFs are presented here for discussion ([Figure 41](#)).

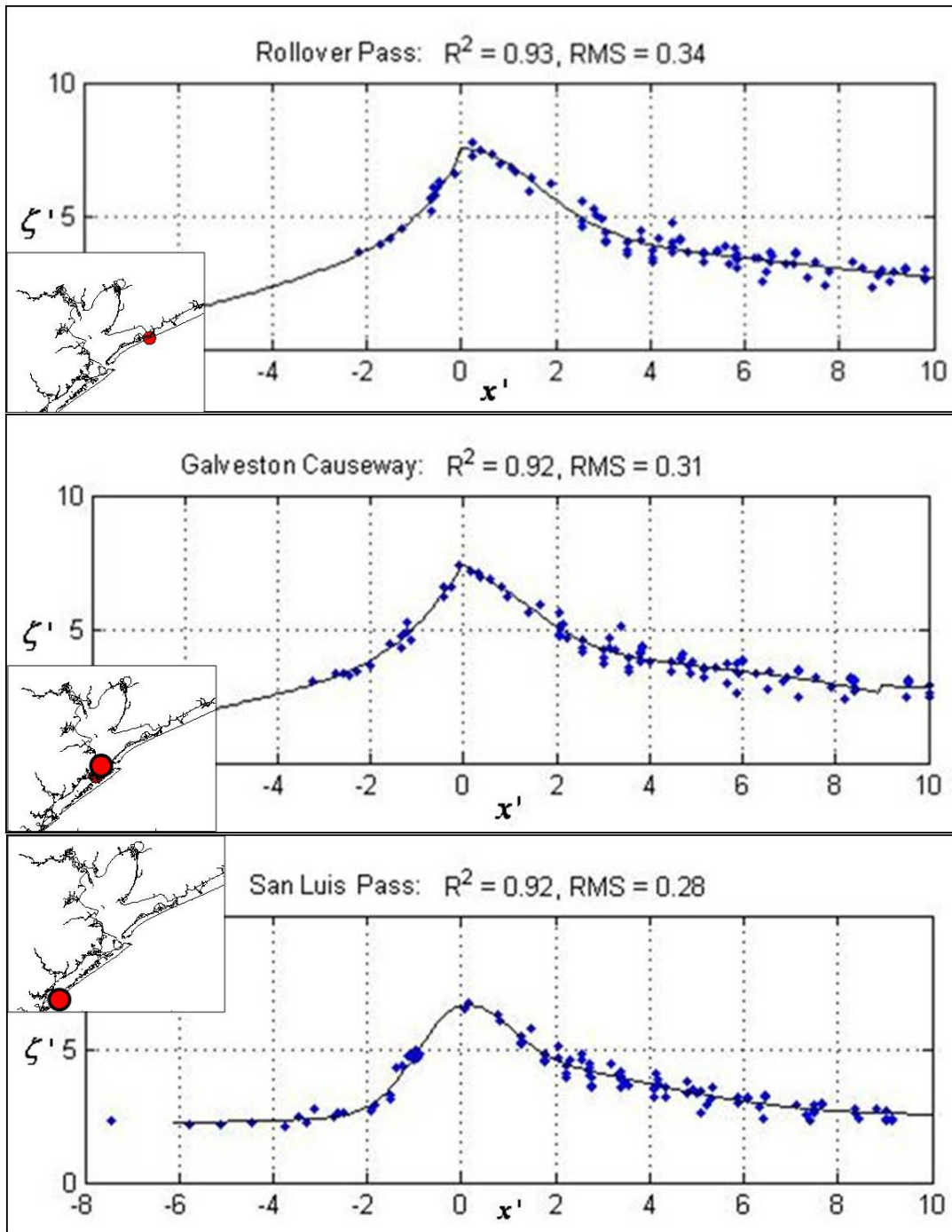


Figure 41. Surge Response Functions Developed at the Three Locations in Galveston.

The SRFs are developed at the location of Rollover Pass (top), Galveston Causeway (middle), and San Luis Pass (bottom). Solid line represents the three-term Gaussian fit to the data.

VALIDATION AND JUSTIFICATION OF SRF METHODOLOGY

By comparing surge predictions made by SRFs to the original numerical simulation output, the accuracy of each SRF can be estimated. Since the SRF is developed by the curve-fitting function of the dimensionless parameters, inherently the SRF itself is a dimensionless, continuous function of the hurricane parameters. Therefore, with given hurricane conditions the SRF provides prediction of dimensional surges by back-calculation from the SRF.

The SRF was used in this way to make predictions of storm surges (ζ_{srf}) based on the hurricane conditions applied by generating synthetic wind fields earlier as forcing input for storm surge simulations (ζ_{sim}). Using the SRFs presented in [Figure 41](#), the SRF predictions (ζ_{srf}) were compared to the ADCIRC model simulation results (ζ_{sim}) and are shown in [Figure 42](#). At the elevation stations on the open coast, the root mean square errors (RMS) of ($\zeta_{srf} - \zeta_{sim}$) were estimated to be between 15 cm and 32 cm. This is consistent with the results obtained by [Irish et al. \(2009\)](#). Considering the accumulative error due to model computation is on the order of 20 to 30 cm ([Westerink et al., 2008](#)), the magnitude of RMS error between the two predictions is reasonable. Therefore, we concluded that the obtained SRFs for the 20 bridge locations represent the surge behavior along the Texas coast with a good accuracy. To better optimize SRF performance, further study on interaction between surges and a bay site environment is in process (Katyal, personal communications).

Note that all surge levels predicted by the SRFs are based on the surge data computed from the numerical model. In the ADCIRC simulations, only the hurricane wind stress and pressure forcing forced the surge. The SRFs thus do not account for additional water level due to wave radiation, astronomical tide, and surface water runoff. Finally, static topography was employed in the ADCIRC model so any additive flooding due to lowering of the barrier islands during storm is not included.

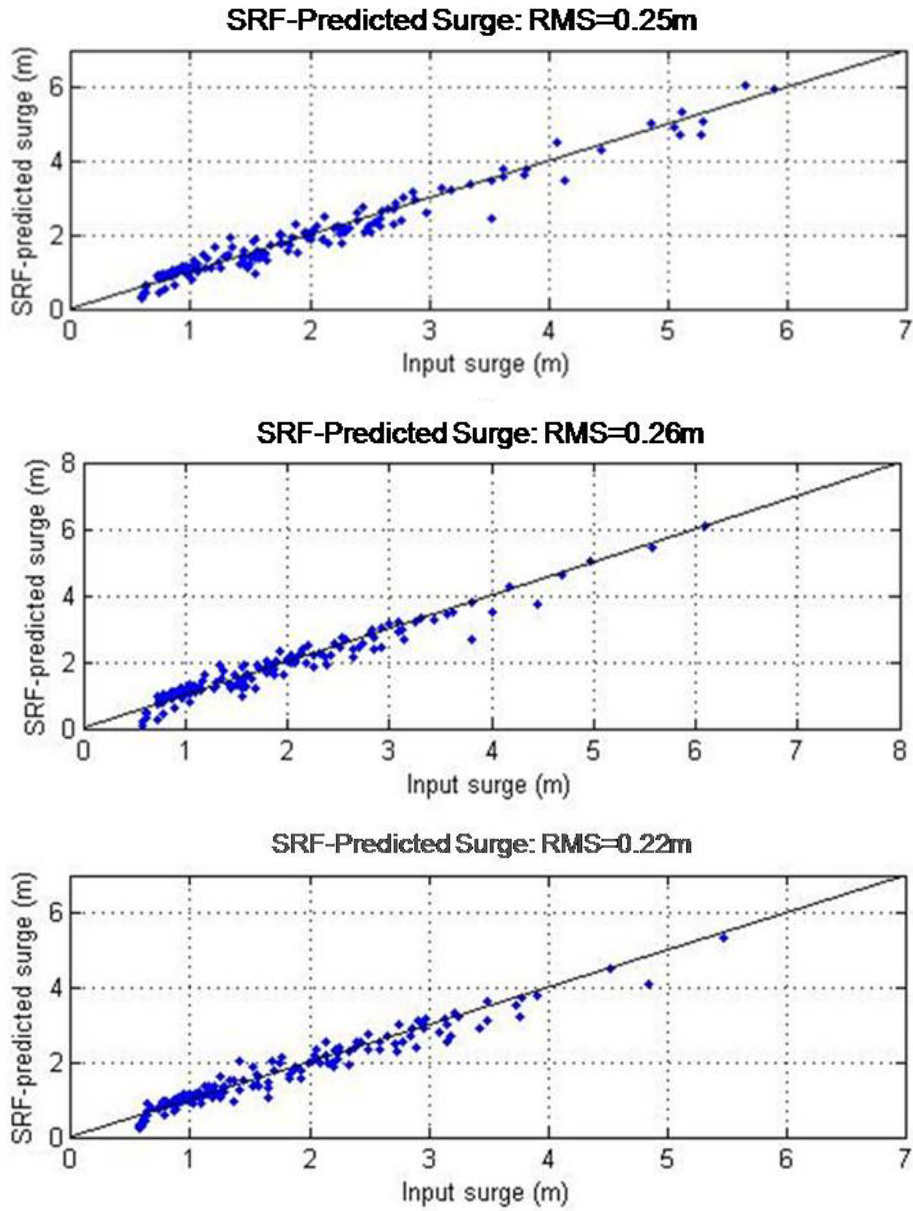


Figure 42. $\zeta_{srf} - \zeta_{sim}$ plots.

The values on the vertical axis are SRF surge predictions while those on the horizontal axis are ADCIRC surge simulation results. Rollover Pass (top), Galveston Causeway (middle), and San Luis Pass (bottom). Solid line indicates exact match.

CHAPTER 9: APPLICATION OF SURGE RESPONSE FUNCTION FOR PEAK SURGE ESTIMATION

Due to its continuous form over hurricane meteorological parameters, the SRF can be utilized to calculate storm surge levels at given locations for any hurricane, once the properties of storm size, intensity, and distance from a point of interest to the hurricane eye at landfall are known. For extreme surge analysis, the SRF was developed based on the peak surges extracted from the entire surface water level history from each ADCIRC simulation. Therefore, the surge prediction made by SRFs may be considered as the peak surge level at that location for the given hurricane meteorology.

To demonstrate and validate the use of the SRF methodology, storm surge predictions for two historical hurricanes (Carla in 1961 and Ike in 2008) were carried out. The SRF predicted surge levels were compared to high-water marks (HWMs) and water level gauge measurements taken during and after these hurricane events.

The focus of this study was to evaluate the extreme surge level response against hurricane forcing represented by the surface wind stress, pressure deficit, and their interaction with local bathymetry. Flood levels derived from other forcing mechanism were not included in the surges predicted by SRF. However, it is noted that processes including wave setup and tide can contribute substantially to overall flood elevation. Thus, when the SRF predictions are compared to observations, some of the differences between the two water levels were anticipated and can be attributed to the effects of wave setup, astronomical tide, land erosion, and runoff. For example, wave setup contributes approximately 10 percent to 20 percent of the total flood level at the open coast. In addition, there is inherently uncertainty with HWM data due to the nature of its collection with respect to debris lines, visual observations, and so forth. Moreover, it has to be noted that HWMs often include individual wave runup.

For comparison between SRF predicted peak surges and Hurricane Carla observations, HWMs given by debris or drift lines on the buildings were used. The HWMs were measured with respect to the Geodetic Vertical Datum (NGVD29), while the SRF predictions were made with respect to MSL. The HWM data were converted to MSL using datum information for the 1983-2001 tidal epoch. This conversion gives MSL to be higher than NGVD29 by about 0.2 m

in the vicinity of the Galveston and 0.3 m in the vicinity of Corpus Christi, based on the benchmark information for the NOAA Galveston Pier 21 and the NOAA Rockport, respectively.

For the comparison between SRF predicted peak surges and Hurricane Ike high-water levels, observed peak water levels based on the time history collected with pressure gauges were used. The water level time series were obtained from pressure gauges deployed by U.S. Geological Survey ([USGS 2005 and 2008](#)) prior to Hurricane Ike's passage. The water level data used for comparison were measured with respect to North America Vertical Datum (NAVD) of 1988. To make them comparable with SRF prediction, these data were converted to MSL. The benchmark data indicate MSL is higher than that measured with respect to NAVD88, about 0.35 m.

HURRICANE CARLA DESCRIPTION

Hurricane Carla was one of the most powerful hurricanes recorded in the United States, especially for the state of Texas. Hurricane Carla was first classified as a hurricane as it passed through the western Caribbean Sea on September 6, 1961, and this storm steadily evolved to a Category 5 hurricane while approaching the Texas coast in the Gulf of Mexico ([Figure 43](#)). At its landfall on September 11, 1961, between Port O'Connor and Port Lavaca in Texas, Carla was a Category 4 hurricane with a lowest pressure of 931 mb, maximum sustain wind speed of 64 m/s, and radius to maximum wind of 56 km ([NOAA, 2009](#)). As a large and intense hurricane moving slowly at 1.8 m/s, a wide span of the Texas coast from Port Lavaca to Galveston experienced some of the highest storm surges ever recorded in this area, 3.3-3.7 m ([NOAA, 2009](#)).

COMPARISON OF PEAK SRF PREDICTIONS WITH HIGH-WATER MARK OBSERVATIONS

Using the hurricane parameters for Hurricane Carla, SRF predictions were made and compared to the HWMs published by [NOAA \(1982\)](#). The peak storm surge levels evaluated from SRF prediction and observed from the HWMs, with respect to MSL, are listed in

Table 17. In addition, the surge levels listed in this table are also plotted on the same graph in order to visualize the comparison (Figure 44).

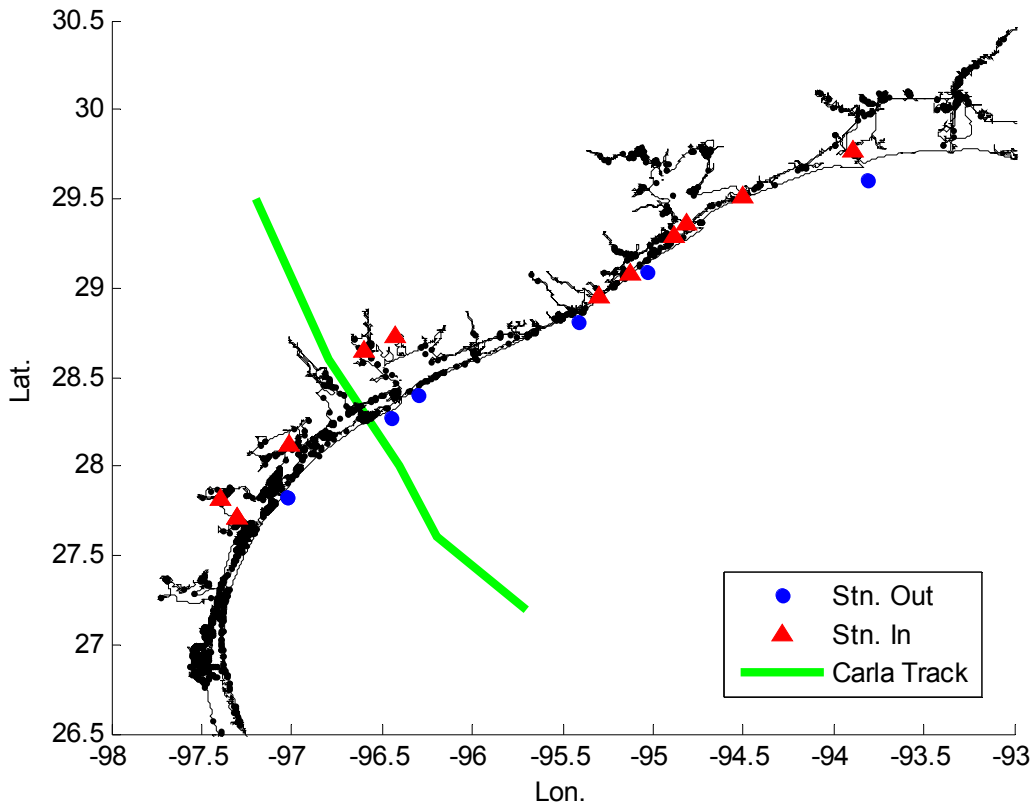


Figure 43. Hurricane Tracking Map and Elevation Stations.
SRF prediction was made at stations marked with triangles and compared to the HWM reported by National Weather Service, NOAA (1982) at the corresponding locations. The solid line shows the Hurricane Carla's storm track with respect to the elevation stations based on information from the Storm Pulse (2009).

Table 17. Hurricane Carla Surge Estimation from HWM and SRF.

Hurricane Carla Surge Comparison			
Station No.	distance from landfall [km]	HWM above MSL [m]	SRF Prediction [m]
51	-43.7	2.8	2.1
53	-41.6	1.6	1.4
58	-30.5	2.6	2.1
65	-16.2	2.0	1.9
77	9.5	3.4	2.5
83	20.6	2.9	2.9
84	20.6	4.5	3.8
88	25.9	5.4	5.2
110	71.2	3.1	3.6
117	80.5	3.7	4.1
127	92.9	3.1	3.8
132	97.0	3.5	3.7
141	111.5	2.5	2.5
147	120.8	2.7	2.6
157	133.5	2.7	3.1
179	164.5	2.5	2.9
182	166.2	2.0	2.1

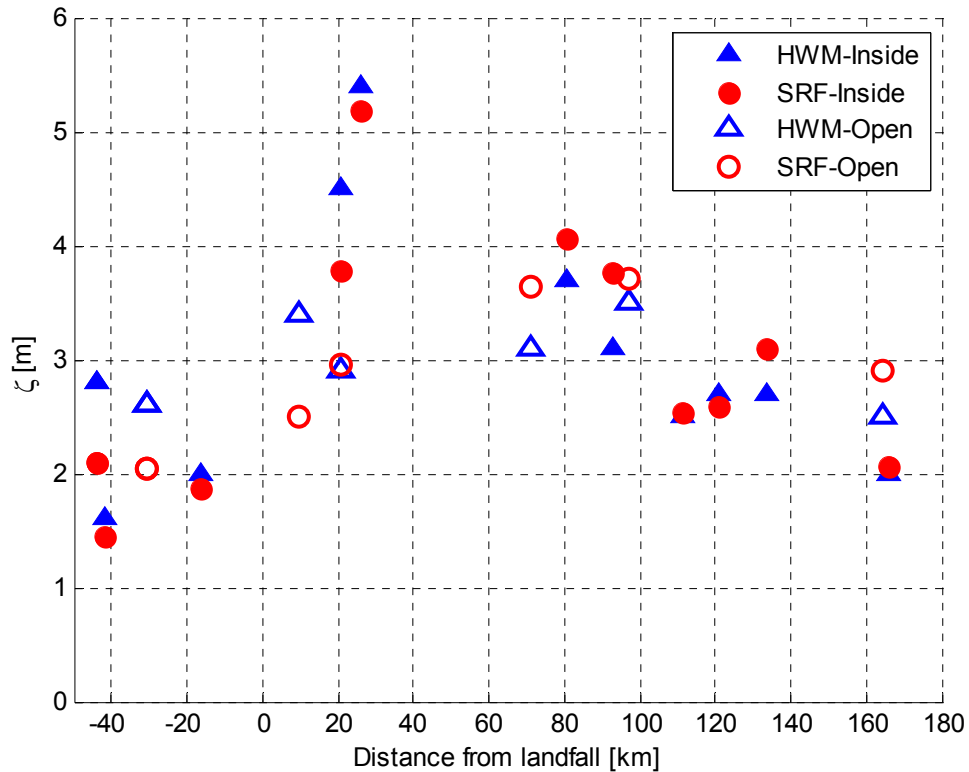


Figure 44. Comparison of the SRF Prediction to HWM for Hurricane Carla.
Surge levels were estimated with respect to MSL.

The comparison showed a clear correlation between the SRF predictions and the historical HWMs. Based on the pairs of data obtained at 17 stations located inside the coastal bays or along the open coast, the root-mean-square (RMS) error was estimated to be 48 cm, and a strong correlation, with the correlation coefficient of 0.87, between two data sources were found. The SRF predictions only include storm surge by wind and pressure deficit, whereas the HWMs include wave effects (i.e., setup and runup) and astronomical tides. The additional effects of waves and tides were more obvious when comparing the difference in surge levels at the stations located on the open coast (hollow marks on Figure 44) than with those located inside a coastal bays (solid marks on Figure 44). Also, the fact that the flood levels recorded through HWM are known to have a high degree of uncertainty may contribute to the differences in the two data sources.

HURRICANE IKE DESCRIPTION

On September 13, 2008, while this study was still in progress, Hurricane Ike struck the Galveston area and caused damage to several coastal bridges and roadways, including the Rollover Pass and Pelican Island Bridges. As Hurricane Ike began moving northwesterly into the Gulf of Mexico, it was upgraded to a Category 4 hurricane. Although Ike's intensity weakened to Category 2 by the time it made landfall at Galveston because of the wide extent of the hurricane force wind field, it resulted in huge storm surges along the Texas coast. Near landfall, the size of the eye was 58 km, the center pressure was 952 mb, and it approached the coast with the speed of 19.3 km/hr. With the given hurricane meteorology, surge predictions were made using the SRFs at several stations located near the eye of Hurricane Ike (Figure 46). The positions of these SRF stations were specified to correspond to the locations of the pressure monitoring probes deployed by USGS prior to Ike's landfall. The SRF predictions were compared to the peak measured water levels from the USGS gauges to verify its accuracy.

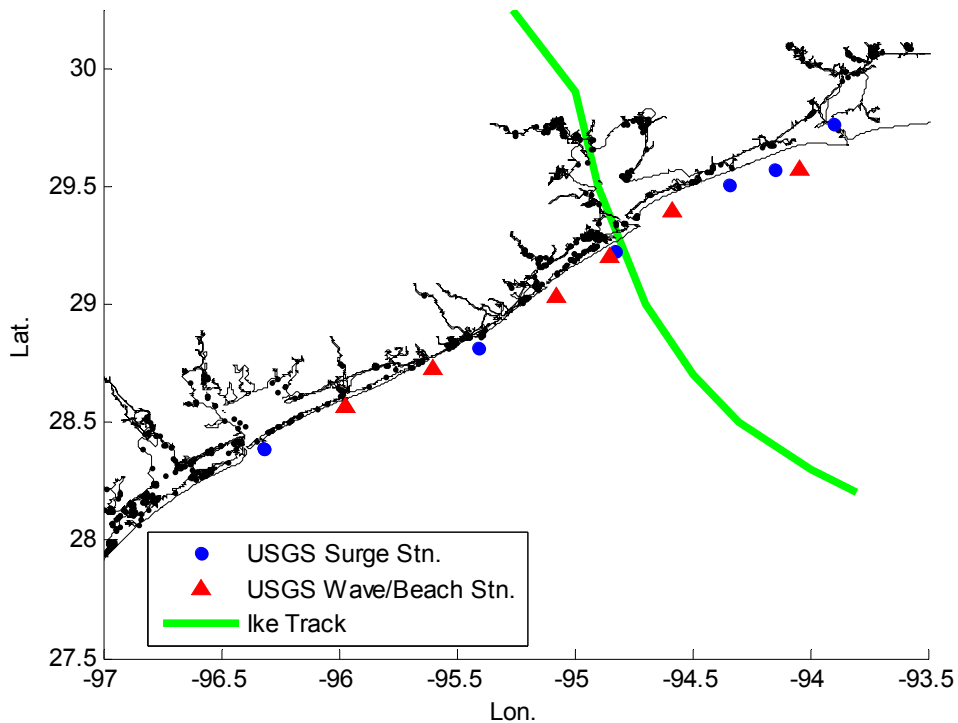


Figure 45. Hurricane Ike Tracking Map and Water Elevation Stations.

SRF predictions were made at stations marked with triangles and compared to the peak water levels measured by USGS (2008) at the corresponding locations. The solid line shows the hurricane storm track with respect to the elevation stations based on information from the National Hurricane Center.

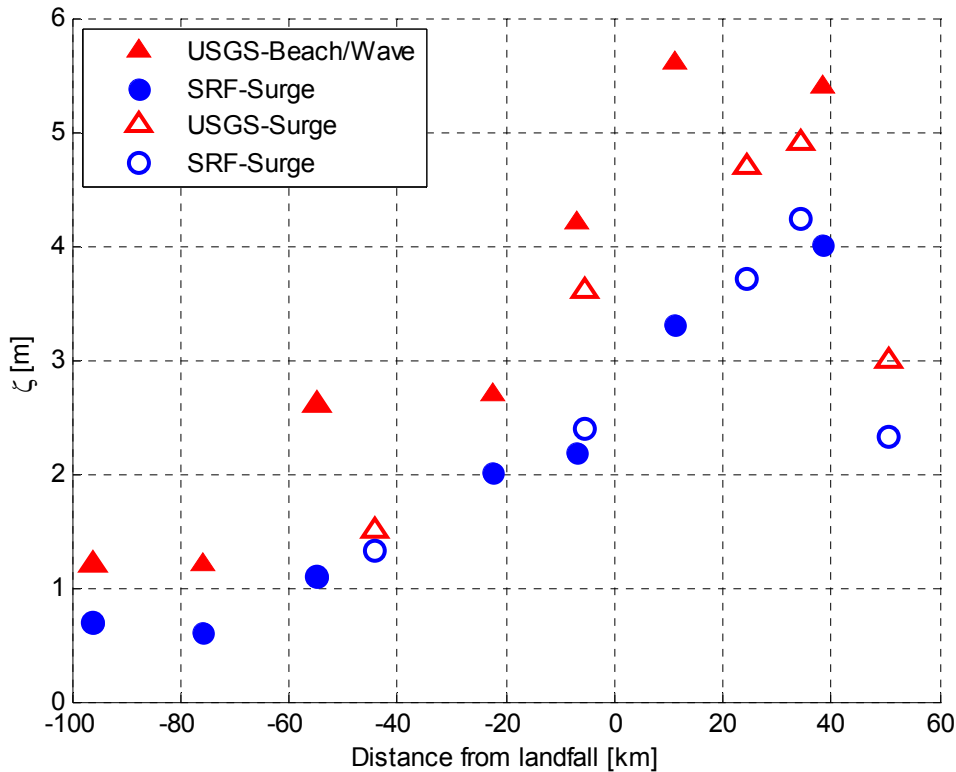
COMPARISON OF THE EXTREME SURGES FROM SRF PREDICTIONS WITH PEAK WATER LEVEL OBSERVATIONS

USGS (2008) has classified the site of recording the peak water level either as a surge station (hollow on Figure 46), or wave/beach station (solid on Figure 46) depending on the gauge configuration at the region. That is, in surge-type flooding the observed water level was presumed to be affected solely by the quasi-steady flood levels, including wave setup. On the other hand, some gauges that do not filter surface waves are classified as a wave/beach type (USGS, 2008). With this discrimination, the surge predictions from the SRFs were compared to the peak water levels at the USGS stations. To examine the alongshore variation in the surge levels, the wave/beach stations located on the open coast were selected. However, at some locations, where the wave/beach stations did not exist nearby, the outer-most surge type stations located behind barrier islands or in bays were selected. In this way, the distance between consecutive stations was kept relatively constant. The numerical prediction results are listed in Table 18 and they are plotted in Figure 46.

The data comparison shows a strong correlation, with a correlation coefficient 0.93, between the SRF predicted values and the USGS measurements. Although the RMS for the 12 measurements is 75 cm, this was anticipated since the SRF predictions did not include the effect of wave setup or tides. However, since the effect of wave setup is smaller behind the barrier islands, much smaller differences between the SRF prediction and the surge-type flood levels are seen; the RMS error is reduced to 43 cm. In addition, larger discrepancies between two sets of data and wider scattering in the USGS data are seen in the data distribution at the east side of Galveston compared to that at the west side stations. Considering the SRF prediction still shows consistency in the surge level trend, the increase of inconsistency between SRF predictions and USGS observations near and on the right side of the hurricane landfall may be explained by the effect of the changes in geographical features such as lowering of barrier islands due to relatively stronger hurricane impact in the east part of Galveston.

Table 18. Hurricane Ike Surge Estimation from Peak Surges and SRF.

Hurricane Ike Surge Predictions			
Station No.	SRF Prediction [ft]	HWM above MSL [m]	SRF Prediction [m]
82	3.0	1.2	0.9
94	2.4	1.2	0.7
105	5.1	2.6	1.6
110	6.3	1.5	1.9
126	8.7	2.7	2.7
138	9.0	4.2	2.7
139	9.8	3.6	3.0
151	13.1	5.6	4.0
161	14.5	4.7	4.4
167	16.3	4.9	5.0
170	16.5	5.4	5.0
182	11.2	3.0	3.4



Surge levels were estimated with respect to MSL at the elevation stations.

Figure 46. Comparison of the SRF Prediction to Peak Water Level Record during Hurricane Ike.

DISCUSSION OF THE COMPARISONS

The two sets of comparisons between the SRF predictions and field measurements demonstrated the performance of SRF in capturing the surge response trends with alongshore spatial changes. In particular, the information on the spatial variation in storm surge levels, produced by the SRFs, can be used in predicting the maximum flooding suspected location, along with the peak surge levels at that location. Furthermore, the surges predicted using several SRFs for a given hurricane condition showed a clear correlation with the observed data for the two hurricanes considered. Owing to the SRF method's ability to utilize any set of hurricane meteorological conditions by turning into the dimensionless input into a dimensionless surge, the study of two hurricanes with different meteorological conditions, making landfall at two different locations along the Texas coast, proved that SRF can be applied for accurate storm surge predictions over a wide range of hurricane conditions.

On the other hand, the SRF method presented here was developed to predict storm surge behavior with respect to the hurricane wind and pressure fields. The storm surge predictions made by these SRFs do not include additional surges generated by wave breaking (wave setup), astronomical tides, and additional flooding induced by changes to geographical features (dune slope change and lowering of the barrier island) during the hurricane events. The exclusion of these factors in the SRFs, in addition to potential errors in the field measurements themselves, introduces a bias between the SRF predictions and the observed data, particularly along the open coast. However, even with the expected bias, the alongshore distributions between two sets of data showed strong correlation. That indicates the difference in flood levels between the two sources of data can be justified by the factors mentioned above. While the SRF method is based on parameterized meteorology, which does not account for natural variability in the hurricane wind field, the relatively good correlation between the SRF predictions and the measurements gives a strong indication that the SRF method is robust enough for general engineering applications.

APPLICATION OF SRF METHOD FOR FLOOD PROBABILITY ESTIMATION

In this study, the water surface response against hurricane meteorology was predicted through the SRF method at 20 Texas coastal bridges. Besides its capability to predict the surge levels for given hurricane conditions, the SRF method has further potential to be applied for flood probability analysis.

We may specify a possible range of properties for the hurricane meteorological parameters at a location of interest in this study such as a coastal region in the Gulf of Mexico. Since SRF is represented by a continuous function with respect to dimensionless parameters based on scaled hurricane meteorological parameters, a set of any given properties for each hurricane parameter can be used as input to the SRF. The set of possible properties for the hurricane meteorology in the region can be converted to form the input sets for SRF. Consequently, peak surge elevations corresponding to the combination of the hurricane properties can be estimated from the SRF.

For illustration, we may consider the possible range of intensities and sizes in the Gulf of Mexico to be from 870 mb, a maximum potential tropical cyclone intensity (MPI) (Tonkin et al., 2000), to 960 mb and from 8 km to 120 km, respectively. We may further assume that we are

interested in surge flood levels generated from storms making landfall within 200 km to the location of interest. Using the SRFs developed earlier, the peak surge levels over this range of conditions can be calculated at the intersection of each R_p , c_p , and x_o set. The surge response surface generated for the selected conditions are represented in the The surge response surfaces were generated from the storm of $cp = 960$ mb, $cp = 930$ mb, $cp = 900$ mb, and $cp = 870$ mb from the top to the bottom, respectively.

In [Figure 47](#), notice that the vertical height at any point on the surface represents the surge levels estimated based on the corresponding given conditions. Therefore, the surge response surfaces indeed represent all possible flood levels due to the entire hurricane meteorology range considered a function of R_p , c_p , and x_o with respect to a fixed location determines the continuous surge response surfaces. The surge response surfaces from the storm of $cp = 960$ mb, $cp = 930$ mb, $c_p = 900$ mb, and $cp = 870$ mb on The surge response surfaces were generated from the storm of $cp = 960$ mb, $cp = 930$ mb, $cp = 900$ mb, and $cp = 870$ mb from the top to the bottom, respectively. Data in [Figure 51](#) are accumulated.

In [Figure 48](#), one should notice that the crest of each surge response surface represents the optimal hurricane condition for generating the highest surge. That is, for a given set of R_p and c_p , the SRF developed at an arbitrary location of interest provides the information on the potential location at which the maximum hurricane flooding may take place, as well as the peak surge level at that location. For extreme-value analysis, it is useful to identify the maximum possible hurricane anticipated at a location of interest. This would provide an upper bound to the stage-frequency (water-level versus return period) distribution. This is the strength of JPM-OS since a logical upper limit on hurricane intensity does exist; based on MPI, a maximum possible surge can be identified. To demonstrate the use of SRF for identifying this upper limit, maximum possible surge levels were calculated at all three bridge locations based on the SRFs presented earlier ([Table 19](#)).

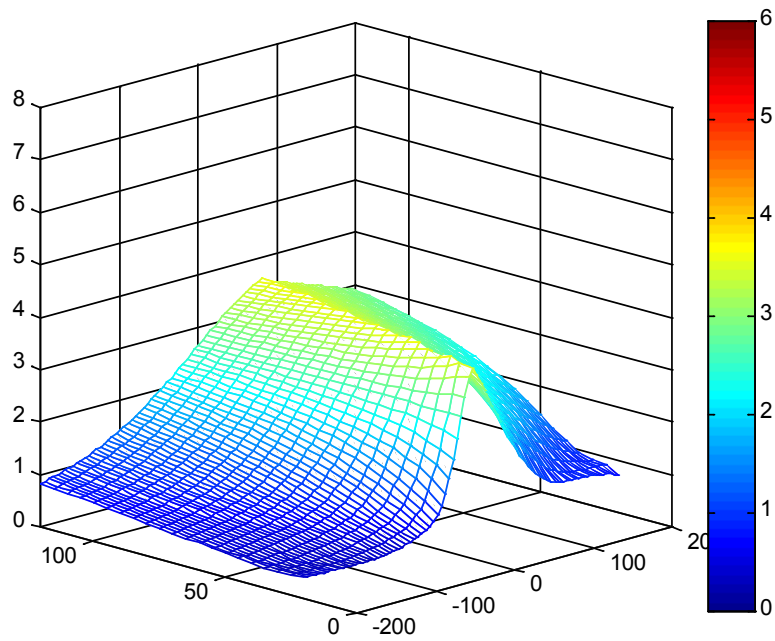
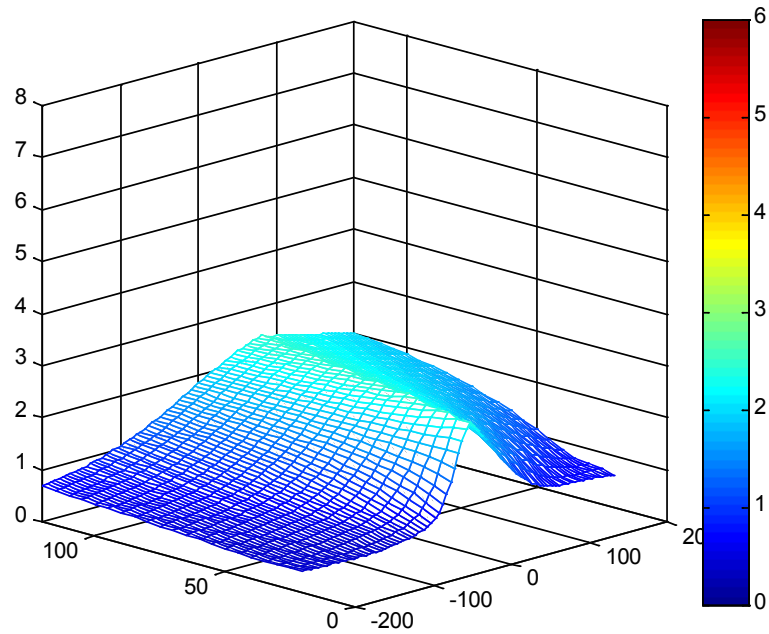


Figure 47. Surge Response Surface Estimated with Respect to the Variation of R_p and x_0 at a Fixed Location.

The surge response surfaces were generated from the storm of $c_p = 960$ mb, $c_p = 930$ mb, $c_p = 900$ mb, and $c_p = 870$ mb from the top to the bottom, respectively.

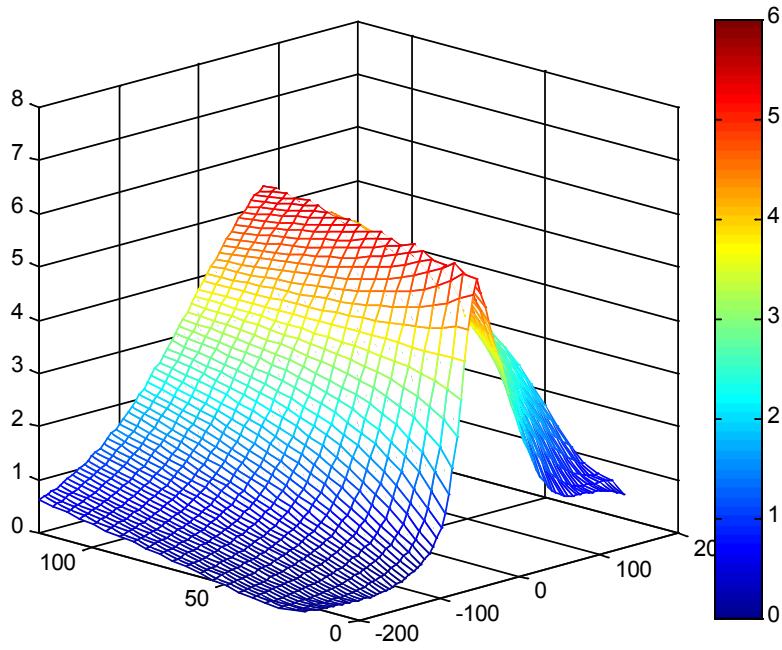
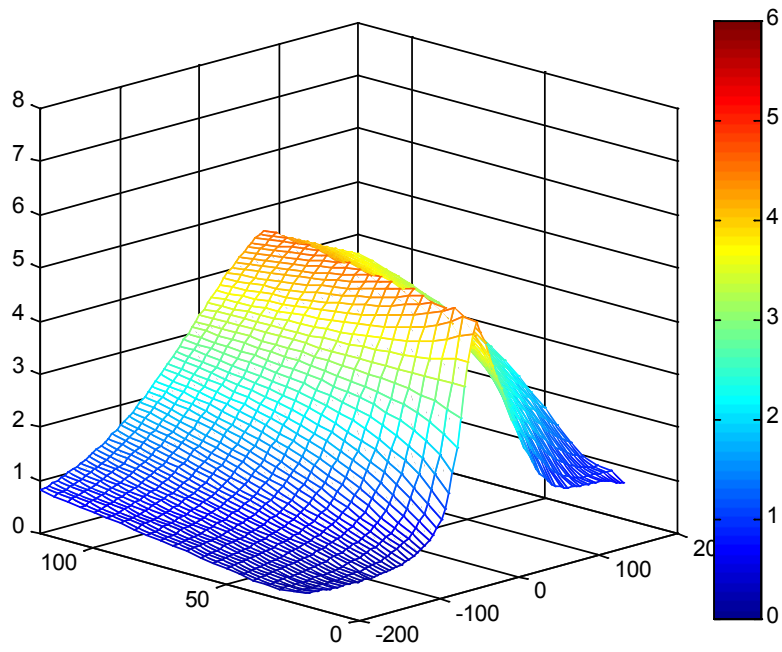


Figure 51. Surge Response Surface Estimated with Respect to the Variation of R_p and x_o at a Fixed Location (Continued).

Table 19. SRF Extreme Surge Predictions at Three Bridges in Galveston.

Bridges	ζ_{max} [m]	c_p [†] [mb]	R_p ^{††} [km]	Peak dist.** [km]
San Luis Pass	6.7	870	50	47.5
Galveston Causeway	5.0	870	116	110
Rollover Pass	7.2	870	44	30

* ζ = Peak surge level due to hurricane of given intensity and size

** Peak dist. = Distance between the bridge and the hurricane landfall that results in the maximum storm surge at the bridge

† c_p = Center pressure of the hurricane in millibar

†† R_p = Radius (size) of the hurricane

In combination with the JPM-OS, SRF can be utilized to estimate flood probability over a full range of hurricane possibilities. According to the JPM-OS method, the storm surge level at a location of interest can be evaluated by the joint probability of the optimally selected meteorological parameters (see Eqn. 4.5). [Niedoroda et al. \(2007 and 2008\)](#) described application of JPM-OS for the flood probability through the documentation of the Mississippi Coastal Flooding Hazard project. Based on a wide review of the history of hurricane meteorology and a series of 228 hurricane simulations, [Niedoroda et al. \(2007\)](#) produced statistical estimation of hurricane surge frequencies and flood level distributions over the coastal regions in Mississippi.

The methodology applied by [Niedoroda et al. \(2007 and 2008\)](#) can be modified to suit the flood probability analysis for a wide range of coastal regions along the entire Texas coast if using the SRF. The approach may be developed from the idea that we may use the SRF developed previously, along with the statistical joint probabilities among the hurricane size (R_p), intensity (c_p) and relative distance from the eye of storm landfall to the location of interest (x_o).

The total range of surge elevation depicted in [Figure 48](#) can be discretized into several infinitesimal bins representing each elevation range. Since the surface in [Figure 48](#) represents all possible flood levels anticipated from the hurricane meteorology of consideration, by associating each point on the response surface into corresponding bins of elevation range the total surge response surface is now transformed to a probability density function for surge. Therefore, with the optimally sampled input properties of the major hurricane meteorological parameters the flood level statistics can be determined.

Furthermore, SRF involves site-dependent parameters such as the size parameter λ and intensity slope m_x , as discussed previously. These parameters determine the shape of surge distribution at a specific location. Therefore, the SRF defined at a region of interest, such as the location of one of the coastal bridges along the Texas coast, provides a means for analyzing the storm surge frequencies that reflect both the meteorological conditions and geographical features.

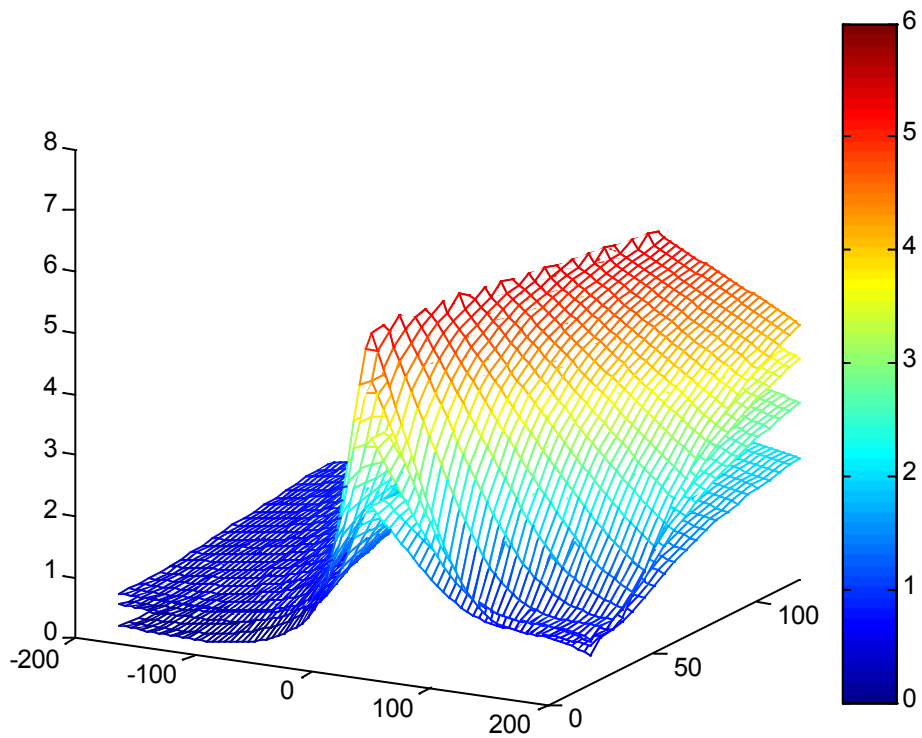


Figure 48. Combined Surge Response Surfaces.

A function of R_p , c_p , and x_o with respect to a fixed location determines the continuous surge response surfaces. The surge response surfaces from the storm of $c_p = 960$ mb, $c_p = 930$ mb, $c_p = 900$ mb, and $c_p = 870$ mb on The surge response surfaces were generated from the storm of $c_p = 960$ mb, $c_p = 930$ mb, $c_p = 900$ mb, and $c_p = 870$ mb from the top to the bottom, respectively.

CHAPTER 10: SUMMARY AND DISCUSSION

Site specific wave parameters (wave height and wave period) have been developed for four bridges along Texas coast. These parameters are developed using results of numerical simulations of wave and storm surge performed at combinations of different hurricane wind and storm surge levels. We observed that extreme wave heights at these four bridges generally increase with hurricane wind speed and storm surge level. At Rollover Pass Bridge, the wave heights are less sensitive to wind speed.

Hurricane Ike provided us an opportunity to validate the capability of the numerical models we used for wave and storm surge simulations. Comparisons between model results and measured wave height and high water mark data indicated that the wave model SWAN and storm surge model ADCIRC are capable of reproduce the extreme wave conditions during Hurricane Ike with high accuracy.

Flood levels derived by hurricane meteorology were estimated near the locations of 20 vulnerable bridges widely spread throughout the Texas coast. To incorporate the wide range of study area with minimum computational workload, the SRF method was optimized for accurate surge predictions. Based on the numerical storm surge simulations of more than 105 storms traveling over 15 parallel tracks, 20 SRFs were developed to characterize storm surge behavior at each target bridge location along the Texas coast. The SRFs performed surge prediction is within 30 cm RMS error range in comparison to the numerically simulated surge levels. Considering the model computation accuracy is in the order of 20 to 30 cm, it was concluded that the obtained SRFs are capable of providing accurate surge prediction in the region of interest.

The capability of SRF in capturing the spatial trends of storm surge for a given hurricane condition was proved through comparison to the historical storm surge records (Carla in 1961 and Ike in 2008). In addition, the application of SRF for the extreme-value analysis of storm surge was demonstrated. The peak surge levels expected at the bridge locations were estimated accordingly to various hurricane conditions assumed based on the hurricane meteorology typically observed in the Gulf of Mexico. From this analysis, it was shown that the SRF can be used to predict the relative distance between the hurricane landfall and the location of the

maximum flooding expected on the given hurricane meteorology. In addition, it can also predict peak surge levels.

Study was undertaken to optimize the use of SRF to produce peak surge predictions over a wide range hurricane meteorological conditions along the Texas coast. The effects of shoreline orientation, storm forward speed, and interaction with complex geographical features inside a bay were considered as insignificant on storm surge response. Such simplifications were justified by partitioning off the entire study area into three regions, within which the assumption of the slowly varying geographical feature is applicable. However, in order to make wide use of SRF methodology and improve the credibility in the predictions from SRF, research to account for the listed variability in the hurricane meteorology and the regional geography remains to be conducted. Moreover, the prediction made by SRF does not include certain forcing factors, such as wave radiation and astronomical tide. For engineering applications, hurricane impact should be evaluated after coupling with the excluded forcing factors by utilizing the SRF surge prediction as an initial estimation. Finally, in order to apply the SRF method for storm surge hazard analysis, further incorporation with the statistical application has to be made.

In 2008, AASHTO published *Guide Specifications for Bridges Vulnerable to Coastal Storms*, which provided equations for computation of wave forces on coastal bridges. The results obtained in this project will enable TxDOT to quickly implement the equations in AASHTO guidelines to determine wave forces on the four bridges studied in this project.

REFERENCES

- AASHTO. (2008) *Guide Specifications for Bridges Vulnerable to Coastal Storms*, American Association of State Highway and Transportation Officials, Washington, D.C.
- Aldama, A., Aguilar, A., Kolar, R., and Westerink, J.J. (2000) “A mass conservation analysis of the GWCE formulation.” *Computational Methods in Water Resources*, 2, 907-912.
- ASCE TCLEE. (2006) “Performance of Transportation Systems During Hurricane Katrina,” draft report, American Society of Civil Engineers, Reston, Virginia.
- Booij, N., Ris, R.C., and Holthuijsen, L.H. (1999) “A Third-Generation Wave Model for Coastal Regions, 1, Model Description and Validation.” *J. Geophys. Res.*, 104(C4), 7649-7666.
- Booij, N., Holthuijsen L.H., Doorn, N. and Kieftenburg, A.T.M.M. (1997) “Diffraction in a spectral wave model.” *Proc. 3rd Intl. Symposium Ocean Wave Measurement and Analysis WAVES 97*, ASCE, New York , pp. 243–255.
- Borgman, L.E., Miller, M., Butler, L., and Reinhard R. (1992) “Empirical simulation of future hurricane storm histories as a tool in engineering and economic analysis.” *Proceedings of 5th International conference of Civil Engineering in the Ocean*, College Station, Texas, 42-65.
- Cardone, V.J., Greenwood, C.V., and Greenwood, J.A. (1992) “Unified program for the specification of hurricane boundary layer winds over surfaces of specified roughness.” *Contract Report CERC-92-1*, U.S. Army Corps of Engineers, Vicksburg, Miss.
- Chow, S.H. (1971) “A study of the wind field in the planetary boundary layer of a moving tropical cyclone,” M.S. Thesis, New York University, New York.
- Collins, E. (2006) “One year later: the repair/rebuild efforts following Hurricane Katrina.” *GoStructural.com*, Online article. <http://www.gostructural.com/article.asp?id=1092>.

- Douglass, S.L., Lindstrom, J., Richards, J.M., and Shaw, J. (2005) “An estimate of the extent of U.S. coastal highways.” Presentation to Transportation Research Board, Hydraulics, Hydrology, and Water Quality Committee Meeting, Washington D.C., Online.
<http://www.southalabama.edu/usacterrec/chighwayestimate.pdf>.
- Google satellite images. (2009a) “Locations of twenty target bridges along Texas coast (red dots).” 1 May. 2009. <http://earth.google.com>.
- Google satellite images. (2009b) “Bridges (the red circles) near the eastern boundary of the Texas coast.” 11 Feb. 2009, <http://earth.google.com>.
- Google satellite images. (2009c) “A bridge (the red circle) at Rollover Pass in Galveston.” 11 Feb. 2009, <http://earth.google.com>.
- Google satellite images. (2009d) “Bridges (the red circles) near the entrance of Galveston Bay” 11 Feb. 2009, <http://earth.google.com>.
- Google satellite images. (2009e) “Bridges (the red circles) of FM 2004 Road (top), and San Luis Pass (bottom) in Galveston.” 11 Feb. 2009, <http://earth.google.com>.
- Google satellite images. (2009f) “Bridges (the red circles) on FM1495 Road (left) and Hwy 332 (right) near Freeport.” 11 Feb. 2009, <http://earth.google.com>.
- Google satellite images. (2009g) “Bridges (the red circles) along Highway 35 in Matagorda Bay.” 11 Feb. 2009, <http://earth.google.com>.
- Google satellite images. (2009h) “A bridge (the red circles) on Lyndon B. Johnson Causeway in Aransas.” 11 Feb. 2009, <http://earth.google.com>.
- Google satellite images. (2009i) “Bridges in Corpus Christi.” 11 Feb. 2009, <http://earth.google.com>.
- Google satellite images. (2009j) “Location (marked by maroon dots) of two damaged bridges in Galveston during Hurricane Ike.” 1 May. 2009, <http://earth.google.com>.
- Gray, W.G. (1982) “Some inadequacies of finite element models.” *Adv. Water Resources*, 5(September), 171-177.

- Gulf Coast Information System. (2006) "Highway 90 bridge damage." Hurricane Katrina damage photos - Mississippi Gulf Coast, Online photos, <http://www.gulf-coast.com/Katrina-Information/Katrina-Pictures/HurricaneKatrinaPictures-2.html>.
- Gumbel, E.J. (1959) "Statistics of Extremes." Oxford University Press, London.
- Ho, F.P., and Myers, V.A. (1975) "Joint Probability Method of Tide Frequency Analysis Applied to Apalachicola Bay and St. George Sound, Florida." *NOAA Technical Report NWS18*, Silver Spring, Maryland.
- Holland, G.J. (1980) "An analytic model of the wind and pressure profiles in hurricanes." *Monthly Weather Review*, 108(80), 1212-1218.
- Irish, J.L., and Cañizares, R., (2009) "Storm-wave flow through tidal inlets and its influence on bay flooding." *J. Waterways Port, Coastal and Ocean Eng.*, 135(2), 52-60.
- Irish, J.L., Resio, D.T., and Cialone, M.A. (2009) "A surge response function approach to coastal hazard assessment—Part 2: quantification of spatial attributes of response functions." *Nat Hazards*, doi: 10.1007/s11069-009-9381-4.
- Irish, J.L., Resio, D.T., and Ratcliff, J.J. (2008) "The influence of storm size on hurricane surge." *J. Phys. Oceanogr.*, 38(9), 2003-2013.
- Irish, J.L., and Resio, D.T. (2009) "A hydrodynamics-based surge scale for hurricanes." *Ocean Eng.*, in press.
- Jones, L. (2009, March 19) "Pelican Island Bridge repair work stuck between agencies." *The Daily News*, Galveston. Online. <http://galvestondailynews.com/story.lasso?ewcd=7d25b30b4537fa83>.
- Kinmark, I.P.E. and Gray, W.G. (1984) "The $2\Delta x$ -test: A tool for analyzing spurious oscillations." *Adv. Water Resources*, 8 (September), 129-135.
- Kolar, R.L. and Westerink, J.J. (2000) "A look back at 20 years of GWC-based shallow water models." *Computational Methods in Water Resources* 2(8), 899-906.

- Luettich, R.A., Westerink, J.J., and Scheffner, N.W. (1991) “ADCIRC: An advanced three-dimensional circulation model for shelves, coasts, and estuaries: Report 1: theory and methodology of ADCIRC-2DDI and ADCIRC-3DL,” *Technical Report DRP-92-6*, U.S. Army Corps of Engineers, Washington, D.C.
- Lynch, D.R. (1983) “Progress in hydrodynamic modeling review of U.S. contributions, 1979-1982.” *Rev. Geophys, Space Phys*, 21(3), 741-754.
- Lynch, D.R. and Gray W.G. (1979) “A wave equation model for finite element tidal computations.” *Comput. Fluids* 7, 207–228.
- National Weather Service. (1982) “Pertinent Meteorological and Hurricane Tide Data for Hurricane Carla”, NOAA Technical Report NWS 32, Silver Spring, Md, August 1982
- National Weather Service. (2008) “Hurricane IKE advisory archive: Advisory 48 ”, National Hurricane Center. Online. <http://www.nhc.noaa.gov/archive/2008/IKE.shtml>.
- Navon, I.M. (1988) “ A review of finite-element methods for solving the shallow-water equations.” *Computer Modeling in Ocean Engineering*, 273-278.
- Niedoroda A.W., Resio, D., Toro, G., Divoky, D., and Reed, C. (2008) “Efficient strategies for the joint probability evaluation of storm surge hazards.” *Proceedings of Solution to Coastal Disasters Congress 2008*, 242-255.
- Niedoroda, A.W., Resio, D., Toro, G., Divoky, D., Das, H., and Reed, C. (2007) “Evaluation of the storm surge hazard in coastal Mississippi.” *Proceedings of 10th International Workshop on Wave Hindcasting and Forecasting and Coastal Hazards, 2007*, Oahu, Hawaii.
- NOAA. (1982) “Pertinent meteorological and hurricane tide data for Hurricane Carl.” *Technical Report NWS32*, Silver Spring, Maryland.
- NOAA. (2009 June 1) “Hurricane Carla.” Hurricane history. Online. <http://www.srh.noaa.gov/crp/docs/research/hurrhistory/Carla/carla.html>.

- Padgett, J., Roches, R.D., Nielson, B., Yashinsky, M., Kwon, O.S., Burdette, N., and Tavera, E. (2008) "Bridge damage and repair costs from Hurricane Katrina." *Journal of Bridge Engineering* 13(1), 6-14.
- Powell, M.D. and Reinhold, T.A. (2007) "Tropical cyclone destructive potential by integrated kinetic energy." *Bull. Amer. Meteor. Soc.*, 88, 513-526.
- Public Information Office of Texas Department of Transportation. (2008) "TxDOT Responds to Hurricane Ike." Houston, Texas, online at Newsrouter.com.
http://www.newsrouter.com/NewsRouter_Uploads/67/TexDOT.pdf.
- Rappleye, C. (2008, October 8) "Repairs to start on Rollover Pass Bridge." *Beaumont Enterprise*. Online. http://www.beaumontenterprise.com/news/local/repairs_to_start_on_rollover_pass_bridge_10-08-2008.html
- Resio D.T. and Westerink, J.J. (2008) "Modeling the physics of storm surges." *Physics Today*, 61(99), 33.
- Resio, D.T., Irish, L.J., and Cialone, M. (2009) "A surge response function approach to coastal hazard assessment. Part 1: Basic concepts." *Nat. Hazards*, 2009, doi: 10.1007/s11069-009-9379-y.
- Ris, R.C.(1997) "Spectral Modeling of Wind Waves in Coastal Areas," Thesis, Delft University of Technology, Delft University Press.
- Ris, R.C., Booij, N., Holthuijsen, L.H., Padilla-Hernandez, R., and Haagsma, J. G. (1998) "SWAN Cycle 2 Users' Manual." For SWAN version 30.75, Unauthorized Electronic Version, Delft Univ. Techn.
- Ris, R.C., Holthuijsen, L.H. and Booij, N. (1999) "A Third-Generation Wave Model for Coastal Regions, 2, Verification." *J. Geophys. Res.*, 104, C4, 7667-7681.
- Rogers, W.E., Kaihatu, J.M., Petit, H., Booij, N., and Holthuijsen, L.H. (2002) "Diffusion reduction in an arbitrary scale third generation wind wave model", *Ocean Engg*, 1357-1390.

- Scheffner, N., Borgman, L., and Mark, D. (1996) "Empirical simulation technique applications to a tropical storm surge frequency analysis of the coast of Delaware." *Journal of Waterway, Port, Coastal, and Ocean Engineering*, 122(2).
- Storm Pulse (2009) "Hurricane Carla Tracking Map", available online at <http://www.stormpulse.com/hurricane-carla-1961>.
- Talbot, J. (2005) "Repairing Florida's Escambia Bay Bridge," Associated Construction Publications, available online at <http://www.acppubs.com/article/CA511040.html>, March 2005.
- Thompson, E.F., and Cardone, V.J. (1996) "Practical modeling of hurricane surface wind fields." *Journal of Waterways, Port, Coastal, and Ocean Engineering*, July/August 1996, 198-205.
- Tonkin, H., Holland, G.J., Holbrook, J., and Henderson-Sellers, A. (2000) "An evaluation of thermodynamic estimates of climatological maximum potential tropical cyclone intensity." *Monthly Weather Review*, 128(March 2000), 746-762.
- U.S. Department of Commerce. (1959) "Meteorological consideration pertinent to standard project hurricane, Atlantic and Gulf Coasts of the United States." *National Hurricane Research Project Rep. 33*, Washington, D.C.
- U.S. Department of Commerce. (1972) "Memorandum HUR-7-120, Revised standard project hurricane criteria for the Atlantic and Gulf Coasts of the United States." *National Hurricane Research Project HUR-7-120*, New Orleans.
- U.S. Department of Commerce. (1979) "Meteorological criteria for standard project hurricane and probable maximum hurricane wind fields, Gulf and East Coasts of the United States.", *NOAA Tech Rep NWS 23*, Washington, D.C.
- U.N. Atlas of the Oceans (2000). "Human settlements on the coast." *USES. Online*. <http://www.oceansatlas.org/servlet/CDSServlet?status=ND10b3Bkb3duJjY9ZW4mMzM9KiYzNz1rb3M~>.

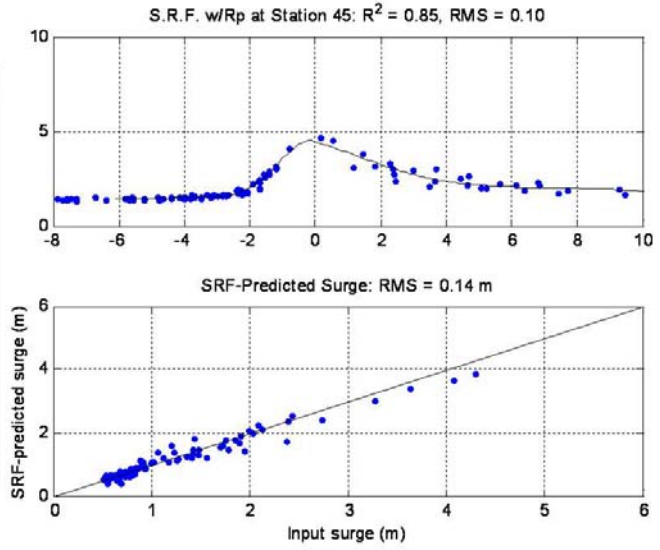
- USACE. (2002) "Coastal Engineering Manual," Engineering Manual 1110-2-1100, U.S. Army Corps of Engineers, Washington, D.C. (in 6 volumes).
- USGS. (2005) "Hurricane Rita surge data, southwestern Louisiana and southeastern Texas, September to November 2005." *Data Series 220*, Reston, VA.
- USGS. (2008) "Monitoring inland storm surge and flooding from Hurricane Ike in Texas and Louisiana, September 2008," *U.S. Geological Survey Open-File Report 2008-1365*, Online. <http://pubs.usgs.gov/of/2008/1365>.
- Westerink, J.J., Luettich, R. A., Feyen, J.C., Atkinson, J.H., Dawson, C., Roberts, H.J., Powell, M.D., Dunion, J.P., Kubatko, E.J., and Pourtaheri, H. (2008). "A basin- to channel-scale unstructured grid hurricane storm surge model applied to southern Louisiana." *Monthly Weather Review*, 136, March 2008, 833-864.
- Westerink J.J., Luettich, R. A., and Scheffner N.W. (1994) "ADCIRC: An advanced three-dimensional circulation model for shelves, coasts, and estuaries: Report 4: Hurricane storm surge modeling using large domains." *Technical Report DRP-92-6*, U.S. Army Corps of Engineers, Washington, D.C.
- Westerink, J.J. and Gray, W.G. (1991) "Progress in surface water modeling." *Reviews of Geophysics*, 29, 210-217.
- Westerink, J. J., Muccino, J. C., and Luettich, R. A. (1991) "Tide and storm surge computations for the Western North Atlantic and Gulf of Mexico." *Estuarine and coastal modeling*, 538-550.
- Westerink, J.J., Luettich, R.A., Baptista, A.M., Scheffner, N.W., and Farrar, P. (1992) "Tide and storm surge predictions using finite element model." *Journal of Hydraulic Engineering*, 118(10), 1373-1390.
- Westerink, J.J., Luettich, R.A., Feyen, J.C., Atkinson, J.H., Dawson, C., Roberts, H.J., Powell, M.D., Dunion, J.P., Kubatko, E.J., and Pourtaheri, H. (2008) "A basin- to channel-scale unstructured grid hurricane storm surge model applied to southern Louisiana." *Monthly Weather Review*, 136, March 2008, 833-864.

Zubier, K., Panchang, V.G. and Demirbilek, Z. (2003) "Simulation of Waves at Duck (North Carolina) Using Two Numerical Models." *Coastal Engineering Journal*, 45(3), 439-469.

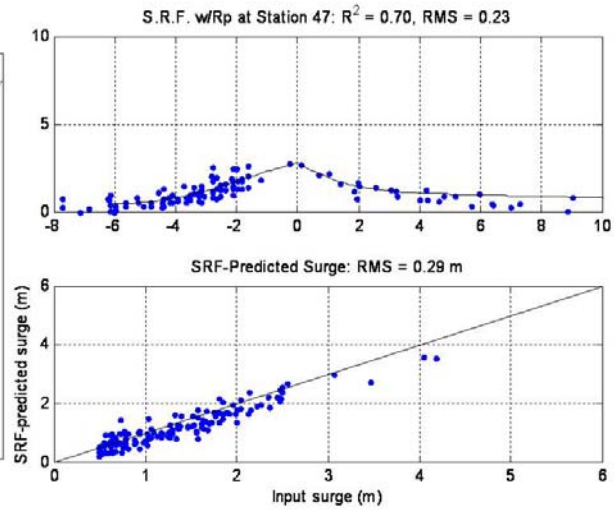
**APPENDIX:
SURGE RESPONSE FUNCTION DEVELOPED
NEAR 17 TEXAS COASTAL BRIDGES**

Table 20. Locations of the 17 Selected Coastal Bridges.

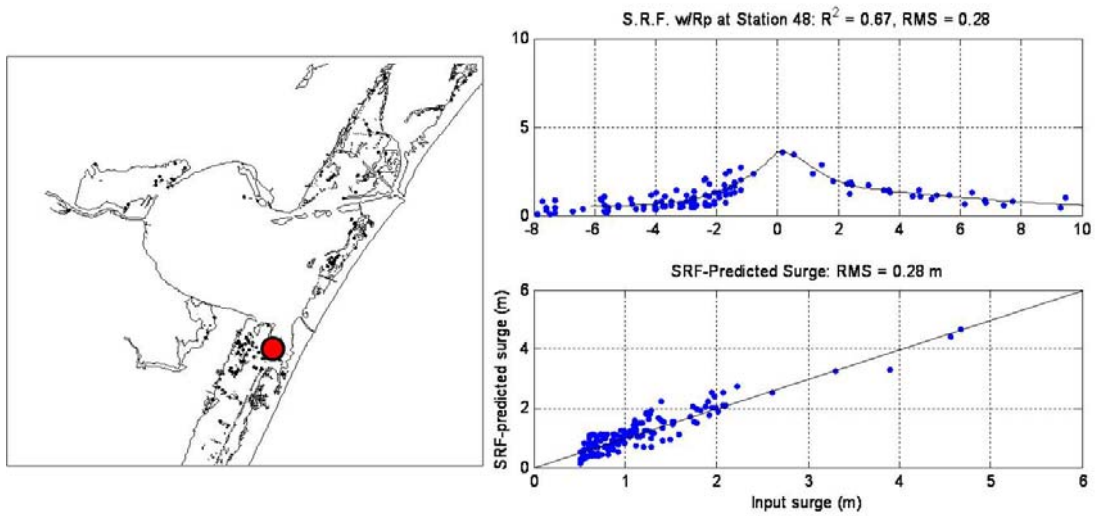
Bridge No.	Stn. No.	Description	Lon.	Lat	Location
1	45	State Hwy Park Road 22_No.1	-97.214	27.619	Corpus Christi
2	47	State Hwy Park Road 22_No.2	-97.240	27.635	
3	48	Kennedy Causeway	-97.261	27.658	
4	51	Padre Island Bridge	-97.312	27.680	
5	53	Nueces Bay Causeway 1	-97.395	27.813	
6	55	Nueces Bay Causeway 2	-97.370	27.844	
7	59	Cemetery Road	-97.104	27.884	
8	65	Johnson Causeway	-97.020	28.120	
9	84	Port Lavaca	-96.598	28.650	Matagorda
10	88	Weedhaven	-96.432	28.732	
11	116	FM1495 Road	-95.341	28.922	Galveston
12	117	Hwy 332	-95.293	28.956	
13	130	FM 2004 Road	-95.207	29.213	
14	142	Pelican Island Bridge	-94.824	29.311	
15	147	Texas City Dike Road	-94.810	29.363	
16	181	Martin Luther King Jr. Drive (Hwy 82)	-93.895	29.766	
17	182	Jetty Road	-93.853	29.696	



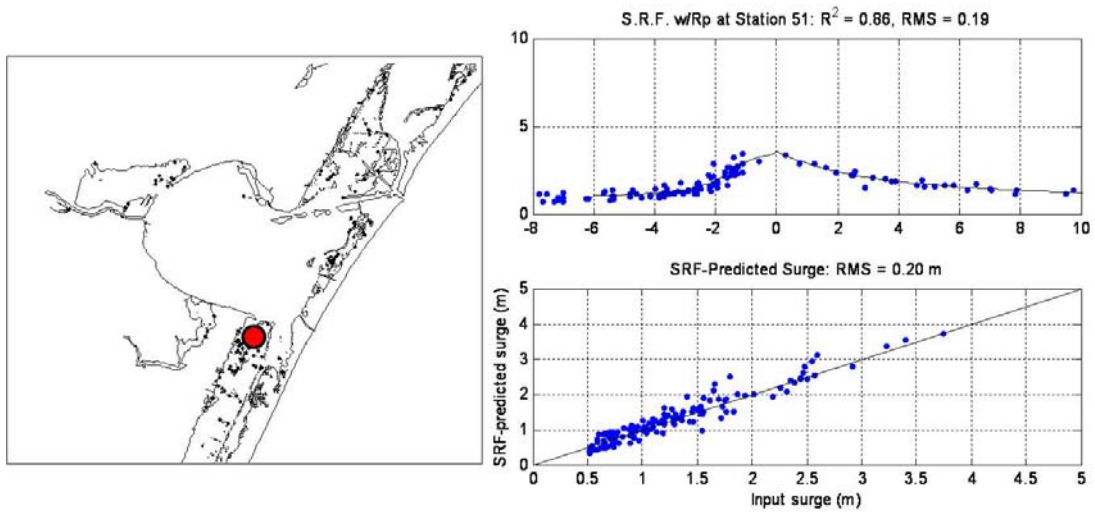
A- 1 Surge response function developed at bridge No. 1. State Hwy Park Road 22 in Corpus Christi.



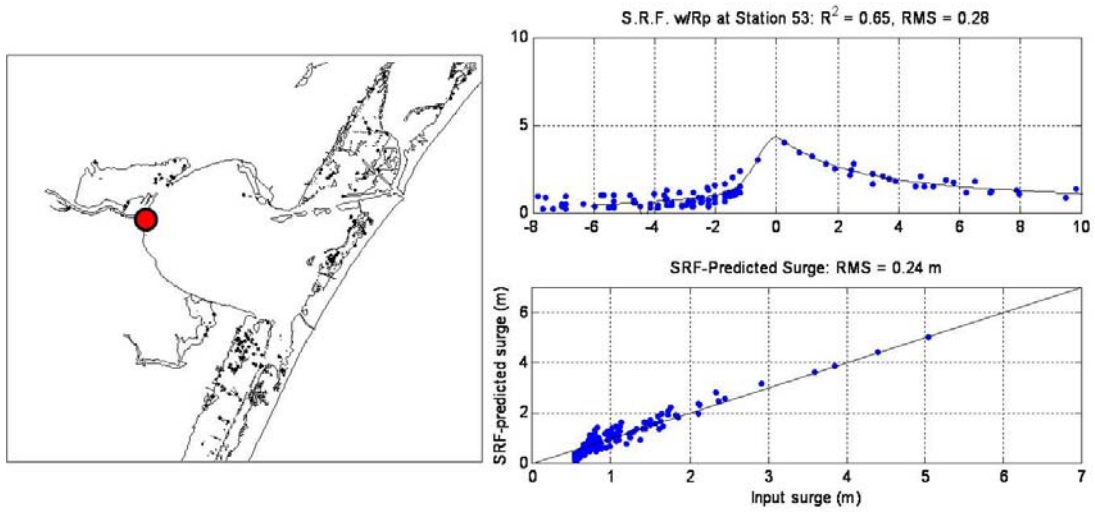
A- 2 Surge response function developed at bridge No. 2. State Hwy Park Road 22 in Corpus Christi.



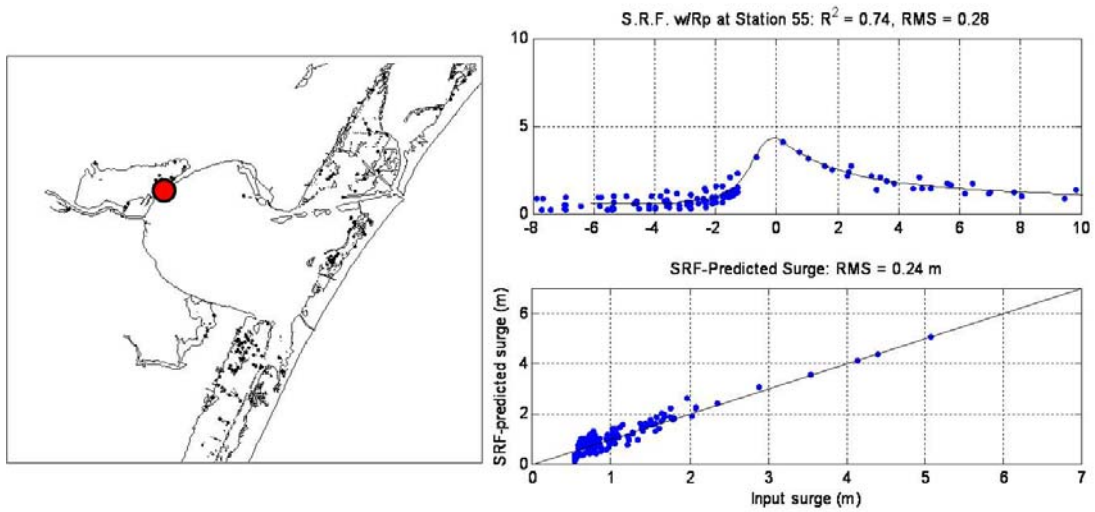
A- 3 Surge response function developed at bridge No. 3 along the Kennedy Causeway in Corpus Christi.



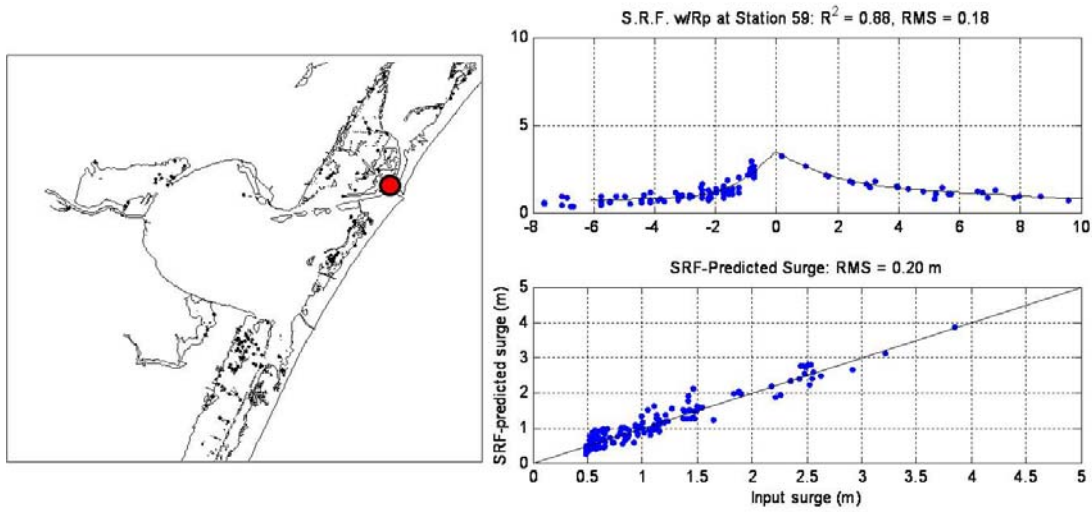
A- 4 Surge response function developed at the bridge No. 4. Padre Island Bridge in Corpus Christi.



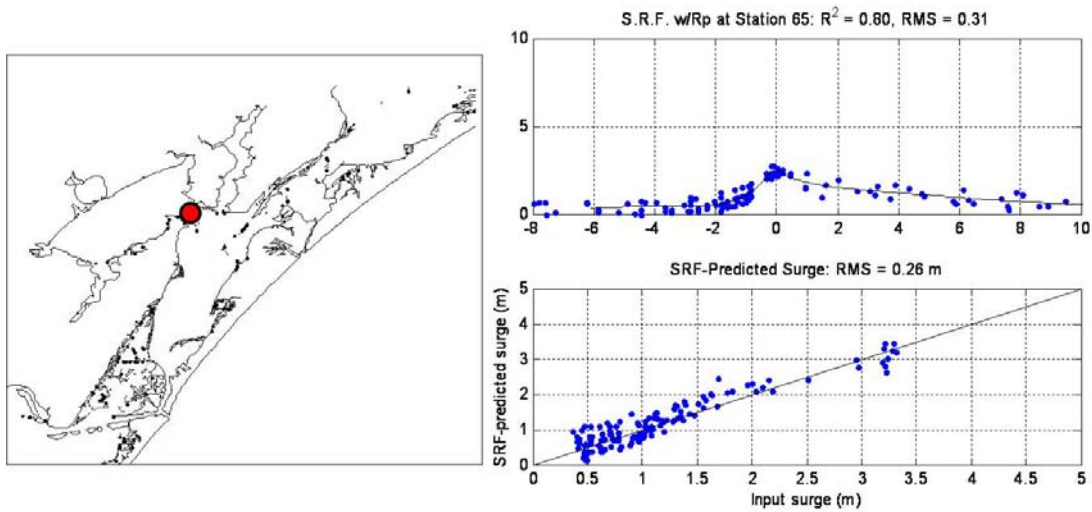
A- 5 Surge response function developed at bridge No. 5 along the Nueces Bay Causeway in Corpus Christi.



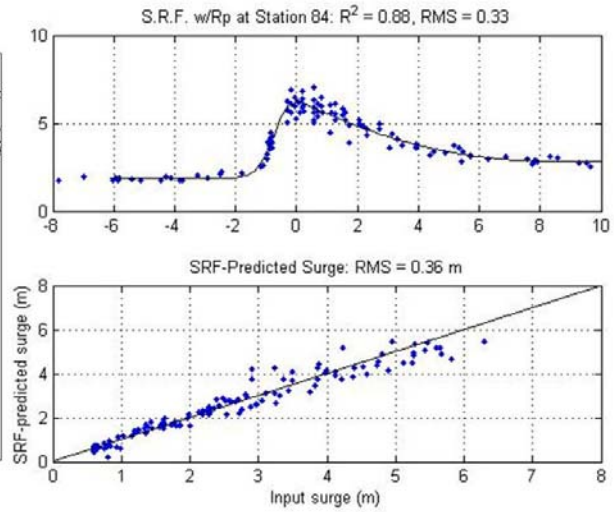
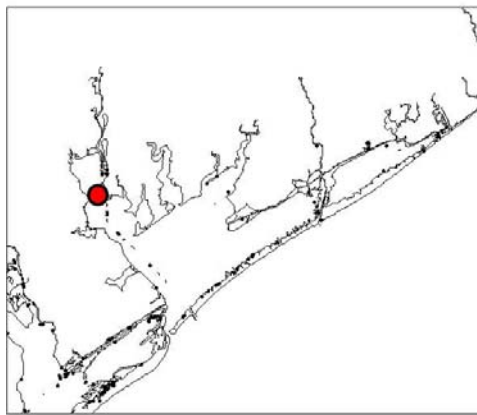
A- 6 Surge response function developed at bridge No. 6 along the Nueces Bay Causeway in Corpus Christi.



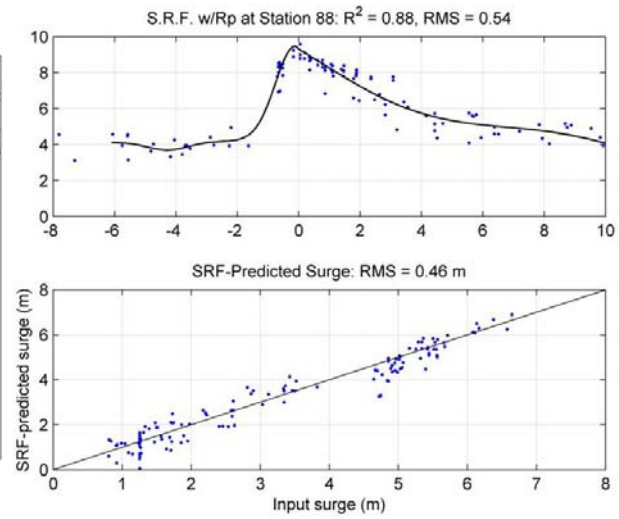
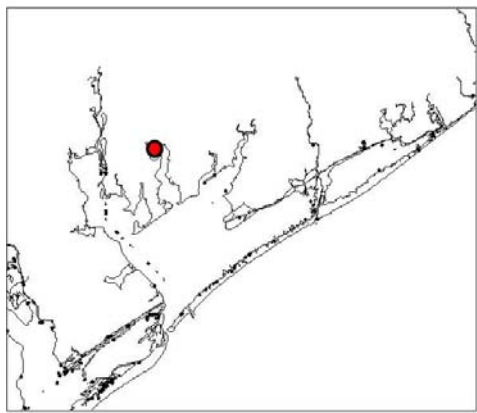
A- 7 Surge response function developed at bridge No. 7 along the Cemetery Road near Corpus Christi.



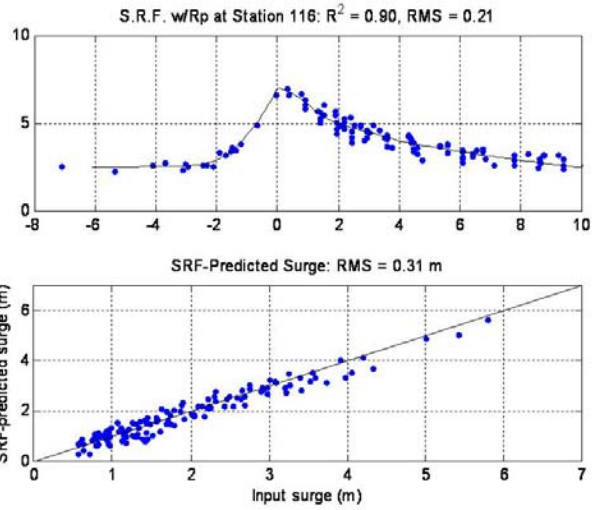
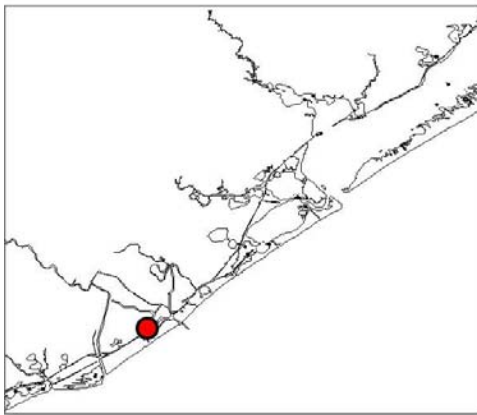
A- 8 Surge response function developed at bridge No. 8 along the Johnson Causeway near Corpus Christi.



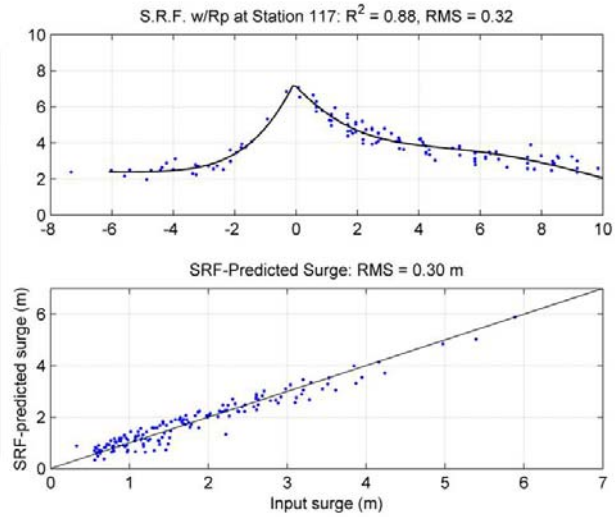
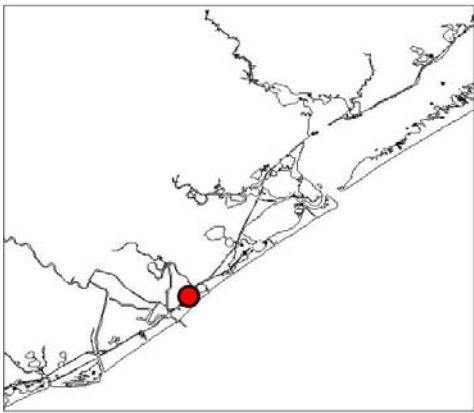
A- 9 Surge response function developed at bridge No. 9. Port Lavaca in Matagorda Bay.



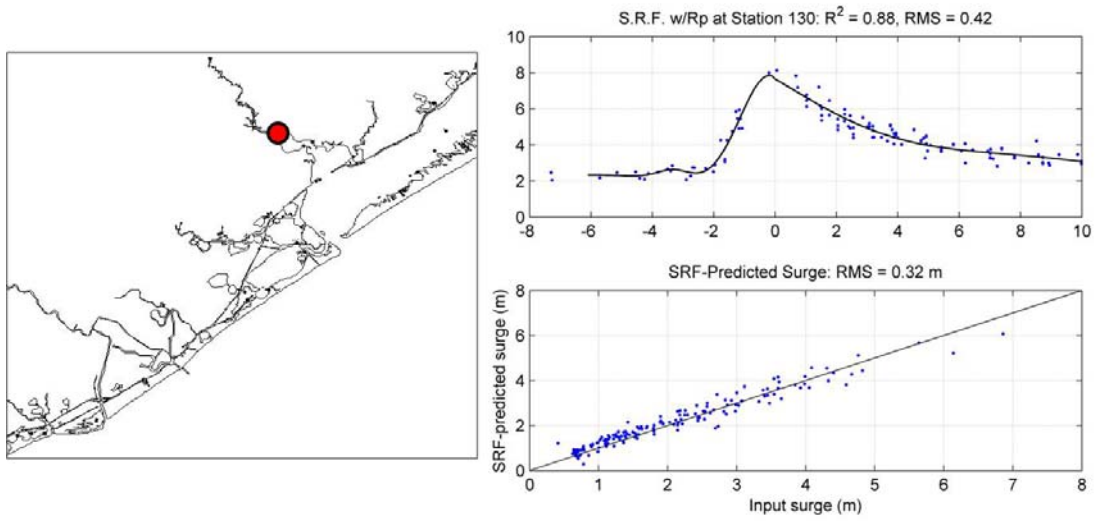
A- 10 Surge response function developed at bridge No. 10 near Weedhaven in Matagorda Bay.



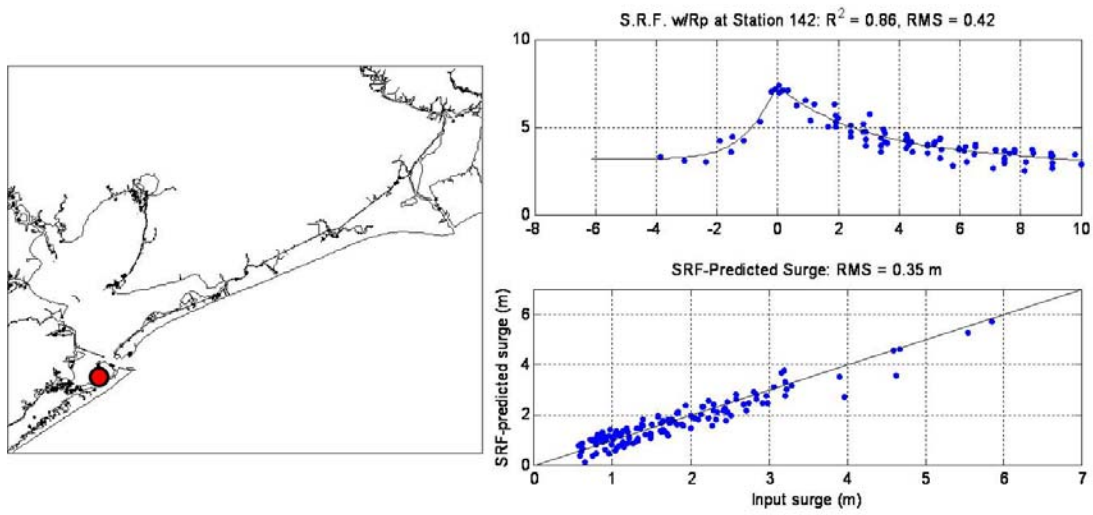
A- 11 Surge response function developed at bridge No. 11 along FM 1495 in Galveston.



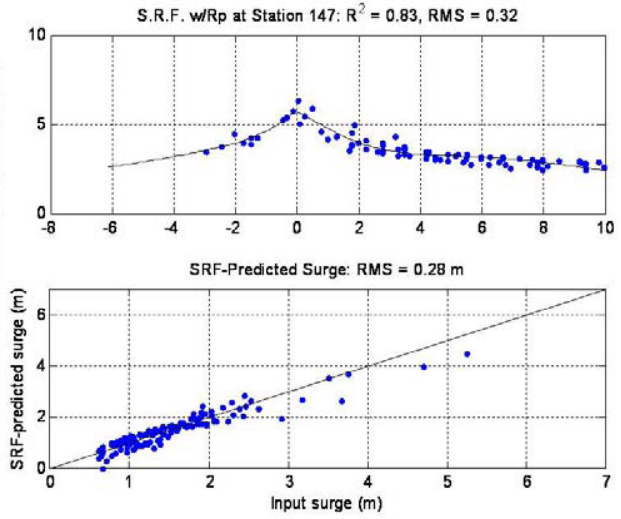
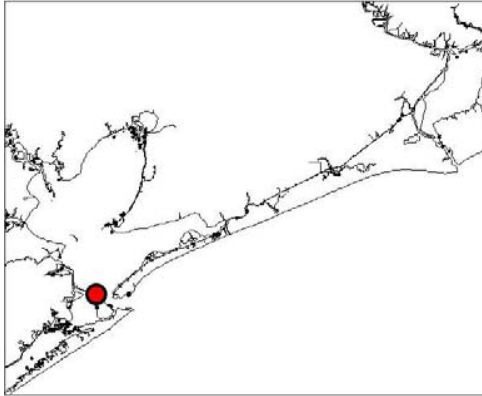
A- 12 Surge response function developed at bridge No. 12 along Hwy 332 in Galveston.



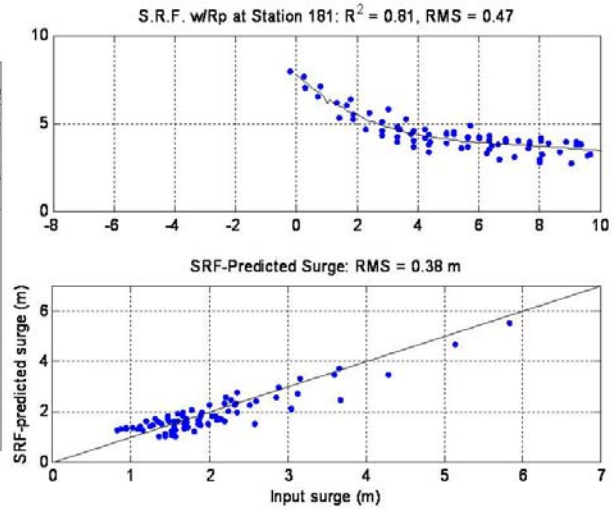
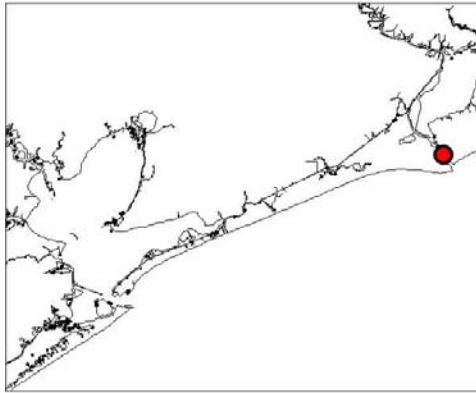
A- 13 Surge response function developed at bridge No. 14. FM 2004 in Galveston.



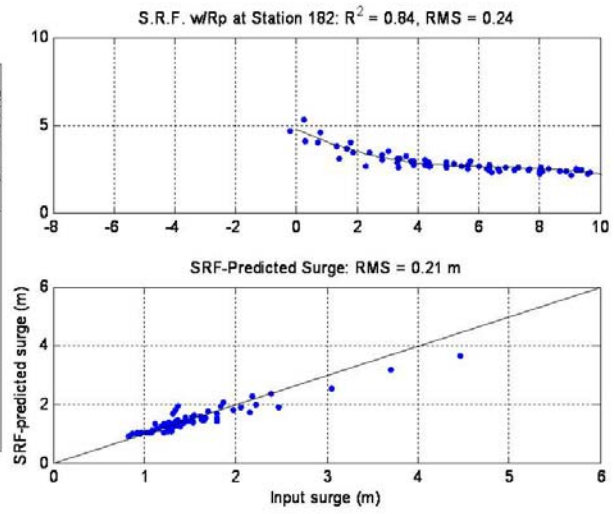
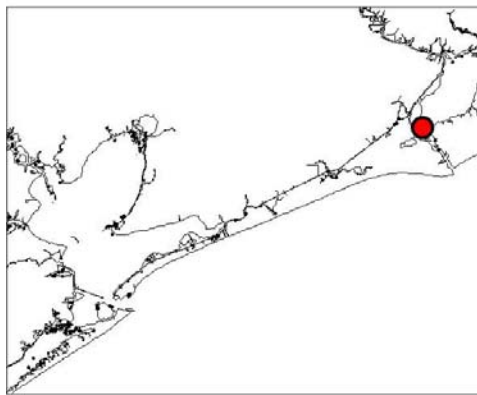
A- 14 Surge response function developed at bridge No. 16. Pelican Island Bridge in Galveston.



A- 15 Surge response function developed at bridge No. 17. Texas City Dike Road in Galveston.



A- 16 Surge response function developed at bridge No. 19. Martin Luther King Jr. Drive (Hwy 82) in Galveston.



A- 17 Surge response function developed at bridge No. 20. Jetty Road in Galveston.